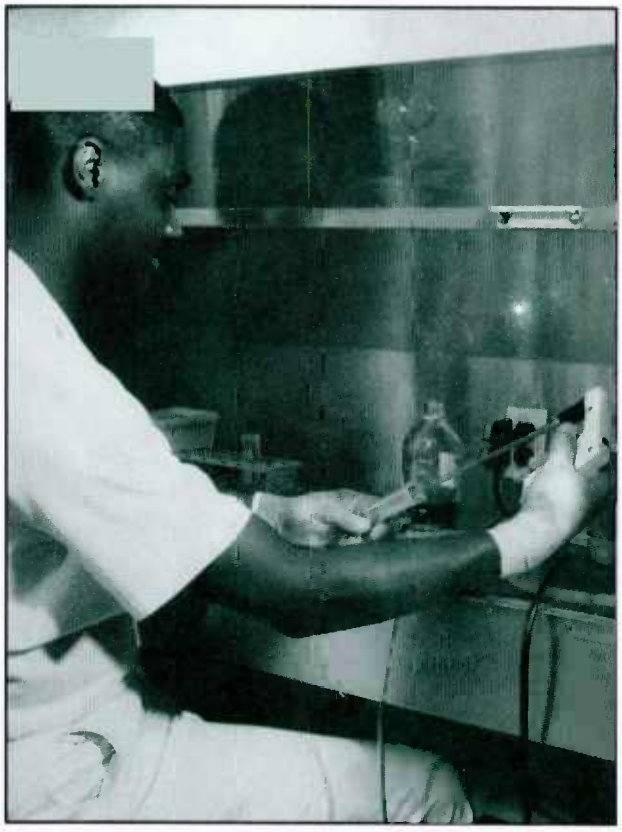

Second Quarter
1994

AFRRI Reports

Armed Forces Radiobiology Research Institute

8901 Wisconsin Avenue • Bethesda, Maryland 20889-5603

On the cover: *Air Force MSgt Kyle Sample, an AFRRI research laboratory technician, performs titration, which allows him to determine cell count, a means of measuring the effects of ionizing radiation. The effort is part of a project to develop treatments for radiation-induced gastrointestinal injury.*

REPORT DOCUMENTATION PAGE

Form Approved
OMB No. 0704-0188

1. AGENCY USE ONLY *(Leave blank)*	2. REPORT DATE	3. REPORT TYPE AND DATES COVERED
	August 1994	Reprints

4. TITLE AND SUBTITLE

AFRRI Reports, Second Quarter 1994

5. FUNDING NUMBERS

PE: NWED QAXM

6. AUTHOR(S)

7. PERFORMING ORGANIZATION NAME(S) AND ADDRESS(ES)

Armed Forces Radiobiology Research Institute
8901 Wisconsin Avenue
Bethesda, MD 20889-5603

8. PERFORMING ORGANIZATION REPORT NUMBER

SR94-9 - SR94-14

9. SPONSORING/MONITORING AGENCY NAME(S) AND ADDRESS(ES)

Uniformed Services University of the Health Sciences
4301 Jones Bridge Road
Bethesda, MD 20814-4799

10. SPONSORING/MONITORING AGENCY REPORT NUMBER

11. SUPPLEMENTARY NOTES

12a. DISTRIBUTION/AVAILABILITY STATEMENT

Approved for public release; distribution unlimited.

12b. DISTRIBUTION CODE

13. ABSTRACT *(Maximum 200 words)*

This volume contains AFRRI Scientific Reports SR94-9 through SR94-14 for April-June 1994.

14. SUBJECT TERMS

15. NUMBER OF PAGES
75

16. PRICE CODE

17. SECURITY CLASSIFICATION OF REPORT	18. SECURITY CLASSIFICATION OF THIS PAGE	19. SECURITY CLASSIFICATION OF ABSTRACT	20. LIMITATION OF ABSTRACT
UNCLASSIFIED	UNCLASSIFIED	UNCLASSIFIED	UL

CONTENTS

Scientific Reports

GASTROENTEROLOGY 1994;106:1405–1417

ALIMENTARY TRACT

Natural Gastric Infection With *Helicobacter pylori* in Monkeys: A Model for Spiral Bacteria Infection in Humans

ANDRE DUBOIS,*,† NANCY FIALA,*,† LILLIE M. HEMAN-ACKAH,§ E. SUSAN DRAZEK,* ANDRZEJ TARNAWSKI,‖ WILLIAM N. FISHBEIN,¶ GUILLERMO I. PEREZ-PEREZ,# and MARTIN J. BLASER#

*Laboratory of Gastrointestinal and Liver Studies, Digestive Diseases Division, Department of Medicine, Uniformed Services University of the Health Sciences, and Departments of †Physiology and §Veterinary Medicine, Armed Forces Radiobiology Research Institute, Bethesda, Maryland; ‖Veterans Administration Medical Center and University of California at Irvine, Long Beach and Irvine, California; ¶Division of Biochemistry, Department of Environmental and Chemical Pathology, Armed Forces Institute of Pathology, Washington, D.C.; and #Division of Infectious Diseases, Department of Medicine, Vanderbilt University School of Medicine, and Department of Veterans Affairs Medical Center, Nashville, Tennessee

Background/Aims: There is no generally accepted model for *Helicobacter pylori* infection in humans. The aim of this study was to examine the natural history and effect of treatment in rhesus monkeys and sequentially define the immune response to *H. pylori* in relation to treatment. *Methods:* Infection and gastritis were graded blindly by histological analysis and culture of biopsy specimens harvested during gastroduodenoscopies in 26 anesthetized colony-bred monkeys. Plasma *H. pylori*–specific immunoglobulin (Ig) G levels were determined by enzyme-linked immunosorbent assay. *Results: H. pylori* and *Gastrospirilum hominis*–like organisms were present in 13 and 9 monkeys, respectively; 3 animals harbored both organisms, whereas 4 monkeys were not infected. Gastritis score was ≤1.5 in animals uninfected or infected only with *G. hominis*–like organisms and ≥2.0 in all *H. pylori*–infected animals. IgG ratios were ≥0.5 in 12 of 13 *H. pylori*–infected animals and in 2 of 13 *H. pylori*–negative animals ($P < 0.001$). One monkey became infected with *H. pylori* during the observation period, with concurrent increase of gastritis and plasma IgG levels. In untreated animals, infection, gastritis, and plasma IgG levels remained unchanged over 7–15 months. Triple therapy eradicated *H. pylori* at 6 months in 4 of 6 animals while suppressing gastritis and plasma IgG levels. *Conclusions:* Rhesus monkeys harboring *H. pylori* are persistently infected and have gastritis and elevated specific IgG levels, all of which may respond to appropriate therapy, whereas *G. hominis* infection is associated with little inflammation.

Since the first report of its isolation in 1983,[1] *Helicobacter pylori,* previously named *Campylobacter pylori,* has been implicated in the pathogenesis of gastritis[2] and duodenal ulcer disease[3] and as a risk factor for adenocarcinoma and lymphoma of the stomach.[4–6] The diagnosis of this infection has been primarily based on identification of the organisms in gastric mucosal biopsy specimens, although noninvasive methods such as the urea breath test[7] and detection of specific serum antibodies[8] have facilitated larger epidemiological studies. Another type of spiral bacterium has also been described in the stomach of patients with gastric cancer[9] and in patients with upper gastrointestinal complaints.[10,11] The provisional name of this bacterium is *Gastrospirillum hominis,* and it has been suggested that it also could be a pathogen.[12,13] More recently, polymerase chain reaction (PCR) amplification of 16S ribosomal RNAs has indicated that this organism belongs in the *Helicobacter* genus, and it appears to be closer to *Helicobacter felis* than to *H. pylori.*[14] Although the name *Helicobacter heilmannii* was initially proposed by these investigators, their examination of different clones led them to conclude that there are probably many species of these bacteria and that it is premature to propose an official name.[14]

Despite the number of observations in humans, we still lack direct experimental evidence for a causal relation between these bacterial infections and subjective symptoms as well as pathological findings. This is caused, in part, by ethical considerations in humans and by the absence of an accepted animal model.

The *Helicobacter* genus presently comprises nine species that have been isolated from different animal species,

Abbreviations used in this paper: ELISA, enzyme-linked immunosorbent assay; FET, Fisher's Exact Test; GHLO, *Gastrospirillum hominis*–like organisms; PCR, polymerase chain reaction.

0016-5085/94/$0.00

including primates.[15] The *Helicobacter* species that have been isolated from naturally infected ferrets, cats, and cheetahs share many properties with *H. pylori* observed in humans,[16–18] although important differences have also been noted. In nonhuman primates, *H. pylori*–like organisms isolated from baboons, pigtailed macaques, and rhesus monkeys have been found to be morphologically and biochemically similar to *H. pylori* isolated from humans.[19–21] However, the DNA homology of the organisms isolated from pigtailed macaques with other members of the *Helicobacter* genus was later found to be <10%.[22] In contrast, *H. pylori*–like organisms isolated from rhesus monkeys have been found to be very similar to human *H. pylori* by all the phenotypic tests that have been applied to date, i.e., total protein profile, antiurease monoclonal antibody, and hyperimmune rabbit antiserum using a 10%–25% linear gradient sodium dodecyl sulfate–polyacrylamide gel electrophoresis system.[21] Furthermore, PCR amplification and partial 16S ribosomal RNA gene sequence analysis has indicated that the rhesus monkey and human isolates are highly homologous.[23a] Taken together, these data strongly suggest that the rhesus monkey isolates that we have grown in vitro are *H. pylori*. In addition, baboons and rhesus monkeys are frequently infected with another gram-negative, urease-positive, tightly coiled spirilla that is identical in morphology to human *G. hominis* by light and electron microscopy.[19,21] Neither human *G. hominis* nor the *G. hominis*–like organisms (GHLO) observed in baboons or rhesus monkeys have been grown in vitro.[24]

Based on these observations, both baboons and rhesus monkeys appear to represent potential models to evaluate the role played by gastric mucosal infection with either of the spiral bacteria found in humans in the production of gastritis and of the associated immune response; these models also permit the evaluation of antimicrobial therapies. However, the genome of *H. pylori*–like organisms isolated from baboons has not yet been characterized, and these animals are bigger and more difficult to handle than rhesus monkeys.

Therefore, the goals of the present study were to determine the natural history of *H. pylori* and GHLO infections in rhesus monkeys; to evaluate the effect of treatment in these animals; and to sequentially define the immune response of infected rhesus monkeys to *H. pylori* in the presence or absence of treatment.

Materials and Methods

Animals

Twenty-six domestic, colony-reared, male rhesus monkeys, *Macaca mulatta* (age, 2–5 years; weight, 3–5 kg), were first quarantined for 90 days in individual stainless steel cages in conventional holding rooms of an animal facility approved by the American Association for Accreditation of Laboratory Animal Care and were subsequently kept in similar individual housing. They had not been used in any other research protocol before being included in the present studies. Animals were provided with tap water ad libitum, commercial primate chow, and fruit. After three negative intradermal tuberculin test results, with tests performed at 2-week intervals, animals were released from quarantine. All subsequent studies were performed between 8 AM and noon after an overnight fast.

Endoscopic Procedures and Biopsies

Each rhesus monkey underwent gastroduodenal endoscopic examination under general anesthesia (atropine sulfate, 0.02 mg/kg intramuscularly followed by ketamine hydrochloride, 10 mg/kg intramuscularly) using a videogastroscope with an outer diameter of 9.8 mm (model 81200; Welch–Allyn, Skaneateles Falls, NY). Between each endoscopy, care was taken to first rinse the endoscopic equipment with water and then disinfect it sequentially with solutions of 2% glutaraldehyde and 95% ethanol. The macroscopic appearance of corpus and antral mucosae was assessed qualitatively but, as previously reported,[21] was not significantly related to any of the other features of infection. In each animal, two pinch biopsy specimens of the gastric mucosa were obtained each from the corpus and the antrum. One of the specimens from each region of the stomach and a specimen obtained from the duodenum were fixed in neutral 10% buffered formalin and routinely processed for light microscopy. Five-micrometer paraffin-embedded sections were processed for H&E and Gram staining and viewed under ×100–×1000 magnification. Initially, Warthin–Starry staining was also performed for identification of spiral bacteria; however, we found that similar accuracy was obtained with H&E and Gram staining and subsequently performed only these preparations. Two additional biopsy specimens were taken each from the corpus and antrum of three *H. pylori*–infected and three GHLO-infected rhesus monkeys. These specimens were fixed in Karnovsky's solution and processed routinely for transmission electron microscopy.[25] Coded ultrathin sections were evaluated to determine the presence and characteristics of *H. pylori* and GHLO using a Philips 400 electron microscope (Philips, Mahwah, NJ) at 80 kV.

Rating of Infection

Based on the appearance of *H. pylori* and GHLO on histological examination,[21] coded H&E- and Gram-stained sections were scored for intensity of infection at ×1000 using a scale of 0–3 as follows: 0, no bacteria; 1, colonies seen in 1–2 of 10 fields of view; 2, colonies seen in 3–8 of 10 fields; and 3, colonies seen in 9–10 of 10 fields. One biopsy specimen from the corpus and one from the antrum were immediately placed in sterile 0.9% NaCl, kept on ice, coded, and then prepared for culture, smears, and urease assay by homogenization with a sterile ground-glass cone-shaped pestle fitting a tapered 1.5-mL Eppendorf tube. Sterile 1–2-μL loops were filled and streaked on agar plates prepared with Mueller–Hin-

ton media supplemented with 5% sheep blood and incubated at 37°C in sealed chambers with an atmosphere of 90% N_2, 5% O_2, and 5% CO_2. Ringed microscope slides were used for smears and Gram stains of 1-μL aliquots of the homogenate and of colonies (dispersed in sterile saline) that grew within 7 days. *H. pylori* identification was based on (1) pinhead-sized "water-spray" colonies positive for urease[26] and oxidase (Becton–Dickinson, Cockeysville, MD) and catalase (formation of bubbles in 3% H_2O_2) activities; (2) presence, in these colonies, of gram-negative curved or "gull-wing" rods; and (3) a kinetic assay showing high urease specific activity (>1 μmol · min^{-1} · mg $protein^{-1}$) plus high-affinity substrate binding (Michaelis constant [K_m] < 1 mmol/L),[27] in at least one culture from each rhesus monkey.

Rating of Gastritis

The presence and extent of gastritis was rated independently from the scoring for infection on coded H&E-stained slides using a scale of 0–3, modified from Marshall and Warren,[28] as follows: 0, intact mucosal lining and essentially no infiltration of the lamina propria with lymphocytes and plasma cells; 1, mild increase of mononuclear infiltration localized in upper half of the mucosa; 2, marked mononuclear infiltration extending from the surface to the muscularis mucosae; and 3, presence of polymorphonuclear leukocytes in glands, which was always associated with marked mononuclear infiltration and surface erosions. Duodenal biopsy specimens were evaluated for the presence of gastric metaplasia. Preobservation or pretreatment infection and gastritis scores of 4 of the 26 rhesus monkeys (1 uninfected, 1 *H. pylori* infected, and 2 GHLO infected) have been included in results previously published.[21]

Measurement of *H. pylori*–Specific Plasma Immunoglobulin G Levels

At each endoscopy, 5 mL of ethylenediaminetetraacetic acid–treated blood was obtained and the plasma was frozen at −70°C. Plasma immunoglobulin G (IgG) levels were determined blindly using a previously described enzyme-linked immunosorbent assay (ELISA) with >95% sensitivity and specificity for human infection.[29,30] In addition, all samples were run a second time using anti-monkey antibody conjugates. In brief, the *H. pylori* antigen used in the ELISA was prepared from bacterial suspensions from five *H. pylori* strains representing a range of antigens. The sonicates from each strain were pooled and diluted in 0.05 mol/L carbonate buffer (pH 9.6) to yield the optimal protein concentration of 10 μg/mL. A 0.1-mL aliquot of this solution was added to each well of a flat-bottomed Immulon 2 plate (Dynatech Laboratories, Alexandria, VA). The screening serum dilutions were 1:800, whereas perioxidase conjugates of goat anti-human (Tago Inc., Burlingame, CA) and anti-monkey (Nordic, Capo Beach, CA) IgG were diluted 1:2000. Results were corrected for day-by-day variation of the ELISA and expressed as optical density ratios. In humans, an IgG ratio > 1.0 has been considered indicative of the presence of anti–*H. pylori* antibodies. All assays were performed at least in duplicate. Tests for possible cross-reactivity of *H. pylori* antibodies had been performed by absorbing serum from *H. pylori*–infected persons who had high values in the IgG ELISA with cells of other enteropathogens.[29] For studies of the time course of infection or of the effect of treatment, all samples collected in a specific animal were run on the same day and were included in the same plate.

Follow-up Examinations and Treatments

Fifteen of the rhesus monkeys (4 uninfected, 6 *H. pylori*–infected, and 5 GHLO-infected as assessed by histological examination and/or culture) were re-evaluated 7–15 months later by endoscopic biopsies and plasma IgG determinations. In addition, two therapeutic trials were performed in 12 of the infected rhesus monkeys. First, 6 rhesus monkeys (2 *H. pylori*–infected and 4 GHLO-infected) were treated with oral amoxicillin plus metronidazole plus bismuth subsalicylate (7, 7, and 10 mg/kg, respectively, three times daily) diluted in Tang (flavored powder that, when reconstituted with water, produces a fruity drink that rhesus monkeys consume readily; General Foods Corp., White Plains, NY) for 4 weeks; endoscopies and plasma IgG determinations were repeated 1 and 3 months later. Second, 6 other rhesus monkeys infected with *H. pylori* were treated with amoxicillin plus metronidazole plus bismuth subsalicylate (7, 7, and 10 mg/kg, respectively) diluted in 5 mL of sterile water and administered intragastrically twice daily for 10 days; endoscopies and plasma IgG determinations were repeated 1 week and 1, 2, 3, 5, and 6 months after the end of treatment.

Statistical Analysis

Results are expressed as means ± SEM. A two-way analysis of variance with repeated measures[31] was used to determine the effects caused by type of infection, by time or treatment, or by an interaction among these two factors. This statistical method takes into account that measurements were repeated sequentially in the same animals by establishing a distinction between a factor that classifies the subjects into groups (grouping factor) and a factor for which each subject is measured at all times (within-subject factor). Computer implementation of this statistical method was performed using locally developed programs. Linear correlation coefficients were calculated using SlideWritePlus software (Advanced Graphic Software, Carlsbad, CA). Fisher's Exact Test (FET) and Mantel–Haenszel corrected χ^2 test were performed when appropriate.

Results

Prevalence of Gastric Infection as Assessed by Light Microscopy and Culture

In 4 of 26 naive (untreated) colony-reared rhesus monkeys, no spiral bacteria were observed by histological analysis of the biopsy specimens harvested from the corpus or antral mucosae; cultures of other gastric biopsy specimens obtained in the same animals were negative. In 13 other rhesus monkeys, *H. pylori* was observed by

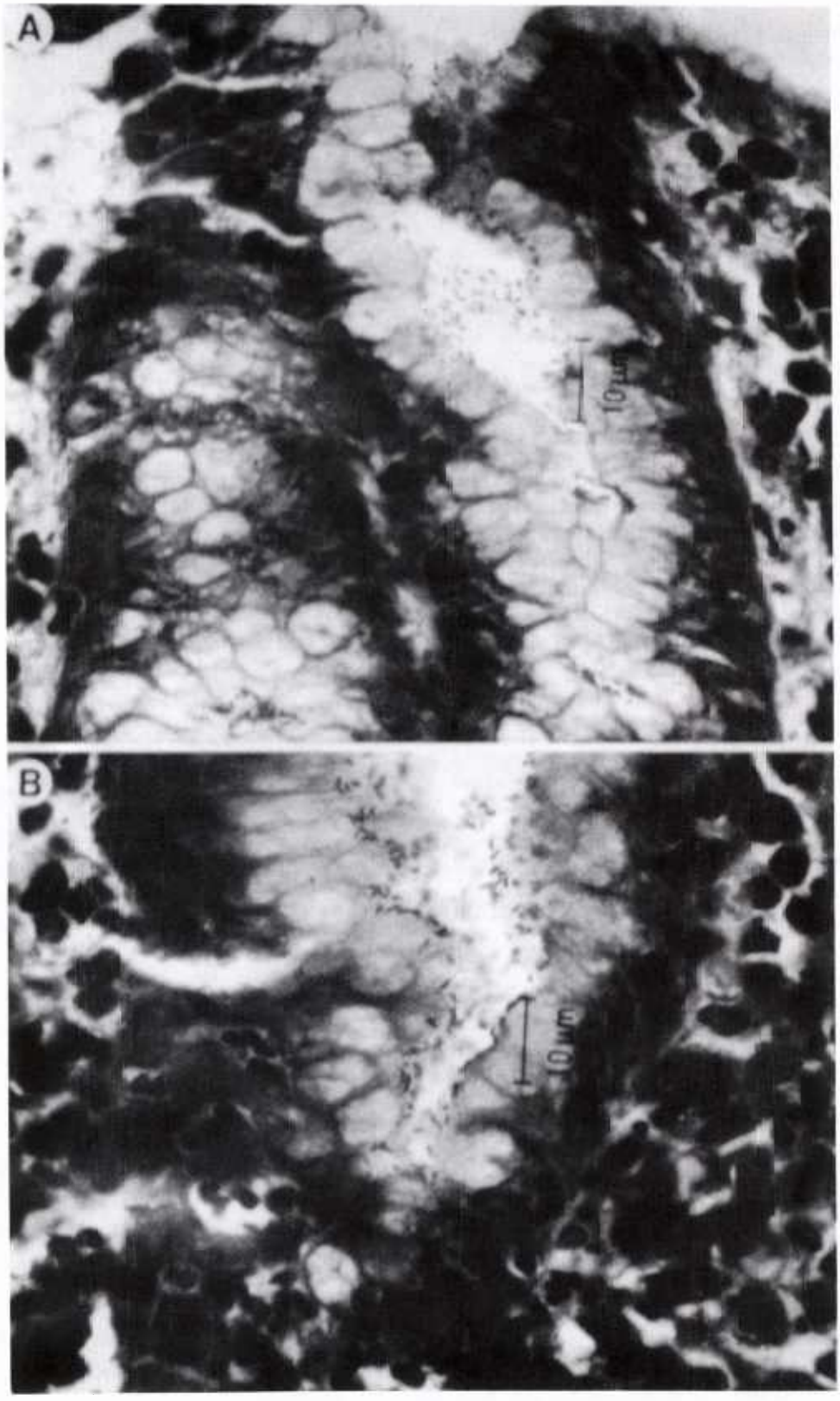

Figure 1. Composite photomicrograph of the (*A*) gastric pit and (*B*) crypt of an *H. pylori*–infected rhesus monkey (H&E; original magnification ×1000). Note the mucous depletion of superficial epithelial cells and the intense mononuclear and neutrophil infiltration.

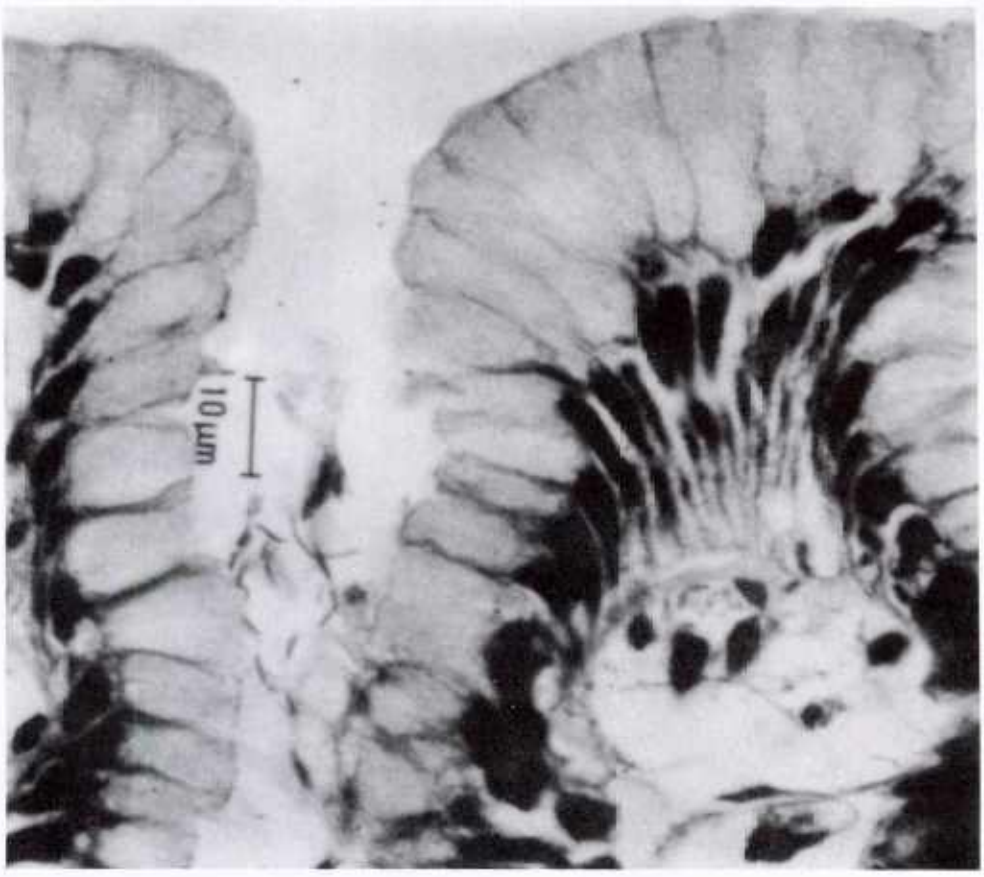

Figure 2. Gastric pit of a GHLO-infected rhesus monkey (H&E; original magnification ×1200). Note the absence of neutrophil infiltration and the discrete mononuclear infiltration.

histological analysis in both the corpus and the antrum (Figure 1) (infection score, 1.38 ± 0.30 and 1.85 ± 0.31, respectively), and the characteristic bacterial growth with high-activity production of a urease with tight substrate binding[32] was found in at least one of the specimens in each of these animals. A small number of GHLO also were observed in the corpus of 3 of these rhesus monkeys. In subsequent analyses, we defined as *H. pylori*–infected those animals that had at least one specimen containing *H. pylori* as evidenced by either light microscopy or culture. In the 9 remaining rhesus monkeys, GHLO alone were observed by histological analysis of the specimens obtained in the corpus and, in addition, in the antrum of 6 of these animals (infection score, 2.67 ± 0.16 and 1.89 ± 0.46, respectively) (Figure 2). As has been reported in human studies,[24] no bacterial growth was observed in the many cultures prepared from these specimens, despite the repeated microscopic observation of the clearly visible, well-stained, long (4–7 µm), corkscrew-like, gram-negative organisms in smears of the same specimens. In contrast, *H. pylori* organisms could not be visualized in the smears of similar specimens harvested from *H. pylori*–infected rhesus monkeys, because they are indistinguishable from the ubiquitous tissue fibrils that also are stained by safranin. All biopsy specimens containing GHLO had urease activity, often manyfold higher than the specimens containing *H. pylori*; in two cases, there was enough material to directly evaluate urea binding affinity by spectrophotometric assay. In both cases, the K_m was <1 mmol/L, as was true for the specimens obtained in *H. pylori*–infected animals; accordingly, no differentiation was possible by this criterion. Indeed, the characteristic urease supports the recent argument based on molecular genetics that GHLO belong within the genus *Helicobacter*.[14] Thus, natural infection with *H. pylori* and/or GHLO were common in this population of rhesus monkeys.

Appearance of Organisms by Transmission Electron Microscopy

H. pylori were observed in close proximity to the surface of epithelial cells. In case of heavy infection, very few microvilli were visible and the bacteria appeared to be attached to pedestals similar to those described in

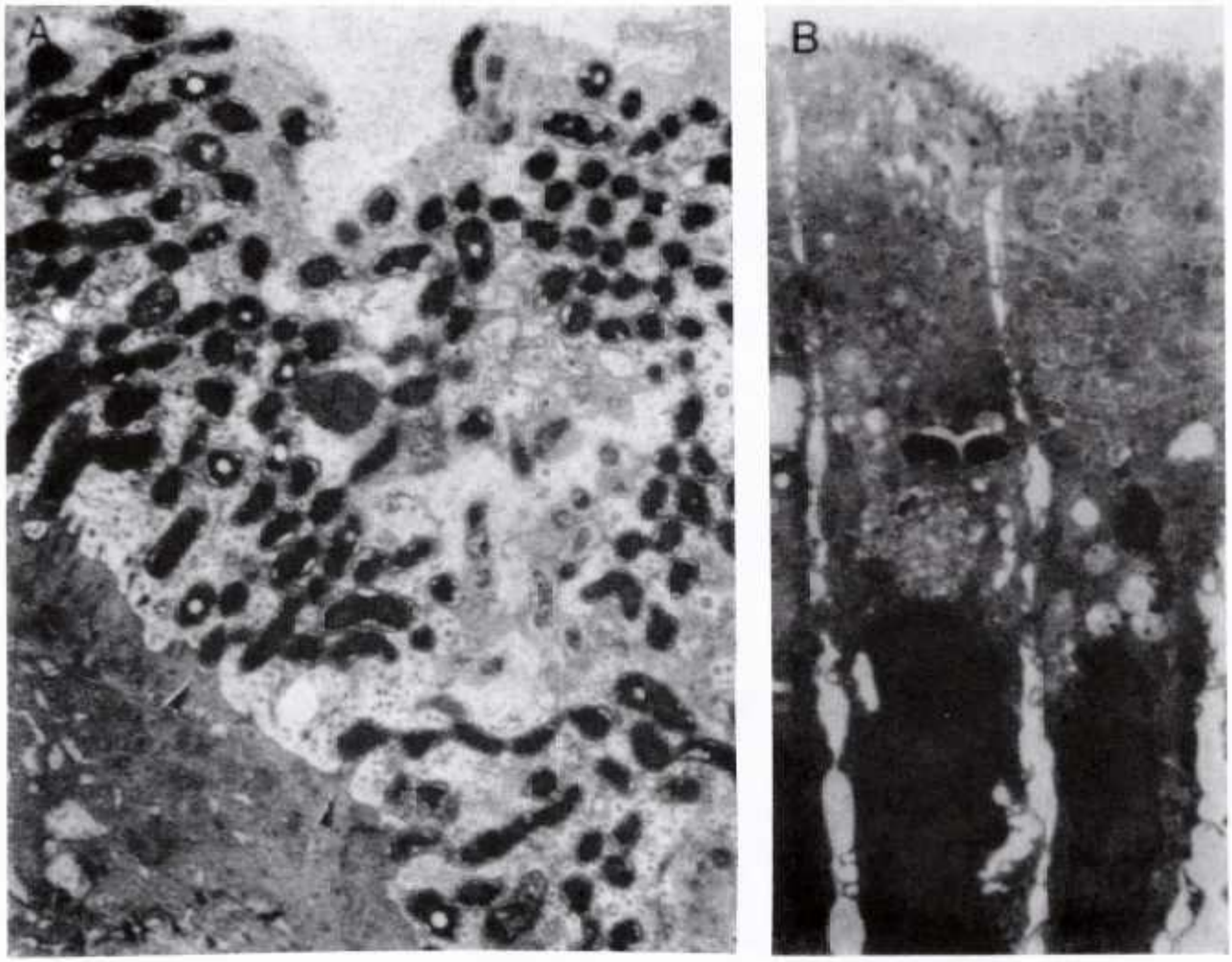

Figure 3. Transmission electron micrographs of *H. pylori*. (*A*) Note the virtual disappearance of microvilli, the formation of pedestals (*arrowheads*), and the close association between *H. pylori* and these pedestals (original magnification ×12,000). (*B*) Intact microvilli and intracellular organelles on two superficial epithelial cells, one of which has two *H. pylori* within its cytoplasm (original magnification ×10,000).

humans[33] (Figure 3*A*, arrows). In contrast, microvilli and intracellular organelles were well preserved in areas of minimal infections, and a few *H. pylori* were occasionally present in the cytoplasm of superficial epithelial cells well below the level of the tight junction (Figure 3*B*). GHLO were never observed in close proximity with, or within the cytoplasms of, surface epithelial cells, and the microvilli were always intact (Figure 4). As previously reported,[21] GHLO, but not *H. pylori*, were often seen within the cytoplasm of parietal cells.

Relationship Between Gastric Inflammation and Infection With Gastric Organisms

For the entire group of 26 animals, inflammation scores of the corpus and antrum were significantly correlated ($r = 0.69$; $P < 0.01$). Therefore, the average of the two scores was subsequently used as an index of the amount of inflammation present in the stomach. All 13 rhesus monkeys infected with *H. pylori*, including 3 animals also infected with GHLO, had mean scores ≥ 2.0 (Figure 5), whereas 3 of 4 apparently uninfected rhesus monkeys had scores ≤ 0.5 ($P = 0.005$; FET, two-tailed). Among the 9 rhesus monkeys infected with GHLO alone, 8 animals had scores ≤ 1.0 (Figure 5); 5 of them had a score of 0 (Figure 5), whereas all 11 rhesus monkeys infected with *H. pylori* alone had scores ≥ 2.0 ($P < 0.001$; FET, two-tailed). Analyzing the data in another way, all 13 rhesus monkeys with mean gastritis scores ≥ 2.0 had detectable *H. pylori* infection compared with 0 of 13 with lower scores ($P < 0.001$; FET, two-tailed). Thus, a mean gastritis score ≥ 2.0 was 100% sensitive and 100% specific for *H. pylori* infection. Finally, gastritis score was significantly greater in *H. pylori*–infected rhesus monkeys than in either the uninfected or the GHLO-infected animals (Figure 5; $P < 0.05$).

Gastric metaplasia of the duodenum was not observed

Figure 4. Transmission electron micrograph of GHLO (original magnification ×18,000). Note that the bacteria are not closely associated with the epithelial cell surface and that microvilli are intact.

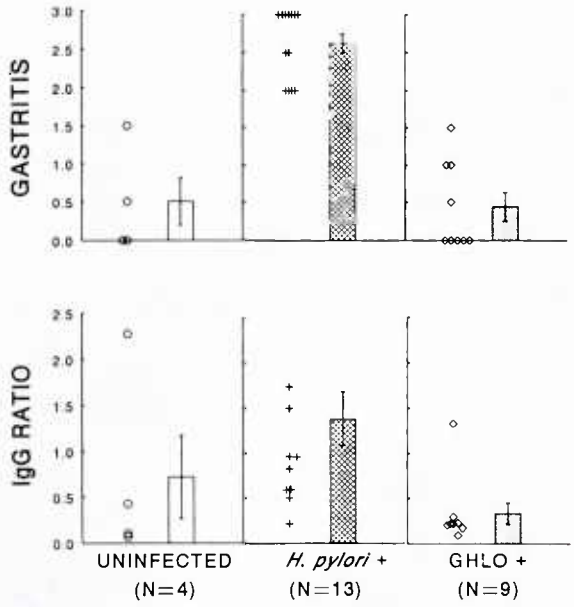

Figure 5. Individual values and means (±SEM) of gastritis scores and plasma IgG ratios in uninfected, *H. pylori*–infected, and GHLO-infected rhesus monkeys as determined by histological analysis and culture. Both gastritis score and plasma IgG were significantly ($P < 0.05$) greater in *H. pylori*–infected rhesus monkeys than in both uninfected and GHLO-infected animals.

in any of the animals, whether infected or not with gastric spiral organisms.

Assessment of Serological Response to *H. pylori*

When using anti-monkey antibody conjugates, *H. pylori*–specific plasma IgG levels were significantly ($P < 0.05$) higher in the *H. pylori*–infected animals than in either GHLO-infected or uninfected rhesus monkeys (Figure 5). In addition, regression analysis showed that plasma IgG ratios were significantly correlated with gastritis scores for the entire group of 26 animals, ($r = 0.52$; $P < 0.01$). Of rhesus monkeys without detectable *H. pylori* infection, 11 of 13 (85%) had IgG optical density ratios of <0.5 compared with only 1 of 13 (8%) with detectable *H. pylori* ($P < 0.001$, Mantel–Haenszel corrected χ^2). The specificity of the ELISA was therefore 92%, and its sensitivity was 85%. In 1 of the 2 animals with an IgG ratio of >0.5 and no detectable *H. pylori* or GHLO infection, the gastritis score was 1.0 in the antrum and 2.0 in the corpus. The other rhesus monkey had a marked infection with GHLO in the corpus (score 3.0) but not in the antrum and a gastritis score of 3.0 in the antrum and 0.0 in the corpus. The high level of inflammation and the *H. pylori*–specific antibodies suggest that these two rhesus monkeys may have been infected with *H. pylori* as well but that the organism had not been detected. In any event, from these studies it is clear that *H. pylori* infection in rhesus monkeys induces a specific immune response that can be accurately detected serologically using *H. pylori* antigens isolated from humans. Similar results were observed with anti-human antibody conjugates ($r = 0.80$; $P < 0.001$), although the specificity (83%) and sensitivity (69%) of the ELISA were slightly less than when using the anti monkey conjugates.

Natural History of Infection With *H. pylori*

Within 12 months of the initial endoscopy, 3 of the 4 uninfected rhesus monkeys had signs of infection. Biopsy specimens obtained in 1 animal showed the presence of *H. pylori* in H&E-stained sections; mean gastritis score increased from 0 to 2.5; IgG ratio increased from 0.07 to 0.65; and culture yielded *H. pylori*. GHLO were observed in the specimens of 2 other previously negative animals, but the cultures remained negative; mean gastritis score increased only slightly from 0 and 0.5 to 1.0 and 1.5, respectively, and IgG ratios remained < 0.5 (0.10 and 0.42 to 0.28 and 0.22, respectively). No infection was detected in the last animal 4 months after the initial endoscopy, although mild gastritis remained present (1.0 vs. 1.5 initially), and the IgG ratio remained high at approximately the same level (1.06 vs. 0.97 initially). In the rhesus monkeys that were initially found to be infected with *H. pylori* (n = 6) or GHLO (n = 5) alone, values for infection, gastritis, and plasma IgG did not change significantly during the subsequent 7–15 months (Table 1). Thus, as in humans, chronic infections with these organisms appear to have relatively stable characteristics.

Effect of Treatment on Infection, Inflammation, and Serological Response

A 4-week treatment with oral amoxicillin plus metronidazole plus bismuth subsalicylate diluted in Tang was given to 6 rhesus monkeys (2 and 4 infected with *H. pylori* and GHLO, respectively). No significant changes were observed in either group of rhesus monkeys for any of the variables assayed (Table 2). We concluded that this treatment was ineffective at eradicating infection.

In a second trial, the same medications given intragastrically twice daily for 10 days to 6 *H. pylori*–infected rhesus monkeys cleared the bacteria both at 5 days and at 1 month in all 6 rhesus monkeys. After 2 months, *H. pylori* infection was again found in 2 rhesus monkeys, indicating relapse or reinfection. The 4 other animals remained negative up to 6 months after treatment, and infection was considered to be eradicated (Figure 6). Infection with GHLO was also present in 3 of the animals

Table 1. Natural History of *H. pylori* or GHLO Infections in Untreated Animals Over Time

Time (*mo*)	Infection score: *H. pylori* or GHLO (light microscopy)[a] Corpus	Antrum	*H. pylori* (culture)[b] Corpus	Antrum	Gastritis score[c] Corpus	Antrum	*H. pylori* IgG ratio[d]
H. pylori–infected (n = 6)							
0	1.8 ± 0.5	2.3 ± 0.4	0.7 ± 0.2	1.0 ± 0.0	2.7 ± 0.3	3.0 ± 0.0	1.15 ± 0.28
7–15	1.2 ± 0.2	2.7 ± 0.1	0.8 ± 0.1	1.0 ± 0.0	2.2 ± 0.1	2.8 ± 0.1	1.66 ± 0.25
GHLO-infected (n = 5)							
0	2.8 ± 0.2	2.2 ± 0.5	0	0	0.4 ± 0.2	0.2 ± 0.2	0.41 ± 0.20
7–11	3.0 ± 0.0	2.4 ± 0.4	0	0	0	0	0.15 ± 0.06

NOTE. Values are means ± SEM for the corpus and antrum.

[a]Coded H&E-stained slides were scored for intensity of infection at 1000× using a scale of 0–3 (0, no bacteria; 1, colonies seen in 1–2 of 10 fields of view; 2, colonies seen in 3–8 of 10 fields; and 3, colonies seen in 9–10 of 10 fields).

[b]Homogenized biopsy specimens were cultured in microaerobic environment, and a score of 1 was given if colonies growing within 7 days were identified as *H. pylori* based on (1) pinhead-sized water-spray colonies positive for urease activity; (2) gram-negative curved or gull-wing rods therefrom; and (3) a kinetic assay showing high urease specific activity, in at least one culture from each rhesus monkey; otherwise, a score of 0 was given.

[c]Gastritis was rated independently from the scoring for infection on coded H&E slides using a scale of 0–3 (0, intact mucosal lining and essentially no infiltration of the lamina propria with lymphocytes and plasma cells; 1, mild increase of mononuclear infiltration, localized in upper half of the mucosa; 2, marked mononuclear infiltration extending from the surface to the muscularis mucosae; and 3, presence of polymorphonuclear leukocytes in glands, which was always associated with marked mononuclear infiltration and surface erosions).

[d]Plasma IgG levels were determined blindly using a modification of a previously described ELISA[29] using antimonkey IgG conjugates.

before treatment, and all 3 were negative for GHLO at 5 days. However, at 1 month, all 3 animals again had evidence for GHLO infection, which was present in an additional animal at 3 months. At 5 and 6 months, all 4 of these rhesus monkeys remained infected with GHLO, although each had been cleared of their *H. pylori* infection. Gastritis scores began to decrease 1 month after therapy; the score was ≤1.0 in all 4 rhesus monkeys in which *H. pylori* had been eradicated, whereas it returned to >2.0 in the 2 animals in which *H. pylori* infection relapsed (Figure 6). *H. pylori*–specific plasma IgG ratios decreased progressively after treatment in the animals in which infection had been eradicated, whereas it remained unchanged in the 2 animals in whom it was not eradicated (Figure 6). Thus, as in humans, both gastritis and specific immune response disappeared with eradication of *H. pylori.*

Discussion

The present data show that infections with *H. pylori* and GHLO were enzootic in our colony. As in humans,[33,34] attachment of *H. pylori* to surface epithelial cells appeared to involve specialized receptors and pedestal formation (Figure 3*A*), and *H. pylori* organisms were rarely observed inside superficial epithelial cells (Figure 3*B*). In contrast, GHLO did not appear to adhere to surface epithelial cells (Figure 4),[10] and they were never seen inside surface epithelial cells, although they were often observed inside parietal cells.[21] In addition, contrary to our earlier series[21] and similar to the observation in humans[10,35] and in rhesus monkeys,[36] we found that *H. pylori* and GHLO could coexist in the same stomach, because 3 rhesus monkeys were proven to be infected with both types of bacteria by histological analysis and culture of *H. pylori.* In these 3 animals, however, the infection score for GHLO was significantly less than in animals infected with this bacterium alone (1.0 in all three animals vs. 2.3 ± 0.2), suggesting antagonism between *H. pylori* and GHLO. However, it is worthwhile noting that the diagnosis of GHLO rests entirely on light and electron microscopic examination of gastric biopsy specimens, because this bacterium has not yet been cultured. It is interesting to note that Reed and Berridge considered that GHLO were commensal organisms.[36]

H. pylori infection, as in humans,[37] was always associated with gastritis in the population of rhesus monkeys studied; this relationship persisted when infected animals were studied longitudinally. In addition, gastritis scores decreased over time in the four animals in which treatment eradicated *H. pylori* (Figure 6), thus indicating that, as in humans, gastritis is induced by *H. pylori* in rhesus monkeys. In contrast, animals apparently infected with only GHLO had minimal gastritis or none at all, which remained stable for months; this observation was confirmed in animals with persistent or new GHLO infection after clearance of *H. pylori.* Finally, gastritis and plasma

Table 2. Response of *H. pylori*–and GHLO-Infected Animals to Ineffective Triple Therapy

	Infection score						
	H. pylori or GHLO (light microscopy)[a]		*H. pylori* (culture)[b]		Gastritis score[c]		
Time (*mo*)	Corpus	Antrum	Corpus	Antrum	Corpus	Antrum	*H. pylori* IgG ratio[d]
H. pylori–infected (n = 2)							
−1	2.0 ± 0.7	3.0 ± 0.0	1.0 ± 0.0	1.0 ± 0.0	3.0 ± 0.0	3.0 ± 0.0	2.75 ± 0.71
1	1.0 ± 0.7	2.5 ± 0.4	0.5 ± 0.5	1.0 ± 0.0	2.8 ± 0.2	3.0 ± 0.0	2.22 ± 0.26
3	1.5 ± 1.1	3.0 ± 0.0	0.5 ± 0.5	1.0 ± 0.0	2.0 ± 0.7	3.0 ± 0.0	3.25 ± 1.11
GHLO-infected (n = 4)							
−1	3.0 ± 0.0	1.0 ± 0.6	0	0	0	1.0 ± 0.5	0.60 ± 0.27
1	2.3 ± 0.7	0.3 ± 0.2	0	0	0.3 ± 0.2	1.0 ± 0.4	0.50 ± 0.28
3	3.0 ± 0.0	1.0 ± 0.6	0	0	0.5 ± 0.4	0.3 ± 0.2	0.79 ± 0.38

NOTE. Values are means ± SEM for the corpus and antrum. Rhesus monkeys were treated with oral amoxicillin plus metronidazole plus bismuth subsalicylate (7, 7, and 10 mg/kg, respectively, three times daily) diluted in Tang for 4 weeks. All other footnotes are exactly as in Table 1.

IgG increased in the animal that became infected with *H. pylori* during the observation period, and the route of infection is at present unclear. Transmission during the endoscopies is possible, although unlikely, because we have taken stringent precautions and have cleaned the videoendoscope with glutaraldehyde and alcohol, rinsing and brushing the biopsy channel. Alternatively, oral-fecal transmission may have occurred in the rhesus monkeys of our colony, because recent publications have indicated that *H. pylori* may be isolated for the stools of ferrets[38] and humans.[39]

The mechanism by which *H. pylori* may cause gastritis is at present unclear. One possible explanation for this inflammatory reaction is that ammonium ions produced by bacterial urease activity[40] have a toxic effect on the gastric superficial epithelial cells. However, we observed that there was no such damage in animals harboring only GHLO, which are strong urease producers, as reported by Heilmann and Borchard[11] and in the present paper. This observation indicates that although urease is probably an important virulence factor that permits survival of these organisms in the gastric acidic environment, it does not necessarily produce gastritis in rhesus monkeys. Another possible cause of gastritis is the *H. pylori* cytotoxin, which has been shown to cause vacuolization in Hela cells[41–44] and may be responsible for the formation of intracellular vacuoles in gastric surface epithelial cells, immediately under the site of adhesion of *H. pylori*.[33] This effect may also be pertinent to rhesus monkeys because similar vacuoles have been observed in this species (Figure 3) and because *H. pylori* isolates cultured from the biopsy specimens of our animals produced the vacuolating cytotoxin at levels similar to those shown for isolates obtained in humans (T. L. Cover and M. J. Blaser, unpublished observations).

Alternatively, gastritis may be caused by antigen-mediated immunopathologic events that characterize this infection.[45,46] The specific immune response may be used as a diagnostic tool because gastric infection with *H. pylori* in humans is accompanied by elevated plasma levels of IgG and IgA.[29] In our study, IgG serology using an antimonkey conjugate was an accurate way to diagnose *H. pylori* infection. The discordance in two rhesus monkeys between high serological and inflammation scores and the inability to identify infection with *H. pylori* indicates that, as in humans,[47] serology may be more accurate than biopsy because it effectively samples the entire stomach. Among the rhesus monkeys studied, there was a significant positive correlation between *H. pylori*–specific plasma IgG level and gastritis score, suggesting that such levels may reflect immunopathogenetic events. In addition, the *H. pylori*–specific plasma IgG persisted over time in animals remaining infected; increased in the rhesus monkey that acquired infection during the observation period; and decreased over a 6-month period after eradication of *H. pylori* after effective therapy. Similar to the observation in humans,[48] the *H. pylori*–specific IgG levels initially decreased even in animals which subsequently relapsed. These findings confirm our previous observation that *H. pylori* organism isolated from the stomach of rhesus monkeys are antigenically related to human *H. pylori*.[21] In addition, they indicate that a modified *H. pylori* IgG ELISA using an antimonkey conjugate may allow the diagnosis of *H. pylori* infection in nonhuman primates, because it appears to reflect mucosal infection with these bacteria. Taken together, these observa-

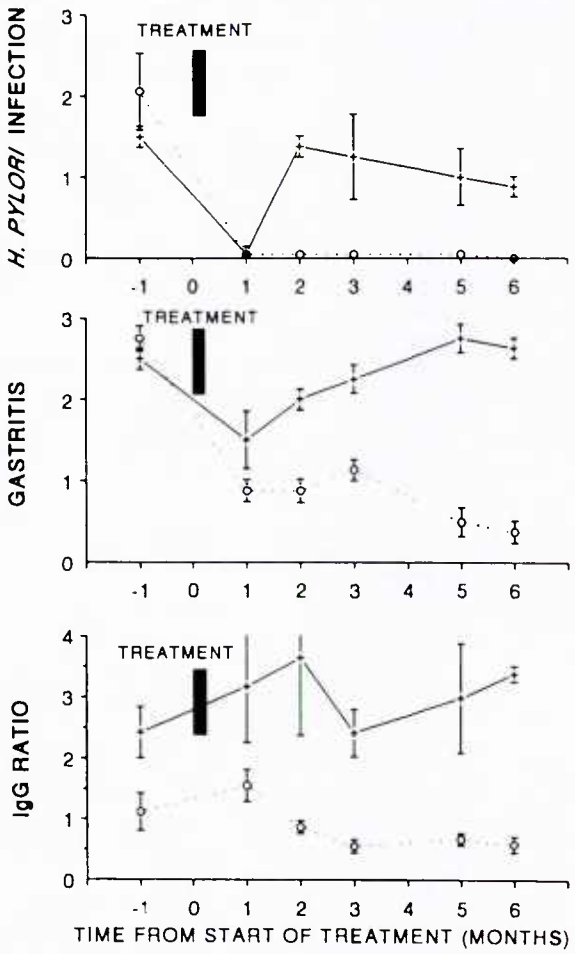

Figure 6. Effect of 10 days of intragastric administration of amoxicillin plus metronidazole plus bismuth subsalicylate (7, 7, and 10 mg/kg, respectively, diluted in distilled water, twice daily) on mean (±SEM) *H. pylori* infection scores, gastritis scores, and plasma IgG in two groups of *H. pylori*–infected rhesus monkeys. In four rhesus monkeys, infections were eradicated at 6 months (○); in two, infections relapsed before 6 months (+).

tions support the view that, as was shown in studies of humans,[47] measurement of plasma IgG levels against *H. pylori* may be superior to biopsy for evaluating the epizootiology of *H. pylori* infection in rhesus monkeys.

Among the 4 rhesus monkeys in which no infection with spiral bacteria was detected at the initial endoscopy, 1 animal had a gastritis score of 1.5 as well as an IgG ratio of 2.27; similarly high values persisted during the 4-month follow-up. Although gastric mucosal biopsy specimens from that animal remained negative for infection, these observations suggest that this rhesus monkey may have been chronically infected with *H. pylori*. Indeed, it is known that negative culture and histology do not exclude the presence of *H. pylori* in biopsy specimens from humans.[47]

Among the 9 GHLO-infected rhesus monkeys from which *H. pylori* could not be isolated, 8 animals had gastritis scores $\leq$ 1.5 and IgG ratio $<$ 0.5. The remaining animal had gastritis scores of 1.0 and a plasma IgG ratio of 1.33, which suggests that a focal infection with *H. pylori* could have been missed because of the prominent GHLO infection at the site of the biopsies. In addition, GHLO infection may have suppressed *H. pylori* growth and viability in culture, leaving mucosal gastritis and an elevated IgG ratio as the only indicator of its presence in that particular biopsy. In humans infected with *G. hominis*, active chronic gastritis was either absent[24] or at least less severe than with *H. pylori* infection.[10,13,49] Furthermore, in these patients, endoscopic biopsy specimens were the only method used to rule out the simultaneous presence of both *H. pylori* and *G. hominis*, and *H. pylori*–specific serum IgG values were not measured. Additional studies will be needed to clarify the interactions between these two bacteria in the gastric mucosa.

The triple-therapy regimen developed for use in humans[50,51] initially decreased the level of *H. pylori* and GHLO infection in rhesus monkeys, but oral dosing with dilution in Tang did not achieve eradication of these bacteria. In contrast, this same regimen given intragastrically achieved clearance of *H. pylori* (but not of GHLO) in all 6 rhesus monkeys at 1 month and in 4 of 6 monkeys up to 6 months after treatment. The relapse observed in 2 rhesus monkeys could be caused by the fact that, as in humans,[52] rapid reinfection or incomplete eradication of these bacteria occurred, possibly as a result of resistance to metronidazole.[53]

In conclusion, the present studies indicate that gastric mucosal infection with *H. pylori* is common in rhesus monkeys and that, as in humans, this infection is associated with the presence of gastritis. In addition, serology allows noninvasive diagnosis of infection and of the response to antimicrobial therapy. Infection with GHLO is common in rhesus monkeys, whereas it is infrequently recognized in humans; however, the role of these organisms in inflammation appears to be low. Thus, naturally occurring *H. pylori* infection in this model may permit greater understanding of the transmission and pathogenesis of infection as well as the development and evaluation of new therapies.

References

1. Marshall B. Unidentified curved bacilli on gastric epithelium in active chronic gastritis. Lancet 1983;1:1273–1275.
2. Blaser MJ. *Helicobacter pylori* and the pathogenesis of gastroduodenal inflammation. J Infect Dis 1990;161:626–633.
3. Marshall BJ, Goodwin CS, Warren JR, Murray R, Blincow ED, Blackbourn SJ, Phillips M, Waters TE, Sanderson CR. Prospective double-blind trial of duodenal ulcer relapse after eradication of *Campylobacter pylori*. Lancet 1988;2:1437–1442.
4. Parsonnet J, Friedman GD, Vandersteen DP, Chang Y, Vogelman

JH, Orentreich N, Sibley RK. *Helicobacter pylori* infection and the risk of gastric carcinoma. New Engl J Med 1991;325:1127–1131.
5. Nomura A, Stemmerman GN, Chyou PH, Kato I, Perez-Perez GI, Blaser MJ. *Helicobacter pylori* infection and gastric carcinoma in a population of Japanese-Americans in Hawaii. N Engl J Med 1991;325:1132–1136.
6. Isaacson PG, Spencer J. Is gastric lymphoma an infectious disease? Hum Pathology 1993;24:569–570.
7. Rauws EAJ. Detecting *Campylobacter pylori* with the ^{13}C- and ^{14}C-urea breath test. Scand J Gastroenterol 1989;24(Suppl 160): 25–26.
8. Booth L, Holdstock G, MacBride H, Hawtin P, Gibson JR, Ireland A, 8amforth J, Du8oulay CE, Lloyd RS, Pearson AD. Clinical importance of *Campylobacter pyloridis* and associated serum IgG and IgA antibody responses in patients undergoing upper gastrointestinal endoscopy. J Clin Pathol 1986;39:215–219.
9. Salomon H, Ueber das Spirillum des Säugetiermagens und sein Verhalten zu den Belegzellen. Int J Med Microbiol 1896;19:433–442.
10. McNulty CAM, Dent JC, Curry A, Uff JS, Ford GA, Gear MWL, Wilkinson SP. New spiral bacterium in gastric mucosa. J Clin Pathol 1989;42:585–591.
11. Heilman KL, 8orchard F. Gastritis due to spiral shaped bacteria other than *Helicobacter pylori:* clinical, histological and ultrastructural findings. Gut 1991;32:137–140.
12. Logan RPH, Karim QN, Polson RJ, Walker MM, Baron JH. *Gastrospirillum hominis* infection of the stomach (letter). Lancet 1989;2:672.
13. Morris A, Ali MR, Thomsen L, Hollis B. Tightly spiral shaped bacteria in the human stomach: another cause of active chronic gastritis? Gut 1990;31:134–138.
14. Solnick JV, O'Rourke J, Lee A, Paster BJ, Dewhirst FE, Tompkins LS. An uncultured gastric spiral organism is a newly identified *Helicobacter* in humans. J Infect Dis 1993;168:379–383.
15. Lee A, O'Rourke J. Gastric bacteria other than *Helicobacter pylori*. Gastroenterol Clin North Am 1993;22:21–42.
16. Fox JG, Cabot E8, Taylor NS, Laraway R. Gastric colonization by *Campylobacter pylori* subsp. *mustelae* in ferrets. Infect Immun 1988;56:2994–2996.
17. Lee A, Hazell SL, O'Rourke J, Kouprach SJ. Isolation of a spiral-shaped bacterium from the cat stomach. Infect Immun 1988;56:2843–2850.
18. Eaton KA, Dewhirst FE, Radin MJ, Fox JG, Paster BJ, Krakowka S, Morgan DR. *Helicobacter acinonyx* sp. *nov.,* isolated from cheetahs with gastritis. Int J Syst 8acteriol 1993;43:99–106.
19. Curry A, Jones DM, Eldridge J. Spiral organisms in the baboon stomach. Lancet 1987;2:634–635.
20. 8rondson MA, Schoenknecht FD. *Campylobacter pylori* isolated from the stomachg of the monkey *Maca nemestrina.* J Clin Microbiol 1988;26:1725–1728.
21. Dubois A, Tarnawski A, Newell DG, Fiala N, Dabros W, Stachura J, Krivan H, Heman-Ackah LM. Gastric injury and invasion of parietal cells by spiral bacteria in rhesus monkeys. Are gastritis and hyperchlorhydria infectious diseases? Gastroenterology 1991; 100:884–891.
22. 8ronsdon MA, Goodwin CS, Sly LI, Chilvers T, Schoenknecht FD. *Helicobacter nemestrinae* sp. *nov.,* a spiral bacterium found in the stomach of a pigtailed macaque (*Macaca nemestrina*). Int J Syst 8acteriol 1991;41:148–153.
23. Ho S-A, Hoyle JA, Lewis FA, Secker AD, Cross D, Mapstone MP, Dixon MF, Wyatt JI, Tomkins DS, Taylor GR, Quirke P. Direct polymerase chain reaction test for detection of *Helicobacter pylori* in humans and animals. J Clin Microbiol 1991;29:2543–2549.
23a. Drazek ES, Dubois A, Holmes RK. Characterization of *Helicobacter pylori* isolates from rhesus monkeys. Abstracts of the 94th general meeting of the American Society for Microbiology. Las Vegas, Nevada, May 23–27, 1994:D262.
24. Fox JG, Lee A. Gastric *Campylobacter*-like organisms: their role in gastric disease of laboratory animals. Lab Anim Sci 1989;39:543–553.
25. Tarnawski A, Hollander D, Cummings D, Krause WJ, Stachura J, Zipser RD, Gergely H. Does sucralfate affect the normal gastric mucosa? Histologic, ultrastructural and functional assessment in the rat. Gastroenterology 1986;90:893–905.
26. Ruiz-Herrera J, Gonzalez J. A continuous method for the measurement of urease activity. Anal Biochem 1969;31:366–374.
27. Dunn BE, Campbell GP, Perez-Perez GI, Blaser MJ. Purification and characterization of *Helicobacter pylori* urease. J Biol Chem 1990;265:9464–9469.
28. Marshall BJ, Warren JR. Unidentified curved bacilli in the stomach of patients with gastritis and peptic ulceration. Lancet 1984;1:1311–1315.
29. Perez-Perez GI, Dworkin BM, Chodos JE, Blaser MJ. *Campylobacter pylori* antibodies in humans. Ann Intern Med 1988; 109:11–17.
30. Drumm B, Perez-Perez GI, Blaser MJ, Sherman PM. Intrafamilial clustering of *Helicobacter* pylori infection. New Engl J Med 1990;322:359–363.
31. Winer BJ. Statistical principles in experimental design. 2nd ed. New York: McGraw-Hill, 1971.
32. Mobley HLT, Cortesia Mi, Rosenthal LE, Jones BD. Characterization of urease from *Campylobacter pylori.* J Clin Microbiol 1988;26:831–836.
33. Hessey SJ, Spencer J, Wyatt JI, Sobala G, Rathbone BJ, Axon ATR, Dixon MF. 8acterial adhesion and disease activity in *Helicobacter*-associated chronic gastritis. Gut 1990;31:134–138.
34. Wyle FA, Tarnawski A, Schulman D, Dabros W. Evidence for gastric mucosal cell invasion by *C. pylori:* an ultrastructural study. J Clin Gastroenterol 12(Suppl 1):S92–S98.
35. Querioz DMM, Cabral MMDA, Nogueira AMMF, 8arbosa AJA, Rocha GA, Mendes EN. Mixed gastric infection by *Gastrospirillum hominis* and *Helicobacter pylori.* Lancet 1990;336:507–508.
36. Reed KD, Berridge BR. *Campylobacter*-like organisms in the gastric mucosa of rhesus monkeys. Lab Anim Sci 1988;38:329–331.
37. Bayerdörffer E, Oertel H, Lehn N, Kasper G, Mannes GA, Sauerbruch T, Stolte M. Topographic association between active gastritis and *Campylobacter pylori* colonization. J Clin Pathol 1989; 42:834–839.
38. Fox JG, Blanco MC, Yan L, Shames B, Polidoro D, Dewhirst FE, Paster 8J. Role of gastric pH in isolation of *Helicobacter mustelae* from the feces of ferrets. Gastroenterology 1993;104:86–92.
39. Thomas JE, Gibson GR, Darboe MK, Dale A, Weaver LT. Isolation of *H. pylori* from human faeces. Lancet 1992;340:1194–1195.
40. Evans DJ, Evans DG, Kirkpatrick SS, Graham DY. Characterization of the *Helicobacter pylori* urease and purification of its subunits. Microb Pathog 1991;10:15–26.
41. Figura N, Guglielmetti P, Rossolini A, 8arberi A, Cusi G, Musmanno RA, Russi M, Quaranta S. Cytotoxin production by *Campylobacter pylori* strains isolated from patients with chronic gastritis only. J Clin Microbiol 1989;27:225–226.
42. Cover TL, Dooley CP, Blaser MJ. Characterization of and human serologic response to proteins in *Helicobacter pylori* broth culture supernatants with vacuolizing cytotoxin activity. Infect Immun 1990;58:603–610.
43. Cover TL, Puryear W, Perez-Perez GI, Blaser MJ. Effect of urease on HeLa cell vacuolation induced by *Helicobacter pylori* cytotoxin. Infect Immun 1991;59:1264–1270.
44. Cover IT, Blaser MJ. Purification and characterization of the vacuolating toxin from *Helicobacter pylori.* J Biol Chem 1992;267: 10570–10575.
45. Ernst PB, Pecquet S. Interactions between *Helicobacter pylori*

and the local mucosal immune system. Scand J Gastroenterol 1991;26(Suppl 187):56–64.

46. Uibo R, Salupere V, Krohn K. Autoimmune reactions to gastric mucosa in chronic gastritis: a review. Scand J Gastroenterol 1991;26(Suppl 186):11–15.
47. Strauss RM, Wang TC, Kelsey PB, Compton CC, Ferraro MJ, Perez-Perez G, Parsonnet J, Blaser MJ. Association of *Helicobacter pylori* infection with dyspeptic symptoms in patients undergoing gastroduodenoscopy. Am J Med 1990;89:464–469.
48. Kosunen TU, Seppala K, Sarna S, Sipponen P. Diagnostic value of decreasing IgG, IgA, and IgM antibody titres after eradication of *Helicobacter pylori*. Lancet 1992;339:893–895.
49. Fléjou JF, Diomandé I, Molas G, Goldfain D, Rotenberg A, Florent M, Potet F. Human chronic gastritis with non–*Helicobacter pylori* spiral organisms (*Gastrospirillum hominis*): four cases and review of the literature. Gastroenterol Clin Biol 1990;14:806–810.
50. Humphreys H, Bourke S, Dooley C, McKenna D, Power B, Keane CT, Sweeney EC, O'Morain C. Effect of treatment on *Campylobacter pylori* in peptic disease: a randomized prospective trial. Gut 1988;29:279–283.
51. Hirschl AM, Hentschel E, Schütze K, Nemec H, Potzi R, Gangl A, Weiss W, Pletschette M, Stanek G, Rotter ML. The efficacy of antimicrobial treatment in *Campylobacter pylori*–associated gastritis and duodenal ulcer. Scand J Gastroenterol 1988;23(Suppl 142):76–81.
52. Hui WM, Ho J, Lam SK. Persistence of *Campylobacter pylori* (CP) during remission and subsequent relapse in duodenal ulcer (DU) (abstr). Gastroenterology 1988;94:A196.
53. Rautelin H, Seppala K, Renkonen OV, Vainio U, Kosunen TU. Role of metronidazole resistance in therapy of *Helicobacter-pylori* infections. Antimicrob Agents Chemother 1992;36:163–166.

Received February 1, 1993. Accepted January 10, 1994.

Address requests for reprints to: Andre Dubois, M.D., Ph.D., Department of Medicine, Uniformed Services University, 4301 Jones Bridge Road, Bethesda, Maryland 20814-4799.

Supported in part by American Registry of Pathology Grant UBFW (to W.N.F.).

The experiments reported in this study were conducted according to the principles set forth in the *Guide for the Care and Use of Laboratory Animals*, Institute of Laboratory Animal Resources, National Research Council, HHS/NIH publication no. 85-23.

The opinions and assertions contained herein are the private ones of the authors and are not to be construed as official or reflecting the views of the Department of Defense, the Uniformed Services University of the Health Sciences, or the Defense Nuclear Agency.

JOURNAL OF CELLULAR PHYSIOLOGY 159:573–581 (1994)

Characterization of Regulatory Volume Decrease in the THP-1 and HL-60 Human Myelocytic Cell Lines

ELAINE K. GALLIN,* TONI M. MASON, AND ARIE MORAN
Department of Physiology, Armed Forces Radiobiology Research Institute, Bethesda, Maryland 20889-5603 (E.K.G., T.M.); Department of Physiology, Faculty of Health Sciences, University of Negev, Beer Sheva, Israel 84105 (A.M.)

Exposure to hypotonic stress produces a transient increase in cell volume followed by a regulatory volume decrease (RVD) in both THP-1 and HL-60 cells. In contrast, cells exposed to hypotonic stress in a high K/low Na Hanks' solution not only failed to volume regulate, but displayed a secondary swelling. Thus, while an outward K gradient was required for RVD, the secondary swelling indicated that hypotonic stress increased permeability in the absence of a negative membrane potential. The K channel blocker quinine (1–4 mM) blocked RVD in both cell types. Gramicidin's ability to overcome the quinine block of RVD indicated that RVD is mediated by a quinine-sensitive cation transport mechanism that is independent of the swelling-induced anion transport mechanism. Barium (1–4 mM), another K channel blocker, slowed the rate of RVD, while 4-aminopyridine, charybdotoxin, tetraethylammonium chloride, tetrabutylammonium chloride, and gadolinium had no effect on RVD. Furthermore, RVD was not mediated by calcium-activated conductances, since it occurred normally in Ca-free medium, in medium containing cadmium, and in BAPTA-loaded cells. Gramicidin produced little or no volume change in isotonic medium, suggesting that basal Cl permeability of both THP-1 and HL-60 cells is low. However, swelling induced an anion efflux pathway that is permeable to both chloride and bromide, but is impermeable to methanesulfonate and glutamate. The anion channel blocker 3,5-diiodosalicylic acid (DISA) antagonized RVD in both cell types. In conclusion, RVD in THP-1 and HL-60 cells is mediated by independent anion and cation transport mechanisms that involve both a DISA-sensitive anion pathway and a quinine-inhibitable K efflux pathway, neither of which requires increases in intracellular calcium to be activated. ©1994 Wiley-Liss, Inc.**

The presence of impermeable intracellular charged particles results in a tendency for all cells to swell. Animal cells counterbalance this tendency by extruding ions through either conductive pathways or coupled transporters (for review, Sarkadi and Parker, 1991). Volume regulation also occurs when cells, such as kidney epithelial cells, are exposed to anisotonic environments (Lewis and Donaldson, 1990). The pathways involved in homeostatic volume regulation have been extensively studied in vitro by placing cells in anisotonic medium. Exposure to hypotonic medium produces a rapid swelling followed by a volume decrease referred to as a regulatory volume decrease (RVD) in many cell types. In some cells, including erythrocytes, RVD is associated with an increase in the activity of electroneutral transporter(s) (Sarkadi and Parker, 1991), while in other cells, such as lymphocytes, K and Cl conductive pathways underlie RVD (Grinstein and Foskett, 1990).

While volume regulatory responses in lymphocytes and erythrocytes have been well characterized, only two studies have examined RVD in cells of the macrophage lineage (monocytes, macrophages, or promonocytic cells). Novak et al. (1988) demonstrated that, in rabbit alveolar macrophages, RVD depends on the K gradient and is due to a ouabain-insensitive loss of K and Cl, which precedes the swelling-induced changes in surface receptor numbers associated with inhibition of receptor-mediated endocytosis. In the promyelocytic cell line HL-60, RVD is associated with a change in actin polymerization, but the shift in actin polymerization is not required for the transduction of the volume regulatory signal (Hallows et al., 1992). While these two studies demonstrated that myeloid cells, like lymphocytes, exhibit RVD, the ionic mechanisms underlying RVD were not investigated.

It is possible that one or more of the K and Cl conductances, which have been characterized in primary cells of the monocytic-macrophage lineage or in macrophage-like cell lines using electrophysiological tech-

Received August 2, 1993; accepted January 4, 1994.

*To whom reprint requests/correspondence should be addressed.

niques (for review see Gallin, 1991), mediate RVD in these cells. As a first step towards exploring this possibility, this study investigated RVD in two human leukemic cell lines; HL-60 cells, which can be induced to differentiate into either macrophage-like cells or neutrophil-like cells, and THP-1 cells, monocytic-like cells that can be differentiated into mature macrophages (Auwerx, 1991). We demonstrate that while RVD in both these cell lines involves the activation of independent cation and anion permeability pathways, the calcium-activated conductances described in macrophages are unlikely to mediate RVD. Furthermore, the cation permeability pathway activated in these two cell lines has a different sensitivity to pharmacological agents than the n-type K channel that mediates RVD in lymphocytes (Grinstein and Foskett, 1990; Deutsch and Lee, 1988).

MATERIALS AND METHODS

Cells

HL-60 cells and THP-1 cells were obtained from American Type Culture Collection (Rockville, MD). HL-60 cells and THP-1 cells were maintained in RPM1-1640 supplemented with 10% fetal bovine serum (FBS; HyClone Laboratories, Logan, UT), penicillin (20 units/ml), streptomycin (20 ng/ml), and glutamine (0.3%). Cells were grown in a 5% CO_2-air incubator at 37°C and split 3:1 twice a week. Cells were maintained for approximately 3 months, at which time new frozen stocks were thawed.

Volume measurements

Volume measurements were carried out electronically using a model ZM Coulter Counter equipped with a 100 μm diameter orifice. The counter was coupled to an IBM compatible personal computer equipped with a Series II Personal Computer Analyzer card (PCAII; Nucleus Inc., Oak Ridge, TN). The PCAII card sorted incoming digitized signals into channels binned to provide histograms in which the channel number was proportional to cell volume. Median cell volume was computed from histograms of approximately 10,000 cells. Polystyrene beads 9–15 μm in diameter (Coulter) in solutions with the same tonicity were used to calibrate the instrument.

Cells were resuspended at approximately 10^6 cells/ml in NaCl Hanks' solution containing 10 mM glucose and 0.5% bovine serum albumin (BSA; normal Hanks') and used for volume analysis within 30 minutes. Volume measurements were performed at room temperature (21–23°C) with control cell volume determined in normal Hanks'. RVD was assessed following dilution with 41% water (0.59× Hanks'). This degree of osmotic stress was chosen because it produced a significant swelling and regulatory response without affecting cell viability. Volume changes were measured over a 30-minute time period and are expressed relative to control cell volume. For later time points where volume changed more slowly, an averaged volume was determined from two to three separate measurements taken over 30 seconds.

Cell viability

Cell viability was assessed with a fluorescent microscope using ethidium bromide and acridine orange. Exposure to 41% hypotonic medium for 30 minutes produced no significant change in cell viability. Addition of quinine (4 mM) in either isotonic or hypotonic medium had no effect on the number of viable cells.

Solutions

Normal Hanks' referred to as Hanks' contained in mM: 150 NaCl, 1.2 $MgCl_2$, 1.6 $CaCl_2$, 4.6 KCl, 10 HEPES, 10 glucose, and 0.5% BSA, titrated with NaOH to pH 7.3. KCl Hanks' contained in mM: 150 KCl, 1.6 $MgCl_2$, 1.2 $CaCl_2$, 5 NaCl, 10 HEPES, 10 glucose, 0.5% BSA, titrated with KOH to pH 7.3. Low sodium Hanks' was made either with N-methylglucamine chloride (NMDGCl) or tetramethylammonium chloride (TMACl) to replace all but 4 mM NaCl. For studies in which anion selectivity was examined, 150 mM chloride was replaced by other anions. For example, Kmethanesulfonate Hanks' contained in mM 150 Kmethanesulfonate, 4.6 KCl, 1.6 $CaCl_2$, 1.2 $MgCl_2$, 10 HEPES, 10 glucose, and 0.5% BSA.

Calcium measurements

Cells were loaded with fura in normal Hanks' containing 2.5 μM fura-2-AM and 0.2 mg/ml of pluronic acid with or without 15 μM BAPTA-AM for 1 hour at room temperature. Cells were centrifuged, and loading medium was replaced with normal Hanks'. Following a 15-minute incubation at room temperature fluorescence ratios (excitation 340 and 380; emission 510) were measured at room temperature using an SLM spectrofluorimeter. After obtaining baseline fluorescence measurements, 41% water was added (3 ml for final cuvette volume) and fluorescence changes were monitored for 5–10 minutes. Calibration was accomplished for each cuvette by adding 15 μl of 10% Triton-X 100 to the cuvette to obtain Fmax, followed by the addition of 50 μl of 0.75 M EGTA/TRIS, pH 8, to obtain Fmin. Complete hydrolysis of the fura-AM was confirmed by comparing the fluorescence ratio at 340/380 of lysed fura-loaded cells in high calcium to the fluorescence ratio of free fura recorded under the same conditions. Intracellular calcium ([Ca]i) was estimated as described by Grynkiewicz et al. (1985) using a Kd of 135 nM for fura measured in 100 mM KCl, pH 7.2, at 20°C.

Chemicals

Gramicidin, 4-acetamido-4′-isothiocyanostilbene-2,2′-disulfonic acid (SITS), 3,5-diiodosalicylic acid (DISA), ouabain, quinine, and tetrabutylammonium chloride (TBACl) were obtained from Sigma (St. Louis, MO), tetraethylammonium chloride from Aldrich (Milwaukee, WI), and charybdotoxin (CTX) from Latoxan (Rosans, France). Gramicidin and DISA were made up as concentrated stocks (100X) in dimethylsulfoxide (DMSO). CTX was made up in Hanks' containing 0.5% BSA and stored in glass vials. CTX's activity was confirmed by demonstrating that it blocked an ionomycin-stimulated K efflux from guinea pig epithelium (Dr. Pamela Gunter-Smith, personal communication). Fura-2-AM, pluronic acid, and BAPTA-AM were obtained from Molecular Probes (Eugene, OR) and made up as 1 mM stock solutions in DMSO.

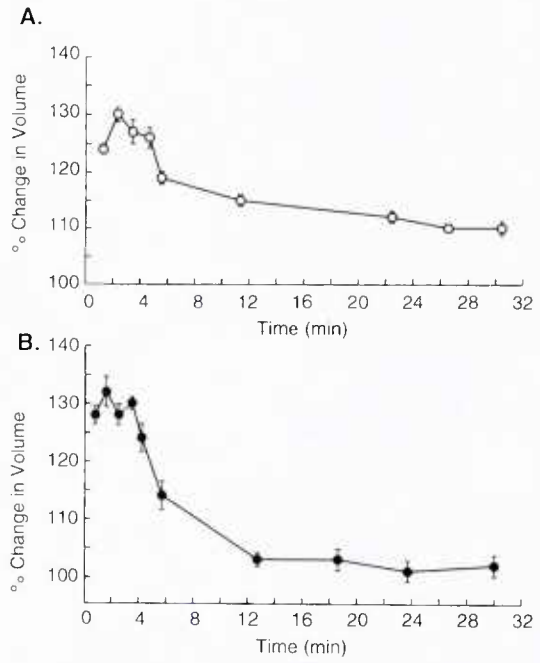

Fig. 1. Time course of regulatory volume changes in **(A)** HL-60 cells and **(B)** THP-1 cells following addition of 41% water at time 0. For this figure and other figures, data are expressed as the percentage volume change compared to control cell volume determined at the beginning of the experiment. Averaged data from three separate runs are shown for each cell type.

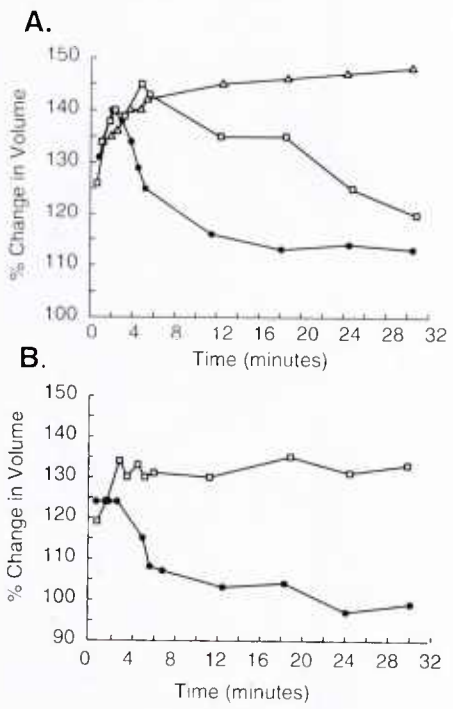

Fig. 2. Effect of quinine on RVD in **(A)** HL-60 cells and **(B)** THP-1 cells. Time course of volume responses of cells in 0.59× NaCl Hanks' (●) and cells in 0.59× NaCl Hanks' containing either 1 mM (□) or 4 mM (△) quinine. For this figure and subsequent figures, each time course is a representative run from a single cuvette of cells (three to four individual time courses were obtained for each experimental condition).

Statistics

All data are expressed as mean ± standard error of mean.

RESULTS

RVD occurs in both THP-1 and HL-60 cells

HL-60 and THP-1 cell populations exhibit unimodal volume distributions under isosmotic and hypotonic conditions. Their mean peak volume under isosmotic conditions was 970 ± 4.1 fL and 580 ± 2.4 fL for THP-1 cells and HL-60 cells, respectively. As reported previously by Hallows et al. (1991), HL-60 cells exhibit a transient swelling followed by a decrease in volume when exposed to hypotonic solution (Fig. 1A). A similar RVD response is also present in the THP-1 cell line following exposure to 0.59× Hanks' (Fig. 1B). Peak swelling occurred between 2 and 4 minutes in both cell types, reaching 125–145% of control cell volume in 0.59× solutions. Cell volume returned to within 10% of control levels within 30 minutes at 21–23°C. RVD was characterized by an initial rapid decrease followed by a slower change in volume. The initial rate of RVD measured during the first 5–6 minutes was −3.31%/min ± 0.12 (n = 17) and − 5.48%/min ± 0.7 (n = 11) for THP-1 and HL-60 cells, respectively.

Role of cation permeability

Potassium channel blockers. Since K conductances have been implicated in RVD responses of other cells (Grinstein and Foskett, 1990; Okada and Hazama, 1989), the effects of several different K channel blockers were tested on HL-60 and THP-1 cells exposed to 0.59× Hanks. In HL-60 cells 1 mM quinine slowed but did not completely block RVD; cell volume at 30 minutes was 120% ± 4.9 (n = 7) of initial control volume compared to a 30-minute volume of 107% ± 3.6 for control measurements in the absence of 1 mM quinine (Fig. 2A). Increasing the quinine concentration to 4 mM blocked RVD completely in HL-60 cells (peak volume vs. 30-minute volume was 142% ± 3.9 vs 139 ± 5.6, n = 3). In contrast, in THP-1 cells, 1 mM quinine completely blocked RVD (volume at 30 minutes was 131% ± 2 of initial control volume, n = 4; Fig. 2B).

Since in some cell types quinine has been reported to affect Cl conductances as well as K conductances (Gogelein and Capek, 1990), experiments were performed using both the cation pore former gramicidin and the K transporter valinomycin to determine whether quinine's block of RVD was due to a block of a cation permeability. Cell volume was monitored in hypotonically stressed cells bathed in medium that contained quinine to which gramicidin was added. Gramicidin, which forms channels permeable to K and Na, enables cells to volume regulate in the presence of a K channel blocker, as long as their anion permeability is unaffected by the K channel blocker. In 0.59× Hanks' containing quinine, addition of gramicidin to THP-1 cells produced a secondary swelling presumably due to the Na influx through gramicidin channels. In contrast, HL-60 cells exposed to gramicidin in 0.59× Hanks' plus

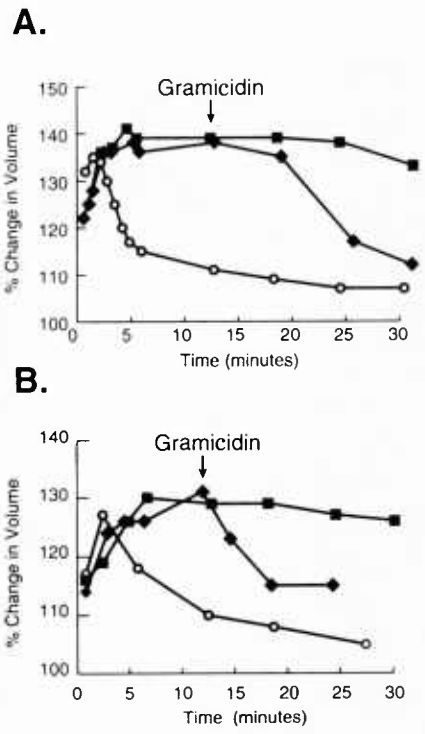

Fig. 3. Gramicidin induces RVD in the presence of 4 mM quinine. Time course of representative volume responses from (A) HL-60 cells in 0.59× NMDG Hanks' and (B) THP-1 cells in 0.59× TMA-Hanks'. Cells in (○) 0.59× Hanks'; (■) 0.59× Hanks + 4 mM quinine; and (◆) 0.59× Hanks' + 4 mM quinine + 1 μM gramicidin added at time indicated by the arrows.

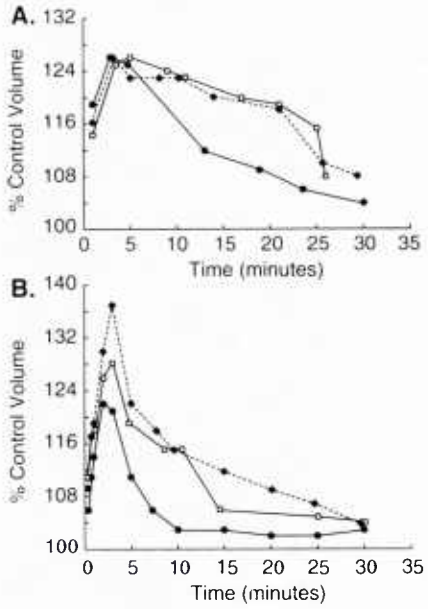

Fig. 4. Effect of barium on RVD response of (A) HL-60 cells and (B) THP-1 cells. Time course of representative volume responses of cells in 0.59× NaCl Hanks' (●), 0.59× NaCl Hanks' containing either 1 (□) or 4 mM BaCl (◆).

TABLE 1. Ability of agents to block RVD

Agent[1]	Concentration	Block[2] HL-60	Block[2] THP-1
Quinine	0.5–1 mM	++	++
Barium	2–4 mM	+	+
4-AP	5 mM	—	—
TEA	10 mM	—	—
TBA	10 mM	—	—
CTX	25 nM	—	—
Cadmium	1 mM	—	—
DISA	0.2 mM	++	++
SITS[3]	0.5–1 mM	+	+
Ouabain	1 mM	—	—
Gadolinium	10–100 μM	—	—

[1]Agents were added immediately before cells were exposed to 0.59X Hanks' and volume was monitored for the next 30 minutes.
[2]++, complete block; +, partial block.
[3]Cells were incubated in SITS for 30 minutes prior to hypotonic stress.

quinine exhibited an RVD response, suggesting that under these conditions the relative electrochemical gradients for K and Na in these two cell types is different. Therefore, to minimize gramicidin-induced influx of Na, experiments on both HL-60 and THP-1 cells were performed in either low Na-NMDGCl Hanks' or low Na-TMA Hanks'. Under these conditions, both HL-60 cells (Fig. 3A) and THP-1 cells (Fig. 3B) exhibit RVD in 0.59× low Na-Hanks' which was blocked by quinine and restored by gramicidin (1 μM) despite the presence of quinine. Similar experiments also were done using the mobile K carrier valinomycin (1 μM) to restore RVD repsonses in quinine-containing Na Hanks'. While the results of these experiments were qualitatively similar to those done using gramicidin in Na-free Hanks', valinomycin was less effective at restoring the quinine-inhibited RVD than gramicidin. The difference in effectiveness between gramicidin and valinomycin probably reflects the fact that the rate of cation flux induced by gramacidin (a channel-forming ionophore) will be considerably greater than that produced by valinomycin (a mobile carrier).

The divalent cation, barium blocks partially or completely several K conductances, including the voltage-gated inwardly rectifying K conductance and the calcium-activated inwardly rectifying K conductance present in macrophages (Gallin, 1991). In HL-60 cells, RVD was slowed, but not blocked by barium (1 mM). Increasing the barium concentration from 1 to 4 mM did not result in further inhibition of RVD (Fig. 4A), while decreasing the barium concentration to 0.5 mM produced a smaller inhibition of the RVD response (data not shown). In THP-1 cells, 4 mM barium was required to significantly slow RVD (Fig. 4B). The K channel blockers, CTX (25 nM), TEACl (10 mM), TBACl (10 mM), and 4-AP (5 mM) had little or no effect on RVD in either cell type (Table 1).

Is the K gradient required for RVD? To determine if the K gradient is required for RVD, both THP-1 and HL-60 cells were placed in a 0.59× KCl Hanks' and cell volume was monitored. Neither cell type exhibited RVD in 0.59× KCl Hanks'. Furthermore, 0.59× KCl Hanks' produced a secondary swelling in both cell types. This is evident in Figure 5 in which representative responses of THP-1 and HL-60 cells to 0.59× KCl

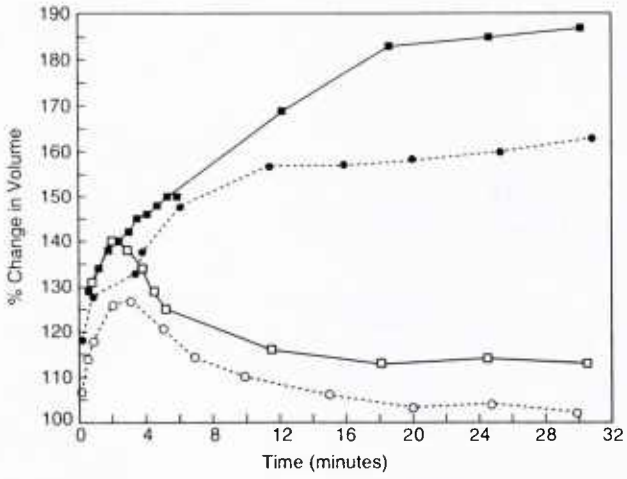

Fig. 5. Comparison of time course of representative volume responses of HL-60 cells (□) and THP-1 cells (○) in 0.59× KCl Hanks' (filled symbols) and 0.59× NaCl Hanks' (open symbols).

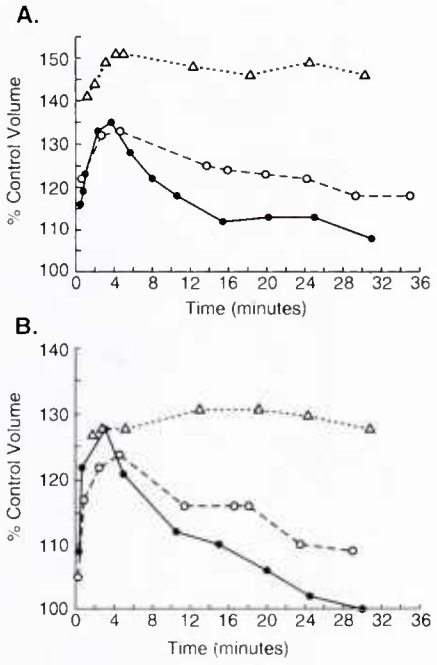

Fig. 6. Time course of representative volume responses of (A) HL-60 cells and (B) THP-1 cells in 0.59× NACl Hanks' (●), 0.59× NaCl Hanks' containing either 1 mM SITS (○) or 0.2 mM DISA (△).

Hanks' are depicted along with RVD responses in 0.59× NaCl Hanks'. The secondary swelling response for HL-60 cells was considerably greater (188% ± 2.1 at 30 minutes [n = 5]) than that for THP-1 cells (159% ± 1.7 at 30 minutes [n = 7]). To determine if the diminished secondary swelling in THP-1 cells compared to HL-60 cells reflects lower cation permeability in THP-1 cells compared to HL-60 cells, gramicidin was added to the bath 10-12 minutes after the hypotonic stress and volume were monitored. Gramicidin had little or no effect on the final volume of THP-1 cells after 30 minutes in 0.59× KCl Hanks' (gramicidin-treated volume was 159%, n = 4), suggesting that the anion permeability or gradient of THP-1 cells accounted for the difference in the magnitude of the secondary swelling.

Anion permeability

Gramicidin produced little or no change in the mean volume of THP-1 or HL-60 cells bathed in isotonic Hanks', indicating that the basal Cl permeability of THP-1 and HL-60 cells is low. In contrast, Cl permeability increased in response to hypotonic stress since, as noted above (Fig. 3) the addition of gramicidin induced RVD when HL-60 and THP-1 cells were bathed in 0.59× Hanks' plus quinine. Furthermore, gramicidin's ability to overcome the quinine-induced block of RVD indicates that the swelling-induced anion and cation permeabilities are independent.

Anion channel blockers. RVD was blocked in both cell types by the anion channel blocker DISA, which has been shown to block RVD in neutrophils (Stoddard et al., 1993). In 0.59× Hanks' the 30-minute volume in DISA-treated cells (0.2 mM) was 136 ± 10 (N = 3) and 136 ± 8 (n = 3) in HL-60 cells and THP-1 cells, respectively. The DISA-induced block of RVD could not be overcome by addition of gramicidin (1 μM). In contrast, SITS (0.5–1 mM) produced only a partial block in THP-1 cells (112% ± 3 of control volume at 30 minutes) and in HL-60 cells (114% ± 4 of control volume at 30 minutes), even when cells were preincubated with 1 mM SITS for 30 minutes before exposure to hypotonic medium (Fig. 6).

Anion selectivity. As noted earlier (Fig. 5), HL-60 cells in 0.59× KCl Hanks' failed to volume regulate and showed a secondary volume increase which was presumably due to an influx of both K and Cl. In order to investigate the selectivity of the anion efflux pathway, the magnitude of the secondary volume increase was monitored in HL-60 cells bathed in 0.59× high K Hanks' containing different anions. As shown in Figure 7, bathing HL-60 cells in Kmethanesulfonate Hanks' or Kglutamate Hanks' abolished the secondary volume increase evident in 0.59× KCl Hanks'. In contrast, cells in Kbromide Hanks' displayed a secondary volume increase similar to that of the cells in KCl Hanks'. Thus, the volume-induced anion efflux mechanism is permeable to both Cl and Br and is impermeable to methanesulfonate and glutamate.

Role of calcium

To determine if a calcium influx was required for the RVD response, volume was monitored in THP-1 and HL-60 cells exposed to 0.59× Hanks' which contained 1.0 mM EGTA and no calcium. RVD occurred normally in both cell types in this solution. Furthermore, cadmium (1 mM), a calcium channel antagonist in other cells, had no effect on RVD in either cell type (Fig. 8).

Despite the absence of a requirement for calcium influx during RVD, it is possible that swelling causes release of [Ca]i stores that in turn can activate calcium-gated channels. To explore this possibility, THP-1 and HL-60 cells were loaded with either fura, or with

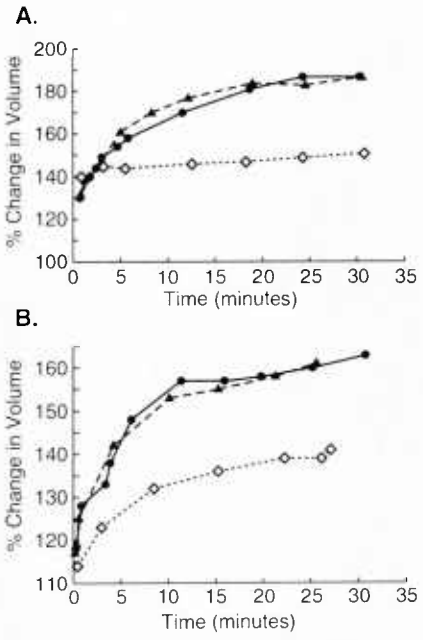

Fig. 7. Time course of representative volume responses of (A) HL-60 cells and (B) THP-1 cells in 0.59× KCl Hanks' (●), 0.59× KBr Hanks' (▲), and in 0.59× Kmethanesulfonate Hanks' (◇).

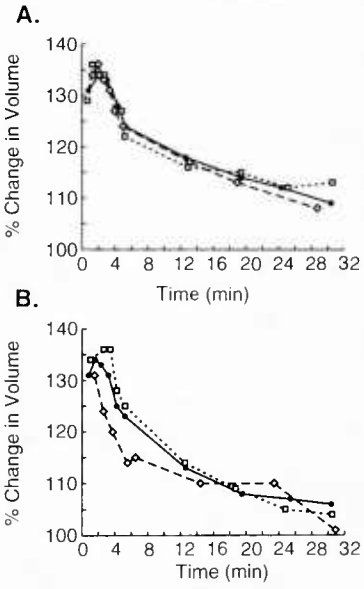

Fig. 8. Time course of representative volume responses of (A) HL-60 cells and (B) THP-1 cells in 0.59× NaCl Hanks' (●), 0.59× NaCl Hanks' containing either 0 calcium/1 mM EGTA (□) or 1 mM CdCl (◇).

BAPTA and fura, and both [Ca]i changes and cell volume were monitored during hypotonic stress. Since volume measurements were performed at room temperature, [Ca]i measurements also were carried out at room temperature. As shown in Figure 9, swelling induced increases in [Ca]i in both THP-1 and HL-60 cells, although the response of THP-1 cells was quite small; the

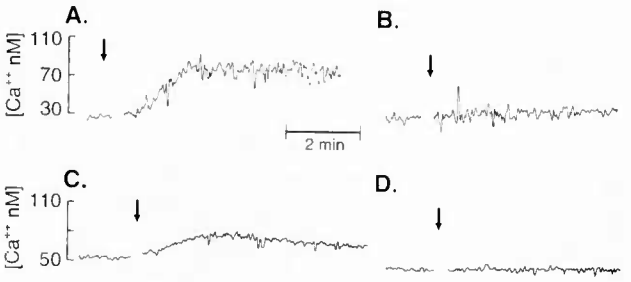

Fig. 9. Effect of swelling on [Ca]i. **A,B:** HL-60 cells and **(C,D)** THP-1 cells were loaded with eithr fura-2 am (A,C) or fura-2-AM plus BAPTA-AM, (B,D). At time indicated by arrows, 41% water was added.

percentage increase in [Ca]i compared to baseline levels obtained before addition of 41% water was 273% ± 26 (n = 6) for HL-60 cells and 154% ± 16 (n = 4) for THP-1 cells. BAPTA loading both cell types abolished the induced [Ca]i rise (Fig. 9). However, BAPTA loading did not block RVD in either cell type in response to either 0.59× NaCl Hanks' or 0.59× Ca-free, EGTA-containing NaCl Hanks' (shown in Fig. 10).

Experiments were also performed to determine if increases in [Ca]i can induce volume changes in the absence of an osmostic stress. In these studies, the volume of cells exposed to either 1 μM ionomycin or 32 nM thapsigargin was compared to the volume of control HL-60 and THP-1 cells in normal Hanks'. No changes in cell volume were apparent during a 30-minute exposure to either thapsigargin or ionomycin in either cell type.

Effect of gadolinium

Stretch-activated channels, which are inhibited by gadolinium (Yang and Sachs, 1989), have been implicated in RVD in astrocytes and other cells (Medrano and Gruenstein, 1993). However, in the presence of 1-100 μM gadolinium chloride, THP-1 and HL-60 cells exhibited normal RVD (data not shown).

DISCUSSION

This study demonstrates that RVD in THP-1 cells, a monocytic cell line, and in HL-60 cells, a promonocytic cell line, involves efflux through independent anion and cationic transport mechanisms. While little data are available about the ionic conductances in HL-60 and THP-1 cells (Wieland et al., 1987, 1990), electrophysiological studies on other myeloid cells have characterized several different K and Cl conductances that may be activated during RVD (Gallin, 1991). In many cases, pharmacological blockers of these ionic conductances have been described. Thus we reasoned that examining the ability of these agents to block RVD in THP-1 and HL-60 cells would provide information about the involvement of these ionic conductances in RVD, and therefore, their presence in these cell lines.

Cation permeability pathway

Surprisingly, quinine was the only K channel antagonist that completely blocked RVD in both cell types; 1 mM quinine blocked RVD in THP-1 cells while 4 mM

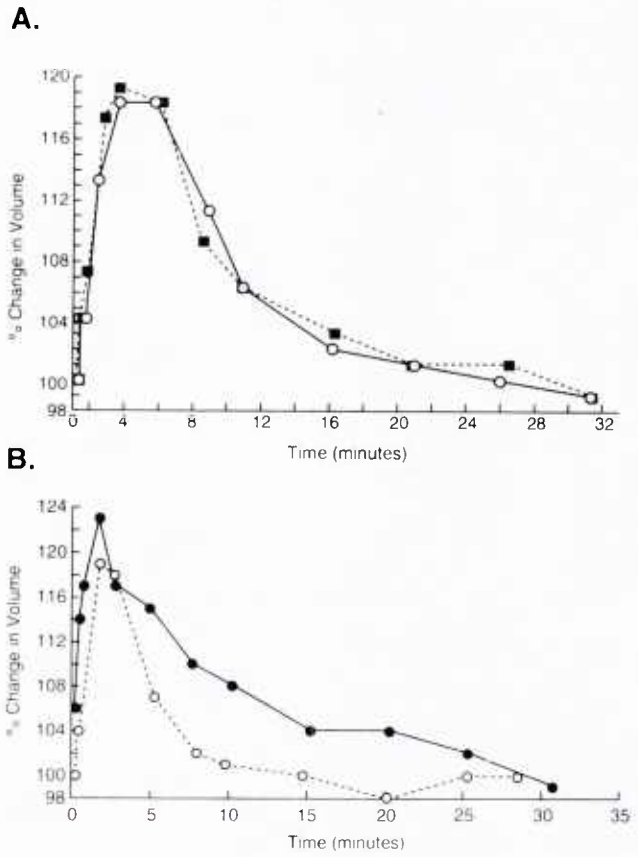

Fig. 10. A: Time course of representative volume responses of control (○) and BAPTA-loaded (■) HL-60 cells in 0.59× 0-calcium/1 mM EGTA NaCl Hanks'. B: Time course of representative volume responses of control (○) and BAPTA-loaded (●) THP-1 cells in 0.59× 0-calcium/1 mM EGTA NaCl Hanks'.

was required to block RVD in HL-60 cells. Although these concentrations of quinine have been reported to effect anionic conductances in some cells (Gogelein and Capek, 1990), the ability of gramicidin (a cationic channel former) to overcome quinine block indicates that in our experiments quinine is blocking RVD through its action on a cationic efflux. In macrophages, quinine blocks Ca-activated K conductances that have been implicated in RVD in other cell types (Okado and Hazama, 1989). Furthermore, we have demonstrated in this study that swelling induces a small increase in [Ca]i in both THP-1 and HL-60 cells which may be due to either a swelling-induced influx of extracellular calcium or release of intracellular calcium stores. Despite these observations, the inability of either BAPTA loading or CTX, an antagonist of Ca-activated K channels to block RVD makes it unlikely that calcium-activated K channels are involved in RVD in these cell lines. Furthermore, the observations that two agents which increase [Ca]i, thapsigargin and ionomycin, fail to change control cell volume, indicates that a [Ca]i increase, which activates Ca-activated K conductances in macrophages (Gallin, 1989), does not itself induce volume changes in these two cell lines.

Barium, the other K channel blocker tested that affected RVD in THP-1 and HL-60 cells, only partially blocked RVD. Perhaps the best characterized K conductance in macrophages is a barium-inhibitable voltage-dependent inwardly rectifying K conductance (Ki). The Ki conductance has been cloned recently (Kubo et al., 1993) and, when present, sets the macrophage resting membrane potential near to the K equilibrium potential (Gallin, 1981). This conductance also enables cells to flip between two stable states of resting membrane potential (Gallin, 1981). Barium block of Ki occurs in 300–500 μM extracellular barium (McKinney and Gallin, 1988). In contrast, 1–4 mM barium was required to slow RVD, but failed to completely inhibit it. Thus, the Ki conductance is unlikely to mediate RVD in HL-60 cells or in THP-1 cells. Partial block of RVD by barium could be due either to a partial block by barium of a single cation conductance or to the involvement of more than one cation conductance in RVD, a barium-sensitive conductance and a barium-insensitive conductance in RVD. In the human colon adenocarcinoma HT-29 cell line, where noise analysis has implicated only one type of K channel in volume regulation, the volume-sensitive K channel is completely blocked by quinine but only partially blocked by barium (Illek et al., 1992). Volume regulation in macrophages may involve a similar K channel.

None of the other K channel blockers tested in THP-1 and HL-60 cells inhibited RVD. Consequently, unlike lymphocytes where a CTX-sensitive "delayed-rectifier type" K conductance has been implicated in RVD (Grinstein and Smith, 1990; Grinstein and Foskett, 1990) or cultured proximal tubule cells where a Ca-activated K conductance (Dube et al., 1990) has been implicated in RVD, volume regulatory responses in myeloid cells do not appear to involve either the Ca-activated K conductances or delayed-rectifier type K conductances that have been described in myeloid cells.

The secondary swelling evident in both THP-1 and HL-60 cells bathed in 0.59× KCl Hanks' indicates that opening of the swelling-induced cation permeability does not depend on the K gradient, nor is it inactivated by depolarization. Our experiments with gadolinium, an antagonist of stretch-activated cation channels, also suggest that these channels are not involved in RVD of HL-60 and THP-1 cells. Further studies using both patch clamp techniques and volume measurements are needed to determine the cation permeability pathway(s) that are involved in RVD in macrophages.

Anion permeability pathway

Addition of gramicidin to either cell type produced little change in cell volume unless cells were exposed to hypotonic medium, indicating that the basal anion permeability of both THP-1 cells and HL-60 cells is low and that it increases following swelling. As in lymphocytes, our studies with high K hypotonic medium containing different anions indicated that the swelling-induced anionic transport pathway is permeable to both Cl and bromide ions but relatively impermeable to methanesulfonate and glutamate (Grinstein et al., 1982). While SITS completely blocks RVD in neutrophils (Stoddard et al., 1993) and other cells, it only produced a partial block of the RVD response in THP-1

and HL-60 cells. On the other hand, RVD was blocked in both cell types by the anion transport blocker DISA and this block could not be overcome by gramicidin. DISA, unlike SITS, is lipophilic and probably crosses the membrane through nonionic diffusion (Simchowtiz et al., 1993). In human neutrophils DISA blocked both RVD and the swelling-induced increases in ^{36}Cl efflux and Cl currents (Stoddard et al., 1993; Simchowtiz et al., 1993). In addition to blocking RVD in several cell types, DISA is a noncompetitive inhibitor of Cl-Cl exchange and Na independent Cl/HCO_3 exchange (Restrepo et al., 1992). Thus, while we can conclude that under our experimental conditions (in HEPES-buffered media without bicarbonate) swelling increases a DISA-inhibitable anionic transport mechanism(s), DISA may block RVD by acting on several different anionic transport mechanisms. In this context, a preliminary report by Hallows et al. (1992) showed that for HL-60 cells suspended in bicarbonate-containing hypotonic medium, the Cl efflux was significantly less than the K efflux, suggesting that additional osmolytes are involved in the RVD response in HL-60 cells. In astrocytes, cell swelling induces a rapid release of taurine, which is markedly reduced by the Cl channel inhibitor DIDS (Pasantes-Morales et al., 1990). If the loss of additional osmolytes also is involved in the RVD response of HL-60 cells maintained in bicarbonate-free medium, then DISA must block both the Cl permeability change and the efflux of the additional osmolytes. Alternatively, it is possible that under the conditions of our experiment, the magnitude of the Cl efflux is similar to that of K efflux and DISA is acting to block only a Cl efflux. Chloride efflux studies will be needed to differentiate between these possibilities.

Delineating the ionic basis of RVD provides information about the ionic transport mechanisms present in myeloid cells, and may even be useful in assessing changes in transport that occur during activation and/or differentiation. Blood monocytes will be exposed to large changes in tonicity during passage through the kidney. On the other hand, tissue macrophages are probably exposed to only small changes in tonicity at sites of inflammation or following changes in metabolism. Volume regulation following swelling induced by enhanced amino acid uptake has been demonstrated in a number of cells including intestinal enterocytes (MacLeoad et al., 1992). It is possible that stimulation of nitrous oxide formation and the subsequent increase in arginine uptake may lead to cell swelling in macrophages.

In conclusion, this study demonstrates that RVD in two myeloid cell lines is mediated by independent quinine-inhibitable cation and DISA-inhibitable anion transport pathways that are not gated by increases in [Ca]i and that the cation permeability pathway mediating RVD in these cells is different from the pathway mediating RVD in lymphocytes.

ACKNOWLEDGMENTS

The authors are grateful to Keith Brockgreitins and Brain Hively for their excellent technical assistance.

LITERATURE CITED

Auwerx, J. (1991) The human leukemia cell line, THP-1: A multifaceted model for the study of monocyte-macrophage differentiation. Experentia, *47*:22–31.

Deutsch, C., and Lee, S.C. (1988) Cell volume regulation in lymphocytes. Renal Physiol. Biochem., *3–5*:260–276.

Dube, L., Parent, L., and Sauve, R. (1990) Hypotonic shock activates a maxi K^+ channel in primary cultured proximal tubule cells. Am. J. Physiol., *25*:F348–F356.

Gallin, E.K. (1981) Voltage clamp studies in macrophages from mouse spleen cultures. Science, *214*:458–460.

Gallin, E.K. (1989) Evidence for a Ca-activated inwardly rectifying K channel in human macrophages, Am. J. Physiol., *257*:C77–C85.

Gallin, E.K. (1991) Ion channels in leukocytes. Physiol. Rev., *71*:775–811.

Gogelein, H., and Capek, K. (1990) Quinine inhibits chloride and nonselective cation channels in isolated rat distal colon cells. Biochem. Biophys. Act., *1027*:191–198.

Grinstein, S., and Foskett, J.K. (1990) Ionic mechanisms of cell volume regulation in leukocytes. Annu. Rev. Physiol., *52*:399–414.

Grinstein, S., and Smith, J.D. (1990) Calcium-independent cell volume regulation in human lymphocytes. J. Gen. Physiol., *95*:97–120.

Grinstein, S., Clarke, C.A., DuPre, A., and Rothstein, A. (1982) Volume-induced increase of anion permeablity in human lymphocytes. J. Gen. Physiol., *80*:801–823.

Grynkiewicz, G., Poenie, M., and Tsien, R. (1985) A new generation of Ca^{+2} indicators with greatly improved fluorescence properties. J. Biol. Chem., *260*:3440–3450.

Hallows, S.K.R., Packman, C.H., and Knauf, P.A. (1991) Acute cell volume changes in anisotonic media affect F-actin content in HL-60 cells. Am. J. Physiol., *261*:C1154–C1161.

Hallows, K.R., Restrepo, D., and Knauf, P. (1992) Control of volume and intracellular pH under hypotonic conditions in human promyelocytic HL-60 cells. J. Gen. Physiol., *100*:60a.

Illek, B., Fisher, H., Kreusel, K., Hegel, U., and Claus, W. (1992) Volume-sensitive basolateral K channels in HT-29/B6 cells: Block by lidocaine, quinidine, NPPB and Ba. Am. J. Physiol., *263*:C674–683.

Kubo, Y., Baldwin, T.J., Jan, Y.N., and Jan, L.Y. (1993) Primary structure and functional expression of mouse inward rectifier potassium channel. Nature, *352*:127–133.

Lewis, S.A., and Donaldson, P. (1990) Ion channels and cell volume regulation: Chaos in an organized system. News in Physiological Sciences *5*:112–119.

MacLeod, R.J., Lembessis, P., and Hamilton, J.R. (1992) Effect of protein kinase C inhibitors on Cl conductance required for volume regulation after L-alanine cotransport. Am. J. Physiol., *262* (Cell. Physiol., *31*):C950–955.

McKinney, L.C., and Gallin, E.K. (1988) Inwardly rectifying whole-cell and single-channel K currents in the murine macrophage cell line J774.1. J. Membr. Biol., *103*:42–53.

Medrano, S., and Gruenstein, E. (1993) Mechanisms of regulatory volume decrese in UC-11MG human astrocytoma cells. Am. J. Physiol., *264*:C1201–1209.

Novak, J.M., Cala, P., Ward, D., Buys, S., and Kaplan, J. (1988) Regulatory volume decrease in alveolar macrophages: Cation loss is not correlated with changes in membrane recycling. J. Cell. Physiol., *137*:243–250.

Okada, Y., and Hazama, A. (1989) Volume regulatory ion channels in epithelial cells. NIPS, *4*:238–242.

Pasantes-Morales, H., Moran, J., and Schousboe, A. (1990) Volume sensitive release of taurine from cultured astrocytes: Properties and mechanism. Glia, *3*:427–432.

Restrepo, D., Cronise, B.L., Snyder, R.B., and Knauf, P.A. (1992) A novel method to differentiate between ping-poing and simultaneous exchange kinetics and its application to the anion exchanger of the HL-60 cell. J. Gen. Physiol., *100*:825–846.

Sarkadi, B., and Parker, J.C. (1991) Activation of ion transport pathways by changes in cell volume. Biochim. Biophys. Acta, *107*:407–427.

Simchowitz, L., Textor, J.A., and Cragoe, E.J. (1993) Cell volume regulation in human neutrophils: 2-(aminomethyl)phenols as Cl^- channel inhibitors. Am. J. Physiol., *265*:C143–C155.

Stoddard, J.S., Steinbach, J.H., and Simchowitz, L. (1993) Whole-cell chloride currents in human neutrophils induced by swelling. Am. J. Physiol., *265*:C156–C165.

Wieland, S.J., Chou, R.H., and Chen, T.A. (1987) Elevation of a potassium current in differentiating human leukemic (HL-60) cells. J. Cell. Physiol., *132*:321–375.

Wieland, S.J., Chou, R.H., and Gong, Q. (1990) Macrophage-colony stimulating factor (CSF-1) modulates a differentiation-specific inward-rectifying potassium current in human leukemic (HL-60) cells. J. Cell. Physiol., *142*:643–651.

Yang, X.C., and Sachs, F. (1989) Block of stretch activated ion channels in Xenopus oocytes by gadolinium and calcium ions. Science, *243*:1068–1071.

Pergamon

Adv. Space Res. Vol. 14, No. 10, pp. (10)583–(10)586, 1994

0273–1177/94 $7.00 + 0.00

SURVIVAL OF IRRADIATED MICE TREATED WITH WR-151327, SYNTHETIC TREHALOSE DICORYNOMYCOLATE, OR OFLOXACIN

G. D. Ledney, T. B. Elliott, M. R. Landauer, R. M. Vigneulle, P. L. Henderson, R. A. Harding and S. P. Tom, Jr

Armed Forces Radiobiology Research Institute, Bethesda, MD 20889-5603, U.S.A.

ABSTRACT

Spaceflight personnel need treatment options that would enhance survival from radiation and would not disrupt task performance. Doses of prophylactic or therapeutic agents known to induce significant short-term (30-day) survival with minimal behavioral (locomotor) changes were used for 180-day survival studies. In protection studies, groups of mice were treated with the phosphorothioate WR-151327 (200 mg/kg, 25% of the LD_{10}) or the immunomodulator, synthetic trehalose dicorynomycolate (S-TDCM; 8 mg/kg), before lethal irradiation with reactor-generated fission neutrons and γ-rays (n/γ=1) or ^{60}Co γ-rays. In therapy studies, groups of mice received either S-TDCM, the antimicrobial ofloxacin, or S-TDCM plus ofloxacin after irradiation. For WR-151327 treated-mice, survival at 180 days for n/γ=1 and γ-irradiated mice was 90% and 92%, respectively; for S-TDCM (protection), 57% and 78%, respectively; for S-TDCM (therapy), 20% and 25%, respectively; for ofloxacin, 38% and 5%, respectively; for S-TDCM combined with ofloxacin, 30% and 30%, respectively; and for saline, 8% and 5%, respectively. Ofloxacin or combined ofloxacin and S-TDCM increased survival from the gram-negative bacterial sepsis that predominated in n/γ=1 irradiated mice. The efficacies of the treatments depended on radiation quality, treatment agent and its mode of use, and microflora of the host.

INTRODUCTION

Protons, electrons, heavy particles, photons, and, to a lesser degree, neutrons compose the major types of ionizing radiation in space. Bombardment of a spacecraft by solar particle events can result in significant increases in secondary photon and neutron production. Serious damage to proliferative cell systems in exposed personnel can result in life-threatening postirradiation sequelae. Of particular concern is the biological effectiveness that neutrons (as well as heavy particles) have over photons. If serious damage is sustained by personnel, radiation-induced performance decrements can jeopardize the mission. Death may ensue if the radiation dose is high enough.

Radioprotective chemicals can induce survival /1-4/. The principal group of radioprotective chemicals are the phosphorothioate compounds developed at the Walter Reed Army Institute of Research. A number of Walter Reed (WR) compounds particularly WR-2721 and WR-151327, have shown promise in protecting against the lethal outcome of gamma and neutron irradiation /1-3/.

Immunomodulators derived from bacterial cells or cloned from various eukaryotic or prokaryotic sources (cell growth factors/cytokines) have also shown promise as radioprotective agents and as substances capable of enhancing non-specific host resistance to bacterial infections and hematopoietic cell recovery following radiation injury. In this regard, synthetic trehalose dicorynomycolate (S-TDCM) is effective in mixed-field-irradiated mice and in γ-irradiated mice /4,5/.

Sepsis is one sequel of radiation damage to host proliferative tissues that may be linked to systemic translocation of bacteria from the gut or from external sources such as the skin and the environment. Antimicrobial agents are effective in treating sepsis in various animal models of radiation injury /6/. The quinolone ofloxacin is effective against sepsis in mixed-field-irradiated mice and in γ-irradiated mice /5,7/.

The purpose of this report is to summarize our findings on the efficacy of WR-151327, S-TDCM, and ofloxacin in increasing survival after lethal doses of mixed-field neutron and γ radiation (n/γ=1) or ^{60}Co γ radiation. Treatment agents were given before (protection) or after (therapy) irradiation, incidence of infection was selectively monitored during maximum host-defense system depression, and survival was recorded for 180 days thereafter.

MATERIALS AND METHODS

Mice

B6D2F1/J female mice were obtained from Jackson Laboratory (Bar Harbor, ME). The animals were maintained in Micro-Isolator cages as previously described /4/. Research was conducted in a facility accredited by the American Association for

Accreditation of Laboratory Animal Care (AAALAC). All procedures involving animals were reviewed and approved by an institutional animal care and use committee.

Irradiations

A TRIGA Mark-F reactor was used for mixed-field irradiation as previously described /5/. Mice were irradiated in aerated, rotating aluminum tubes at a dose rate of 0.38 Gy/min to a total dose of 5.6 Gy with an equal mixture of neutrons and photons having a mean energy of 0.8 MeV.

A ^{60} Co γ bilateral radiation facility was used for γ photon irradiation. Mice were irradiated in aerated Plexiglas containers at 0.4 Gy/min to a total dose of 10.25 Gy. Dosimetry for both radiation sources was previously described /8/. Dose response survival studies indicated that the radiation doses used were lethal to 80%-100% of untreated mice over a 30-day time period.

Treatment Agents

WR-151327 (U.S. Biosciences Inc, West Conshohocken, PA) was dissolved in neutralized saline, filtered, and injected ip (200 mg/kg in 0.25 ml) 30 min before irradiation. This dose of WR-151327 resulted in minimal reduction of locomotor activity, an index of behavioral toxicity. The locomotor decrement produced by 200 mg/kg WR-151327 can be mitigated by administration of caffeine (data not shown), similar to the effect observed for the related phosphorothioate, WR-3689 /9/.

S-TDCM (Ribi ImmunoChem Research, Inc. Hamilton, MT) was prepared in 0.2% Tween-80 0.9% saline and injected ip (8 mg/kg in 0.5 ml) 22-24 hr before or 1 hr after irradiation. This S-TDCM dose induced no reduction in locomotor activity (data not reported).

L-ofloxacin (Ortho Pharmaceutical Corp, Raritan, NJ) was dissolved in sterile water before use, and 40 mg/kg in 0.1 ml water was fed to mice at 24-hr intervals starting 3 days after irradiation and ending 21 days later. Locomotor activity assessment of mice treated with ofloxacin was precluded by the daily treatments.

Ceftriaxone (Roche Laboratories, Nutley, NJ) was reconstituted and diluted in sterile water and 75 mg/kg/day was injected sc daily at 24-hr intervals starting 1 day after irradiation and ending 21 days later. Locomotor activity assessment of mice treated with ceftriaxone was precluded by the daily treatments.

Bacteria

Specimens of liver from euthanized mice were processed from day 5 to day 18 to determine the incidence of bacteremia after irradiation. The bacteria were isolated on sheep blood agar and MacConkey agar (BBL, Cockeysville, MD), incubated in air and 5% CO_2 at 35 C, and identified by standard techniques /10/.

Experimental Design and Statistical Analyses

In the therapy and sepsis studies, experimental groups were paired as to radiation quality and treatment agent. Paired experiments were performed with mice from a single shipment. All experiments were done with animals received at monthly intervals over a 2-year period. Survival data for mice were obtained for 180 days after irradiation. Comparisons were made by the generalized Savage (Mantel-Cox) procedure /11/. Incidence of bacteria in the livers after irradiation were evaluated by chi square analysis /12/.

RESULTS

Survival incidence of irradiated mice 180 days after treatment usage is shown in Figure 1. WR-151327 and S-TDCM given before γ irradiation resulted in 92% and 78% survival, respectively, and were less effective in n/γ=1-irradiated mice (90% and 57%, respectively). S-TDCM therapy given alone after irradiation resulted in 20% and 25% survival of n/γ=1 and γ-irradiated mice, respectively. S-TDCM therapy with ofloxacin resulted in 30% survival in all irradiated mice. Ofloxacin therapy given alone to n/γ=1- and γ-irradiated mice resulted in 38% and 5% survival, respectively.

Incidence and major types of bacteria found in the livers of mice up to 18 days after irradiation are presented in Figure 2. More positive liver cultures were found in n/γ=1-irradiated mice than in γ-irradiated mice. However, antimicrobial therapy with ofloxacin and ceftriaxone reversed this finding. Gram-negative bacterial sepsis (Escherichia coli and Proteus sp.) predominated in n/γ=1-irradiated mice even with antimicrobial therapy. Gram-positive bacterial sepsis (streptococci, enterococci, and staphylococci) predominated in γ-irradiated mice and was not treated in this study.

DISCUSSION

During solar particle events the environment within a space vehicle may contain a mixture of γ photons and neutrons. One sequel to unmitigated injury from these radiations is performance degradation. Radioprotective agents may also result in performance decrement /9/. For this reason we evaluated the effectiveness of relatively low doses of various radioprotective agents that are known to protect against neutrons and γ photons /2-5/. Since it is not always possible in space environments to avoid radiation hazards, therapies for such injury were also evaluated. S-TDCM and ofloxacin are two agents that enhance

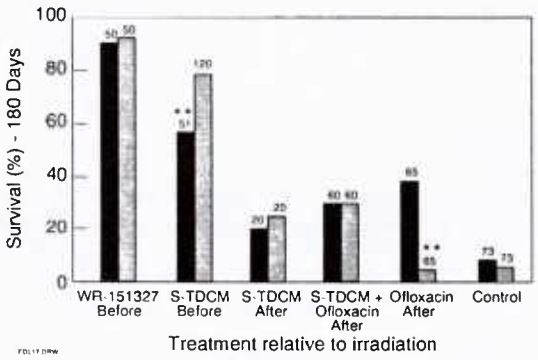

Fig. 1. Incidence of survival in B6D2F1/J mice 180 days after 5.6 Gy mixed field (n/γ=1) or 10.25 Gy γ-irradiation and treatments with WR-151327, S-TDCM, or ofloxacin. Statistical differences determined by chi-square analysis (* = P<0.05; ** = P<0.01). All treatments of γ-irradiated mice increased survival compared to saline-treated controls (P<0.01) except for ofloxacin therapy. All treatments of n/γ=1-irradiated mice increased survival compared to saline-treated controls (P<0.01) except for S-TDCM therapy. Numbers at top of bars indicate total mice in each experiment.

survival in various mouse models of radiation injury /4-7, 13,14/. In this present work, protection against n/γ=1 radiation and γ radiation was sustained over 180 days after administration of WR-151327 and S-TDCM. The difference in the mechansim of action of these two agents may be that WR-151327 protects against radiation-induced hydroxyl radicals that damage sensitive targets, and S-TDCM increases survival by augmenting hematopoietic system recovery /14,15/ and activating nonspecific host defenses against bacterial infection /14,16/.

Therapy with S-TDCM increased survival for γ-irradiated mice, and, to a lesser extent, for n/γ=1 irradiated animals. In comparison, in other work (data not reported), recombinant human granulocyte colony stimulating factor (rh-G-CSF) did not increase survival in any of the irradiated mice. The reason for this difference is not clear, but S-TDCM, because of its adjuvant nature, may be better able to augment recovery of lethally irradiated hematopoietic proliferative tissues /14,15/. S-TDCM enhances macrophage antibacterial activity while rh-G-CSF stimulates production of new granulocytes. Macrophages are radioresistant cells, and their activation by S-TDCM would aid against the early gram-negative bacterial sepsis that predominated after n/γ=1 irradiation and the late gram-positive bacterial sepsis that predominated after γ-irradiation.

The antimicrobial ofloxacin is effective against gram-negative bacteria but not gram-positive bacteria. Since gram-negative bacterial sepsis was paramount in mixed-field-irradiated mice, ofloxacin provided antimicrobial coverage and sufficent time for hematopoietic and nonspecific host recovery to occur. Ofloxacin was provided orally and is absorbable through the gut mucosa, thus reaching bacteria that may have translocated systemically from the injured gut. Interestingly, ceftriaxone, an antimicrobial effective against gram-negative as well as gram-positive bacteria, was ineffective in the present study (data not reported). Ceftriaxone is not absorbed from the gut and must be injected into mice. Daily penetration of the skin for 21 days induced significant local hemorrhage and opportunity for skin-associated gram-positive bacteria to infect the injection site. Clearly, an orally absorbable antimicrobial agent offers a therapeutic advantage over an antimicrobial given by another route in an irradiated host, even when the bacterial coverage is generally the same.

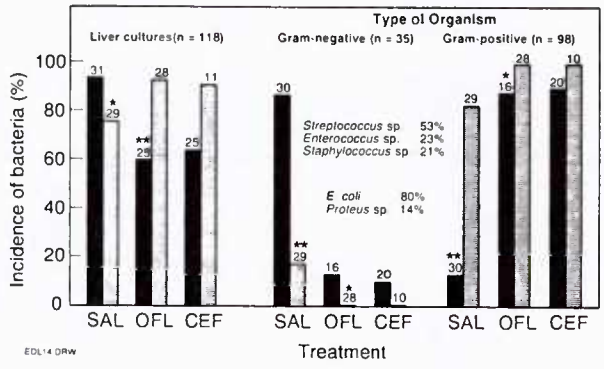

Fig. 2. Incidence and type of bacteria in B6D2F1/J mice treated with saline (SAL), ofloxacin (OFL), or ceftriaxone (CEF) after 5.6 Gy mixed field (n/γ=1) or 10.25 Gy γ irradiation. Statistical differences determined by chi-square analysis (* = P< 0.05; ** = P<0.01). Numbers at top of bars signify number of mice tested in each indicated category. The number (n) of gram positive and gram negative bacteria isolated were greater than the number of animals tested.

In summary, comparatively low doses of the phosphorothioate WR-151327 and the immunomodulator S-TDCM increase survival from lethal radiations expected in a space vehicle. Therapy is possible for postirradiation sepsis with S-TDCM and the antimicrobial ofloxacin. The success of therapy regimens will depend on the type of infections involved, the mode of treatment, and the quality of radiation.

ACKNOWLEDGEMENTS

This research was supported by the Armed Forces Radiobiology Research Institute, Defense Nuclear Agency. Research was conducted according to the principles in the Guide for the Care and Use of Laboratory Animals prepared by the Institute of Laboratory Resources, National Research Council.

REFERENCES

1. J.F. Weiss and M.G. Simic, Perspectives in Radioprotection, Pergamon Press, New York, 1988.

2. C.P. Sigestad, D.J. Grdina, A.M. Connor and W.R. Hanson, A comparison of radioprotection from three neutron sources and ^{60}Co by WR-2721 and WR-151327, Radiat. Res. 106, 224-233 (1986).

3. L.S. Steel, A.J. Jacobs, L.J. Giambarresi and W.E. Jackson III, Protection of mice against fission neutron irradiation by WR-2721 or WR-151327, Radiat. Res. 109, 469-478 (1987).

4. D.G. McChesney, G.D. Ledney and G.S. Madonna, Trehalose dimycolate enhances survival of fission neutron-irradiated mice and Klebsiella pneumoniae-challenged irradiated mice, Radiat. Res. 121, 71-75 (1990).

5. G.D. Ledney, G.S. Madonna, T.B. Elliott, M.M. Moore and W.E. Jackson III, Therapy of infections in mice irradiated in mixed neutron/photon fields and inflicted with wound trauma: A review of current work, Radiat. Res. 128, S18-S28 (1991).

6. I. Brook, G.D. Ledney, G.S. Madonna, R. M. DeBell and R.I. Walker, Therapies for radiation injuries: Research perspectives, Mil. Med. 157, 130-136 (1992).

7. I. Brook and G.D. Ledney, Ofloxacin and Penicillin G combination therapy in prevention of bacterial translocation and animal mortality after irradiation, Antimicrob. Agents Chemother. 35, 1685-1687 (1991).

8. D.A. Stewart, G.D. Ledney, W.H. Baker, E.G. Daxon and P.A. Sheehy, Bone marrow transplantation of mice exposed to a modified fission neutron (N/G-30:1) field, Radiat. Res. 92, 268-279 (1982).

9. M.R. Landauer, H.D. Davis, K.S. Kumar and J.F. Weiss, Behavioral toxicity of selected radioprotectors, Adv. Space Res. 12, #2-3, (2)273-(2)283 (1992).

10. E.H. Lennette, A. Balows, W. Hausler and J.H. Shadomy, (eds.) Manual of Clinical Microbiology, 4th ed. American Society for Microbiology, Washington, D.C., 1985.

11. E.T. Lee, Statistical Methods for Survival Data Analysis, pp. 122-129, Lifetime Learning Publ., Belmont, CA., 1980.

12. R.G.D. Steel and J.H. Torrie, Principles and Procedures of Statistics, pp. 366-387, McGraw-Hill, New York, 1960.

13. G.S. Madonna, G.D. Ledney, M.M. Moore, T.B. Elliott and I. Brook, Treatment of mice with sepsis following irradiation and trauma with antibiotics and synthetic trehalose dicorynomycolate (S-TDCM), J. Trauma 31, 316-325 (1991).

14. G.S. Madonna, G.D. Ledney, T.B. Elliott, I. Brook, J.T. Ulrich, K.R. Myers, M.L. Patchen and R.I. Walker, Trehalose dimycolate enhances resistance to infection in neutropenic animals, Infect. Immun. 57, 2495-2501 (1989).

15. D.A. Stewart, G.D. Ledney, G.S. Madonna, S.M. Stiefel and M.M. Moore, Synthetic trehalose dicorynomycolate (S-TDCM) increases hematopoietic cell proliferation in fission neutron (n/g=1) irradiated mice, J. Mil. Med. Lab. Sci. 19, 208-213 (1990).

16. E. Yarkoni and A. Bekierkunst, Non-specific resistance against infection with Salmonella typhi and Salmonella typhimurium induced in mice by cord factor (trehalose 6,6'-dimycolate) and its analogues, Infect. Immun. 14, 1125-1129 (1976).

Biotherapy 7: 13–26, 1994.

Mast cell growth factor (C-*Kit* Ligand) in combination with granulocyte-macrophage colony-stimulating factor and interleukin–3: *in vivo* hemopoietic effects in irradiated mice compared to *in vitro* effects

M.L. Patchen[1], R. Fischer[1], T.J. MacVittie[1], F.R. Seiler[2] and D.E. Williams[3]
[1]*Department of Experimental Hematology, Armed Forces Radiobiology, Research Institute Bethesda, MD, USA;* [2]*Research Laboratories of Behringwerke, AG, Marburg, Germany;* [3]*Immunex Corporation, Seattle, WA, USA*

Received 19 July 1993; accepted in final form 1 September 1993

Key words: C-kit Ligand, GM-CSF, Hemopoiesis, IL–3, MGF, Myelosuppression, Radiation, SCF

Abstract

In the presence of hemopoietic cytokines such as granulocyte-macrophage colony-stimulating factor (GM-CSF) and interleukin–3 (IL–3), mast cell growth factor (MGF; also known as steel factor, stem cell factor, and c-*kit* ligand) has proven to be a potent hemopoietic regulator *in vitro*. In these studies, we examined the *in vivo* effects of MGF in combination with GM-CSF or GM-CSF plus IL–3. Effects were based on the ability of these cytokines to stimulate recovery from radiation-induced hemopoietic aplasia. Female B6D2F1 mice were exposed to a sublethal 7.75-Gy dose of ^{60}Co radiation followed by subcutaneous administration of either saline, recombinant murine (rm) MGF (100 μg/kg/day), rmGM-CSF (100 μg/kg/day), rmIL–3 (100 μg/kg/day), or combinations of these cytokines on days 1–17 postirradiation. Recoveries of bone marrow and splenic spleen colony-forming units (CFU-s), granulocyte macrophage colony-forming cells (GM-CFC), and peripheral white blood cells (WBC), red blood cells (RBC) and platelets (PLT) were determined on days 14 and 17 during the postirradiation recovery period. MGF administered in combination with GM-CSF or in combination with GM-CSF plus IL–3 either produced no greater response than GM-CSF alone or down-regulated the GM-CSF-induced recovery. These results sharply contrasted results of *in vitro* studies evaluating the effects of these cytokines on induction of GM-CFC colony formation from bone marrow cells obtained from normal or irradiated B6D2F1 mice, in which MGF synergized with GM-CSF or GM-CSF plus IL–3 to increase both GM-CFC colony numbers and colony size. These studies demonstrate a dichotomy between MGF-induced effects *in vivo* and *in vitro* and emphasize that caution should be taken in attempting to predict cytokine interactions *in vivo* in hemopoietically injured animals based on *in vitro* cytokine effects.

Abbreviations: GM-CSF; Granulocyte-Macrophage Colonly-Stimulating Factor; IL–3: Interleukin–3; MGF: Mast Cell Growth Factor; SCF: Stem Cell Factor; rm: Recombinant Murine; CFU-s: Colony Forming Unit-Spleen; GM-CFC: Granulocyte Macrophage Colony-Forming Cell; WBC: White Blood Cells; RBC: Red Blood Cells; PLT: Platelets; SLF: Steel Factor; G-CSF: Granulocyte Colonly-Stimulating Factor; IL–1: Interleukin–1; IL–6: Interleukin–6; Epo: Erythropoietin; CFC: Colony-Forming Cell; Sl: Steel; BFU-e: Erythroid Burst Forming Units; s.c.: Subcutaneous; PEG: Polyethyleneglycol; PIXY321: GM-CSF/IL–3 Fusion Protein.

Introduction

One of the most recent cytokines implicated in hemopoietic regulation is c-*kit* ligand, also known as mast cell growth factor (MGF), steel factor (SLF), and stem cell factor (SCF) [1–3]. C-*kit* ligand has been ascribed numerous hemopoietic and nonhemopoietic effects, although it was initially identified and purified based on its ability to stimulate mast cell growth [2–5].

Multiple studies have focused on the *in vitro* effects of this factor, demonstrating that alone it has limited hemopoietic activity, but when combined with other hemopoietic cytokines, including granulocyte colony-stimulating factor (G-CSF), granulocyte macrophage colony-stimulating factor (GM-CSF), interleukin–1 (IL–1), interleukin–3 (IL–3), interleukin–6 (IL–6), and erythropoietin (Epo), it synergizes to increase both the number and size of colonies generated from hemopoietic progenitors [3–11], and in some instances, to increase the replating potential of primitive progenitors [12]. Furthermore, in combination with such factors, c-*kit* ligand also synergistically enhances the *in vitro* expansion of hemopoietic progenitors grown in liquid cultures [13–15]. These effects are thought to result not only from the ability of c-*kit* ligand to potentiate progenitor cell proliferation but also from its ability to enhance progenitor cell survival [14, 16]. The observations that c-*kit* ligand in combination with other cytokines appears to generate large numbers of both committed colony-forming cells (CFC) and pre-CFC suggest that this factor may act earlier than other hemopoietic factors described to date [9, 17].

The most notable evidence that c-*kit* ligand is involved in hemopoietic regulation *in vivo* is the fact that mice with mutations at the *Steel (Sl)* locus, which encodes c-*kit* ligand, are defective in hemopoietic cell development [18–21]. Furthermore, the macrocytic anemia, deficiencies in tissue mast cells, abnormalities in megakaryocytopoiesis, and reduced granulocytopoiesis that occur in *Steel* mice can be partially corrected by the administration of c-*kit* ligand [22]. In addition to the data accumulated in *Steel* mice, a limited number of studies have recently reported the ability of c-*kit* ligand to stimulate hemopoiesis in normal mice, rats, canines, and nonhuman primates [23–26]. Among the effects reported following c-*kit* ligand administration *in vivo* are increases in peripheral blood erythrocyte, neutrophil, lymphocyte, monocyte, eosinophil, and basophil numbers, as well as increases in bone marrow cellularity, GM-CFC, and erythroid burst-forming units (BFU-e), and (in mice) increases in splenic GM-CFC and CFU-s. In addition to these studies performed with c-*kit* ligand in normal animals, the ability of this factor to moderately stimulate hemopoietic regeneration in a more clinically relevant condition of radiation-induced hemopoietic aplasia has also recently been demonstrated [26–27].

We have previously demonstrated the ability of GM-CSF or GM-CSF plus IL–3 to accelerate hemopoietic recovery in irradiated primates [28–29]. Because *in vitro* studies have demonstrated synergistic hemopoietic stimulation produced by c-*kit* ligand combined with GM-CSF or GM-CSF plus IL–3 [6–8, 14–16, 30–31], we evaluated whether coadministration of c-*kit* ligand with these cytokines would further enhance their ability to accelerate hemopoietic regeneration following radiation-induced hemopoietic aplasia.

We report that MGF administered *in vivo* either does not affect, or in some cases even downregulates, regenerative responses induced by GM-CSF or GM-CSF plus IL–3 in irradiated mice, and that these effects sharply contrast the ability of MGF to synergize with these cytokines *in vitro*.

Materials and methods

Cytokines

Recombinant murine c-*kit* ligand, henceforth referred to as MGF, was provided by Immunex (Seattle, WA). Recombinant murine GM-CSF and IL–3 were provided by Behringwerke AG (Marburg, Germany). Cytokines were expressed in yeast and purified to homogeneity as previous-

ly described [10, 32]. Endotoxin contamination of cytokines was below the limit of detection using the limulus amebocyte lysate assay. Each cytokine was administered subcutaneously (s.c.) in a 0.1-ml volume at the dose of 100 μg/kg. Cytokine doses were based on preliminary dose-response studies performed in our laboratory [27; Patchen, unpublished]. In combination studies, mice received each cytokine at a separate injection site. All injections were initiated 1 day following irradiation and continued daily for 17 days. Control mice were injected with an equal volume of sterile saline.

Mice

B6D2F1 female mice (~20 g) were purchased from Jackson Laboratories (Bar Harbor, ME). Mice were maintained in an AAALAC (American Association for Accreditation of Laboratory Animal Care) accredited facility in Micro-Isolator cages on hardwood-chip contact bedding and were provided commercial rodent chow and acidified water (pH 2.5) *ad libitum*. Animal rooms were equipped with full-spectrum light from 6 a.m. to 6 p.m. and were maintained at 70 °F ± 2 °F with 50% ± 10% relative humidity using at least 10 air changes per hour of 100% conditioned fresh air. Upon arrival, all mice were quarantined and samples from cage water bottles were cultured to detect any mice infected with oropharyngeal *Pseudomonas* sp. Only healthy mice were released for experimentation. All animal experiments were approved by the Institute Animal Care and Use Committee prior to performance.

Irradiation

The ^{60}Co source at the Armed Forces Radiobiology Research Institute was used to administer bilateral total-body gamma radiation. Mice were placed in ventilated Plexiglas containers and irradiated with 7.75 Gy at a dose rate of 0.4 Gy/min. Dosimetry was performed using ionization chambers [33] with calibration factors traceable to the National Institute of Standards and Technology. The tissue-to-air ratio was determined to be 0.96. Dose variation within the exposure field was < 3%.

Peripheral Blood Cell Counts

Blood was obtained from halothane-anesthetized mice by cardiac puncture using a heparinized syringe attached to a 20-gauge needle. White blood cell (WBC), red blood cell (RBC), and platelet (PLT) counts were performed using a Coulter counter.

Cell Suspensions

Cell suspensions for each assay represented tissues from three normal, irradiated, or irradiated and cytokine-treated mice at each time point. Cells were flushed from femurs with 3 ml of McCoy's 5A medium (Flow Labs, McLean, VA) containing 10% heat-inactivated fetal bovine serum (Hyclone Labs, Logan, UT). Spleens were pressed through a stainless steel mesh screen, and the cells were washed from the screen with 6 ml medium. The number of nucleated cells in the suspensions was determined by Coulter counter. Femurs and spleens were removed from mice euthanized by cervical dislocation.

Granulocyte-Macrophage Colony-Forming Cell Assay

For *in vivo* studies, hemopoietic progenitor cells committed to granulocyte and/or macrophage development were assayed using a double-layer agar granulocyte-macrophage colony-forming cell (GM-CFC) assay in which mouse endotoxin serum (5% v/v) was added to feeder layers as a source of colony-stimulating factors [34]. In studies evaluating the direct *in vitro* effects of cytokines on colony formation, a single-layer agar culture system was used in which normal bone marrow cells and cytokines were prepared in a 0.33% agar-media suspension at the concentration of 5×10^4 cells per ml and 2 ml of this suspension was plated into 35-mm culture dishes. Colonies (> 50 cells) were counted after 10 days of incubation in a 37 °C humidified environ-

ment containing 5% $C0_2$. Triplicate plates were cultured for each cell suspension.

Spleen Colony Forming Unit Assay

Exogenous spleen colony-forming units (CFU-s) were evaluated by the method of Till and McCulloch [35]. Recipient mice were exposed to 9 Gy of total-body radiation to reduce endogenous hemopoietic stem cells. Three to five h later, bone marrow or spleen cells were intravenously (i.v.) injected into the irradiated recipients. Twelve days after transplantation, the recipients were euthanized by cervical dislocation, and their spleens were removed. The spleens were fixed in Bouin's solution, and grossly visible spleen colonies were counted. Each treatment group consisted of five mice.

Statistics

Results of replicate experiments were pooled and are represented as the mean ± standard error (SE) of pooled data. Statistical differences were determined by Behrens-Fisher t-test analysis. Significance level was set at $p < 0.05$.

Experimental Design for in Vivo Studies

The ability to accelerate hemopoietic regeneration in a murine model of severe radiation-induced hemopoietic hypoplasia was used to evaluate the potential of MGF to synergize with GM-CSF or GM-CSF plus IL–3 in inducing hemopoietic progenitor cell expansion *in vivo*. In preliminary studies (Table 1), it was determined that a sublethal 7.75 Gy ^{60}Co radiation exposure induced severe hemopoietic hypoplasia from which recovery (especially in the spleen) became evident between days 14 and 17 postirradiation. Based on these preliminary studies, subsequent studies evaluating the ability of cytokines to accelerate hemopoietic recovery focused on evaluation of bone marrow and splenic cellularity, CFU-s, and GM-CFC recoveries, as well as peripheral WBC, RBC, and PLT recoveries on days 14 and 17 postirradiation.

Results

In Vivo Studies in Irradiated Mice

The effects of MGF plus GM-CSF on bone marrow and splenic CFU-s, GM-CFC, and peripheral blood cell recoveries in sublethally irradiated mice are illustrated in Figures 1, 2, and 3, respectively. MGF alone, at the dose used in these studies, had no effect on CFU-s recovery. In contrast, GM-CSF alone induced accelerated marrow and splenic CFU-s recoveries, which were evident as early as day 14 postirradiation. MGF administered in combination with GM-CSF, however, had no further effect than GM-CSF alone on bone marrow CFU-s recovery (Fig. 1A), and even down-modulated the splenic CFU-s recovery (Fig. 1B) induced by GM-CSF alone. Though less significant, similar patterns were observed for GM-CFC (Fig. 2) and peripheral WBC (Fig. 3A) recoveries in mice treated with MGF plus GM-CSF. RBC and PLT recoveries in these mice, however, were not down-modulated (Fig. 3B and 3C).

In an additional study, MGF was administered to sublethally irradiated mice in combination with GM-CSF plus IL–3 and CFU-s (Fig. 4) and GM-CFC (Fig. 5) recovery evaluated on day 17 postirradiation. The appropriate obligatory single- and double-factor controls were also simultaneously evaluated. Administration of MGF alone or MGF plus GM-CSF induced recovery patterns identical to the results described above. IL–3 alone produced a stimulation of only splenic CFU-s and GM-CFC recovery. However, when IL–3 was administered in combination with GM-CSF, it enhanced bone marrow and splenic CFU-s and GM-CFC recoveries over those induced by GM-CSF alone; this stimulatory interaction was more pronounced in the spleen than in the bone marrow. In contrast, mice administered MGF in combination with GM-CSF plus IL–3 exhibited CFU-s and GM-CFC recoveries that were again reduced to the same level or below the level of recovery induced by GM-CSF alone. Interesting, however, was the observation that MGF in combination with IL–3 did enhance CFU-s and GM-CFC recoveries beyond those induced by MGF or IL–3

Table 1. Recovery of bone marrow and splenic cellularity, CFU-s and GM-CFC following a 7.75 Gy ^{60}Co exposure.

	Unirradiated	Irrad Day 7	Irrad Day 10	Irrad Day 14	Irrad Day 17	Irrad Day 21
Cells/Femur (millions)	12.4 ± 0.6	1.2 ± 0.1	1.8 ± 0.3	3.6 ± 0.4	3.8 ± 0.6	5.1 ± 0.5
CFU-s/Fumur	6,837 ± 198	9 ± 1	13 ± 2	328 ± 29	531 ± 37	1,084 ± 118
GM-CFC/Femur	11,478 ± 406	0 ± 0	89 ± 11	370 ± 83	1,219 ± 186	1,498 ± 136
Cells/Spleen (millions)	155.8 ± 6.1	12.7 ± 0.7	12.9 ± 0.7	35.9 ± 4.4	144.9 ± 11.4	242.5 ± 40.7
CFU-s/Spleen	2.878 ± 188	0 ± 0	8 ± 3	383 ± 42	2,135 ± 309	2,614 ± 256
GM-CFC/Spleen	3,036 ± 180	0 ± 0	0 ± 0	357 ± 40	3,053 ± 521	17,543 ± 982

Data represent the mean ± SE of values obtained from two replicate experiments.

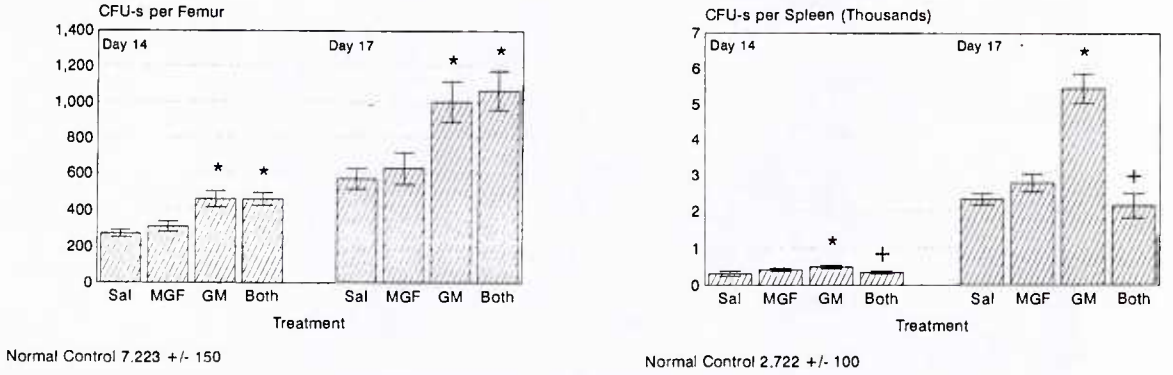

Fig. 1. Effect of MGF plus GM-CSF (each 100 μg/kg/d, s.c.) on postirradiation recovery of bone marrow and splenic CFU-s recovery in sublethally irradiated (7.75 Gy) B6D2F1 mice. Data represent the mean ± SE of values obtained from three replicate experiments. * $p < 0.05$, with respect to saline controls; + $p < 0.05$, with respect to GM-CSF values.

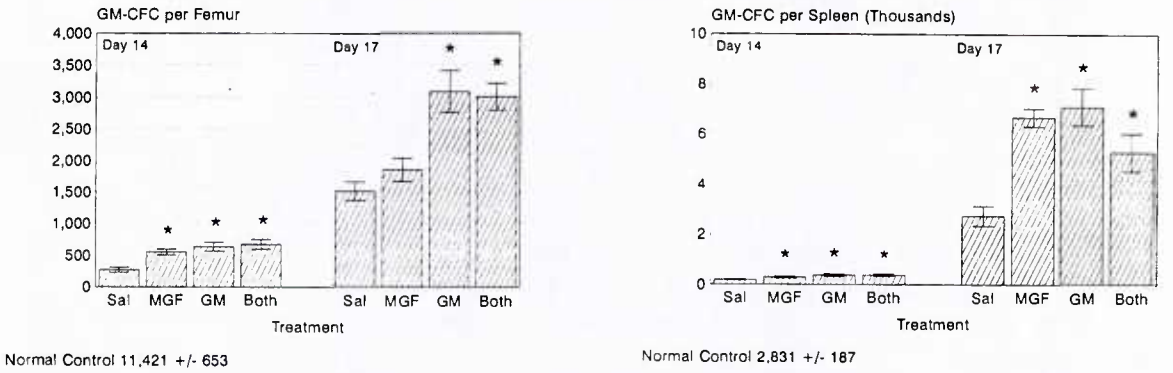

Fig. 2. Effect of MGF plus GM-CSF (each 100 μg/kg/d, s.c.) on postirradiation recovery of bone marrow and splenic GM-CFC recovery in sublethally irradiated (7.75 Gy) B6D2F1 mice. Data represent the mean ± SE of values obtained from three replicate experiments. * $p < 0.05$, with respect to saline controls; + $p < 0.05$, with respect to GM-CSF values.

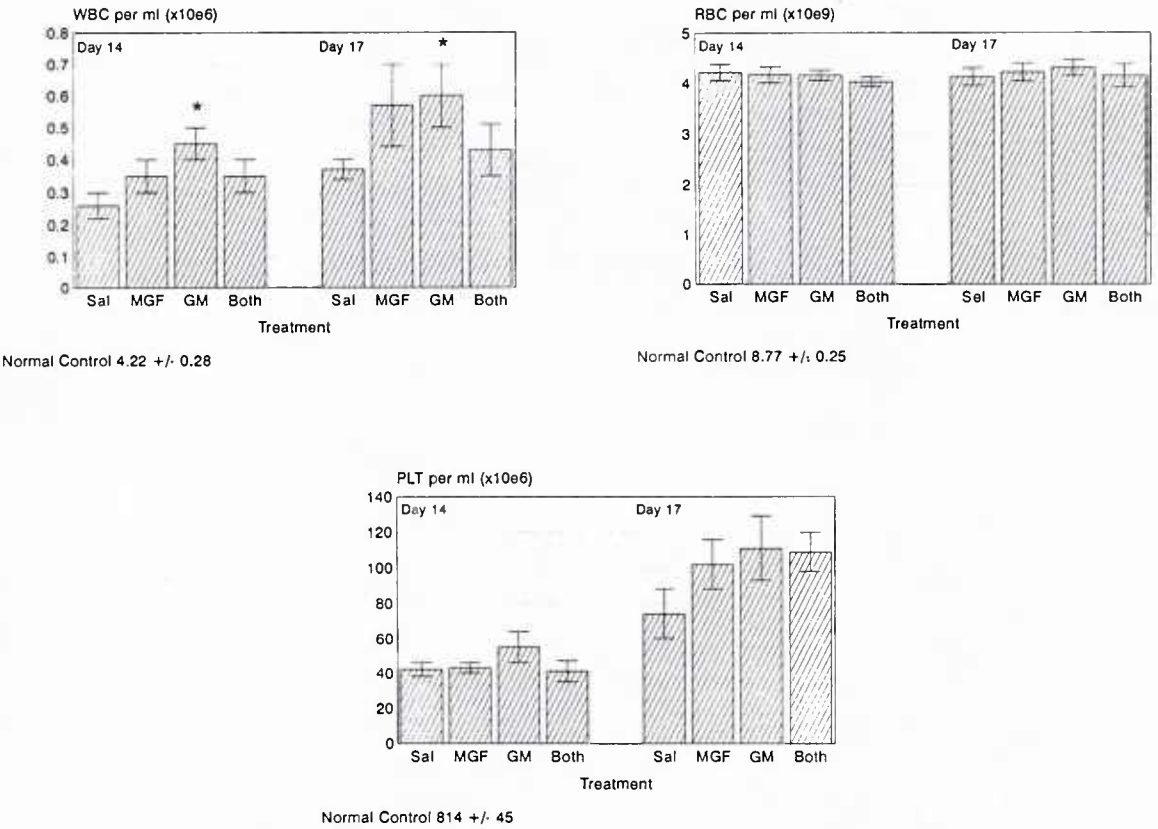

Fig. 3. Effect of MGF plus GM-CSF (each 100 μg/kg/d, s.c.) on postirradiation recovery of peripheral blood white blood cells, red blood cells, and platelets in sublethally irradiated (7.75 Gy) B6D2F1 mice. Data represent the mean ± SE of values obtained from three replicate experiments. * $p < 0.05$, with respect to saline controls; + $p < 0.05$, with respect to GM-CSF values.

alone. Splenic effects were more significant than bone marrow effects; however, MGF plus IL–3 treatment did not induce recovery surpassing that induced by GM-CSF plus IL–3.

In Vitro Studies Performed with Bone Marrow Cells Obtained from Normal Mice

Because results of our *in vivo* studies contrasted dramatically with previously published results of *in vitro* studies demonstrating synergistic stimulatory effects of MGF combined with GM-CSF or GM-CSF plus IL–3 [6–8, 14–16, 30–31], we performed *in vitro* studies to verify our cytokine activities. Initial *in vitro* studies focused on determining the ability of MGF alone or in combination with GM-CSF or GM-CSF plus IL–3 (as well as the respective single- and double-factor obligatory controls) to alter GM-CFC colony formation when directly cultured with bone marrow cells obtained from normal mice. Results are presented in Table 2 and Figure 6.

In these initial studies, colony-stimulating effects of MGF alone were evaluated at concentrations of 0.125 ng/plate, 12.5 ng/plate, and 25 ng/plate. No colony formation was evident at the 0.125-ng concentration; however, sporadic cluster (< 50 cells) and colony formation became evident at higher MGF concentrations, with 12.4 ± 0.7 colonies per plate being observed at the 25-ng concentration. IL–3 alone (0.125 ng/plate) induced no colony formation, and GM-CSF at the

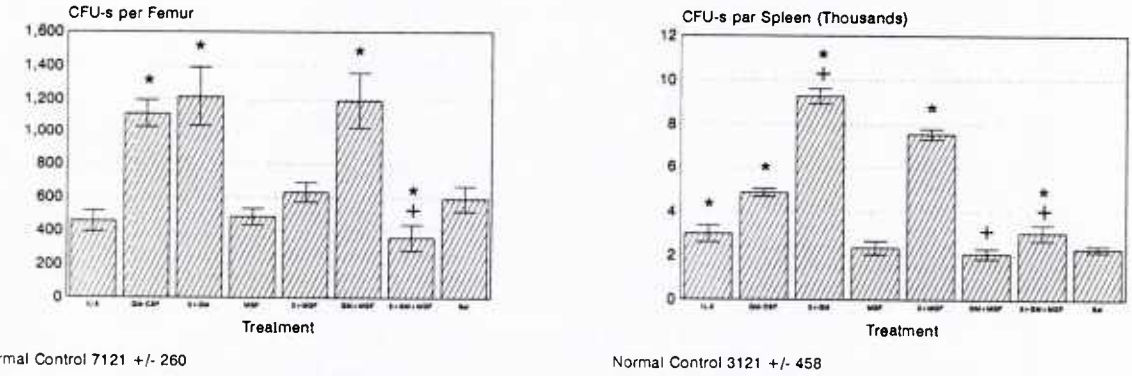

Fig. 4. Effects of MGF plus GM-CSF and IL–3 (each 100 μg/kg/d, s.c.) on postirradiation recovery of bone marrow and splenic CFU-s recovery in sublethally irradiated B6D2F1 mice. Data represent the mean ± SE of values obtained from one experiment. * $p < 0.05$, with respect to saline controls; + $p < 0.05$, with respect to GM-CSF values.

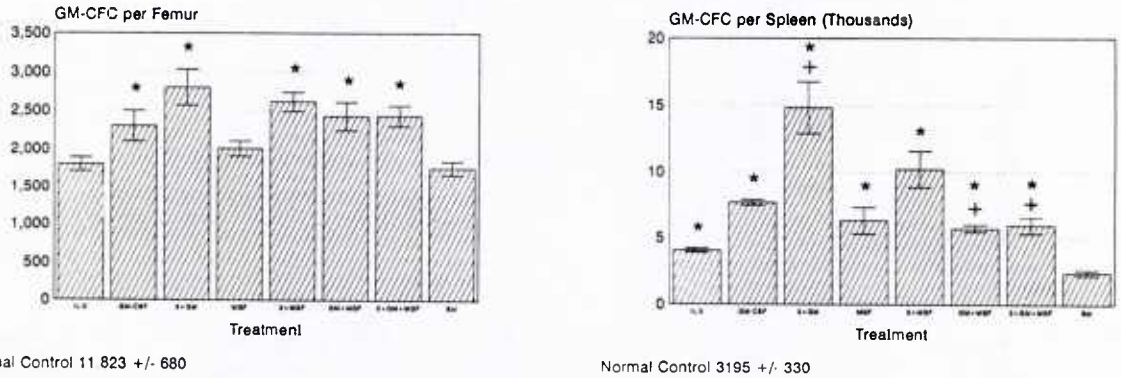

Fig. 5. Effects of MGF plus GM-CSF and IL–3 (each 100 μg/kg/d, s.c.) on postirradiation recovery of bone marrow and splenic GM-CFC recovery in sublethally irradiated (7.75 Gy) B6D2F1 mice. Data represent the mean ± SE of values obtained from one experiment. * $p < 0.05$, with respect to saline controls; + $p < 0.05$, with respect to GM-CSF values.

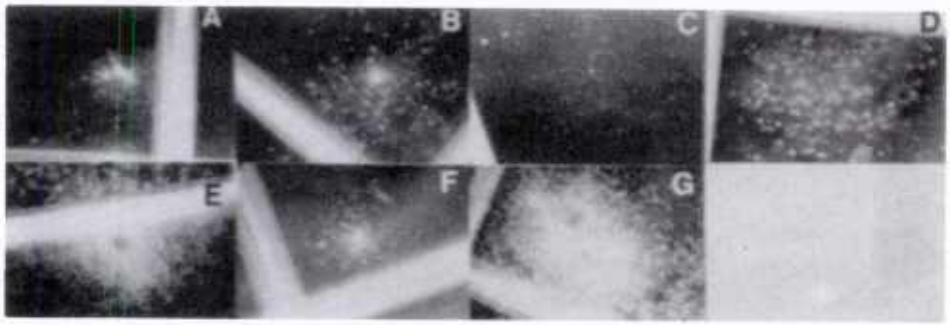

Fig. 6. Photographs of normal B6D2F1 bone marrow GM-CFC colonies grown *in vitro* in the presence of various cytokines. Cultures contained 1×10^5 cells and 0.125 ng/plate of GM-CSF, 0.125 ng/plate of IL–3, 25 ng/plate of MGF, or combinations of the respective cytokine concentrations. All photos at 11X magnification. The "lines" apparent in the pictures represent culture plate grid-lines and were purposely photographed in each shot to give perspective to the colony size. A: MGF; B: GM-CSF; C: IL–3; D: GM-CSF plus IL–3; E: MGF plus GM-CSF; F: MGF plus IL–3; G: MGF plus GM-CSF plus IL–3.

Table 2. Effects of MGF, GM-CSF, and IL–3 on normal bone marrow GM-CFC colony formation when added *in vitro* to GM-CFC cultures[a].

	No MGF	0.125 ng MGF	12.5 ng MGF	25.0 ng MGF
—	—	0.0 ± 0.0	2.1 ± 0.6	12.4 ± 0.7
+ GM-CSF	29.8 ± 2.6	32.5 ± 2.3	61.0 ± 8.0	75.8 ± 7.0
			($p < 0.04$)	($p < 0.002$)
+ IL-3	0.0 ± 0.0	0.0 ± 0.0	8.2 ± 1.9	25.3 ± 2.2
			($p < 0.04$)	($p < 0.0001$)
+ GM-CSF + IL-3	35.7 ± 3.6	40.2 ± 5.7	73.5 ± 7.5	91.3 ± 7.7
			($p < 0.008$)	($p < 0.0001$)

[a] GM-CFC numbers per 1×10^5 normal B6D2F1 bone marrow cells cultured for 10 days in 0.33% soft agar. GM-CSF and IL–3 concentrations were always 0.125 ng/plt; MGF concentration varied and is indicated for each group. Data represent the mean ± SE of values obtained from four replicate experiments. Endotoxin serum control cultures had 84.3 ± 4.6 colonies.

same concentration induced suboptimal colony formation compared to control colony formation generated by endotoxin serum (29.8 ± 2.6 colonies vs 84.3 ± 4.6 colonies, $p < 0.0001$). When these concentrations of IL–3 and GM-CSF were used in combination, a slight enhancement in GM-CFC colony number and a clear enhancement in colony size were observed in comparison to GM-CSF-induced growth alone (Fig. 6).

To investigate potential synergistic effects of MGF, bone marrow cells were cultured with the 0.125-ng/plate concentrations of GM-CSF and IL–3 in the presence of increasing concentrations of MGF. MGF interacted with GM-CSF and IL–3 to increase both GM-CFC colony number and colony size (Table 2; Fig. 6). The effects were directly proportional to MGF concentration, with the lowest concentration producing no significant interactive effects. When all three cytokines were combined, an even more dramatic synergy was observed, especially with respect to colony size (Table 2; Fig. 6).

An additional interesting observation was an increase in the appearance of obvious "doublet" colonies which were detected at a frequency of 7.5 ± 2.5 per 10^5 bone marrow cells in cultures stimulated with endotoxin sera (Table 3). These colonies appeared to arise from a single division of a primitive cell, from which each daughter cell then proliferated to form large overlapping individual colonies. In cytokine cultures, such colonies were only observed in cultures containing the higher concentrations of MGF in combination with GM-CSF, or in combination with GM-CSF plus IL–3; the addition of IL–3 to MGF plus GM-CSF significantly increased the incidence of these characteristic "doublet" colonies in the cultures (e.g., 30.0 ± 4.1 vs 14.5 ± 0.5, $p < 0.005$).

In Vitro Studies Performed with Bone Marrow Cells Obtained from Irradiated Mice

Because the possibility existed that hemopoietic progenitor cells in irradiated mice may respond differently to cytokines than hemopoietic progenitor cells in normal mice, additional *in vitro* studies were performed using bone marrow target cells obtained from mice 17 days after exposure to 7.75 Gy ^{60}Co. In these studies, bone marrow cells were cultured in the presence of the cytokine concentrations inducing the most dramatic effects on normal bone marrow cells i.e., 25 ng/plate of MGF, 0.125 ng/plate of GM-CSF, 0.125 ng/plate of IL–3, and the respective combinations (Table 4). Although the total number of colonies obtained from 10^5 irradiated bone marrow cells was in all instances less than the total number of colonies obtained from the same number of normal bone

Table 3. Effects of MGF, GM-CSF, and IL–3 on normal bone marrow "Doublet" GM-CFC colony formation when added *in vitro* to GM-CFC cultures[a].

	No MGF	0.125 ng MGF	12.5 ng MGF	25.0 ng MGF
—	—	0.0 ± 0.0	0.0 ± 0.0	0.0 ± 0.0
+ GM-CSF	0.0 ± 0.0	0.0 ± 0.0	6.5 ± 1.5 ($p < 0.02$)	14.5 ± 0.5 ($p < 0.0001$)
+ IL-3	0.0 ± 0.0	0.0 ± 0.0	0.0 ± 0.0	0.0 ± 0.0
+ GM-CSF + IL-3	0.0 ± 0.0	0.0 ± 0.0	9.0 ± 2.0 ($p < 0.02$)	30.0 ± 4.1 ($p < 0.0001$)

[a] GM-CFC numbers per 1×10^5 normal B6D2F1 bone marrow cells cultured for 10 days in 0.33% soft agar. GM-CSF and IL–3 concentrations were always 0.125 ng/plt; MGF concentration varied and is indicated for each group. Data represent the mean ± SE of values obtained from four replicate experiments. Endotoxin serum control cultures had 7.5 ± 2.5 doublet colonies.

marrow cells, results were qualitatively similar in that the addition of MGF to cultures containing GM-CSF, IL–3, or GM-CSF plus IL–3 clearly enhanced the colony formation stimulated by these factors alone.

Discussion

Morbidity and mortality associated with high-dose irradiation can be directly attributed to infectious and hemorrhagic complications resulting from radiation-induced neutropenia and thrombocytopenia. Sustained hemopoietic recovery following chemotherapy or radiation exposure requires surviving pluripotent stem cells to self-renew as well as to differentiate into multipotent and committed progenitors capable of giving rise to functional mature cells. In recent years, administration of single hemopoietic growth factors, including G-CSF, GM-CSF, MGF, IL–1 and IL–6, has been shown to stimulate hemopoietic regeneration when administered following radiation- or chemotherapy-induced myelosuppression [13, 27, 29, 36–41]. In addition, some cytokine combinations have proven to surpass the effectiveness of single agents [28–29, 42]. In particular, the combination of GM-CSF plus IL–3 has proven to be quite effective in accelerating the postirradiation regeneration of both neutrophils and platelets [29], as has the recently developed GM-CSF/IL–3 fusion protein, PIXY321 [43]. Because c-*kit* ligand, *in vitro*, has been shown to synergize with GM-CSF or GM-CSF plus IL–3 in stimulating progenitor cell proliferation and expansion [6–8, 14–16, 30–31], we hypothesized that administration of MGF in combination with these cytokines *in vivo* may further improve hemopoietic regeneration beyond that obtained with only GM-CSF or GM-CSF plus IL–3. Unexpectedly, MGF did not further enhance the regenerative hemopoietic effects of GM-CSF or GM-CSF plus IL–3 in sublethally irradiated mice. Furthermore, in some instances, hemopoietic responses induced by these cytokines *in vivo* were actually down-regulated by coadministration of MGF.

Our *in vivo* results directly contrast both results of previous *in vitro* studies demonstrating synergistic hemopoietic stimulation with c-*kit* ligand in combination with GM-CSF or GM-CSF plus IL–3, and *in vitro* results generated in our own laboratory. The *in vitro* data presented in Tables 2–4 and Figure 6 clearly demonstrate that our MGF was capable of augmenting GM-CSF-stimulated or GM-CSF-plus-IL–3-stimulated GM-CFC colony formation from bone marrow cells obtained from either normal or irradiated mice, thus eliminating the possibility that regenerating bone marrow

Table 4. Effects of MGF, GM-CSF, and IL–3 on irradiated bone marrow GM-CFC colony formation when added *in vitro* to GM-CFC cultures[a].

	MGF Present	Regular Col	Doublet Col
+ GM-CSF	No	22.6 ± 2.2	1.0 ± 0.4
	Yes	38.3 ± 1.7	4.3 ± 0.9
		($p < 0.0001$)	($p < 0.05$)
+ IL-3	No	0.0 ± 0.0	0.0 ± 0.0
	Yes	2.0 ± 0.7	0.0 ± 0.0
+ GM-CSF + IL-3	No	27.4 ± 1.5	1.7 ± 0.2
	Yes	41.9 ± 2.3	5.2 ± 0.9
		($p < 0.0001$)	($p < 0.05$)
—	Yes	0.0 ± 0.0	0.0 ± 0.0

[a] GM-CFC numbers per 1×10^5 bone marrow cells obtained from 7.75-Gy irradiated B6D2F1 mice on day 17 postexposure and cultured for 10 days in 0.33% soft agar. GM-CSF and IL–3 concentrations were always 0.125 ng/plt; MGF concentration was 25 ng/plt. Data represents the mean ± SE of values obtained from four replicate experiments. Endotoxin serum control cultures had 35.2 ± 3.1 regular colonies and 1.9 ± 0.3 doublet colonies.

cells in irradiated mice are somehow unresponsive to MGF-mediated effects. Furthermore, since the same MGF, GM-CSF, and IL–3 cytokine stocks were used for both our *in vivo* and our *in vitro* studies, and since *in vitro* studies were performed at a later time than *in vivo* studies, differences in cytokine batches, or loss of cytokine activities can be excluded as explanations for the contrasting effects observed in *in vivo* versus *in vitro* studies.

Although the possibility that the MGF dose used in our *in vivo* studies induced suppression because it was too high cannot be eliminated, this seems unlikely since the 100 ug/kg/d MGF dose used was at the low end of the 100–200 ug/kg/d MGF dose range which we have shown to be capable of accelerating hemopoietic recovery in myelosuppressed animals [27]. Our studies do, however, suggest that cytokine dose ratios may play a critical role in eliciting synergistic hemopoietic responses. In our *in vitro* studies performed with normal bone marrow cells, no MGF-induced synergy was observed in GM-CSF, IL–3, or GM-CSF plus IL–3 cultures when the MGF concentration was equal to other cytokine concentrations (i.e., 0.125 ng/plate of each cytokine); however, when MGF concentration exceeded the other cytokine concentrations by 100–200 fold (i.e., the 12.5 ng/plate and 25 ng/plate MGF concentrations), extremely significant enhancement in colony formation was observed. Hence, these results suggest that an excessive MGF concentration may be required in order to obtain synergy. Since our *in vivo* studies employed an equal dose of each cytokine (100 μg/kg/d), it may be that the MGF dose administered *in vivo* was simply insufficient to observe synergy. However, because individual cytokines differ pharmacokineticaly, and pharmacokinetics can dramatically alter the bioavailability of agents *in vivo*, it is difficult to directly compare *in vitro* and *in vivo* cytokine dose relationships. Although the MGF dose used in our *in vivo* studies was not synergistic with GM-CSF or GM-CSF plus IL–3, it was biologically active as evidenced by the fact that, in some instances,

this MGF dose actually *down-regulated* responses induced by GM-CSF alone or GM-CSF plus IL–3.

The reason for the hemopoietic down-modulation observed *in vivo* following MGF coadministered with GM-CSF or GM-CSF plus IL–3 is uncertain. C-*kit* ligand is known to exist both as an integral membrane-associated protein possessing an extracellular domain, transmembrane domain, and intracytoplasmic domain, as well as to exist as a soluble protein produced by proteolytic cleavage of the membrane-associated form [3, 6, 10, 44]. The membrane-associated protein is readily produced by hemopoietic stromal elements [44–46]. In spite of the fact that hemopoietic precursor cells can clearly respond to soluble c-*kit* ligand [22], it has been suggested that the stromal membrane-bound form is perhaps more important than the soluble form in regulating *in situ* hemopoiesis [44–46]. The MGF used in our studies was a soluble c-*kit* ligand. Since irradiation alone has been shown to increase c-*kit* ligand expression [47], in conjunction with exogenous MGF administration, c-*kit* ligand concentration may have become sufficient in irradiated mice to saturate c-*kit* (i.e., the c-*kit* ligand receptors) present on hemopoietic precursor cells. Such receptor blockade could prevent the binding of hemopoietic precursor cells to hemopoietic stromal elements *via* membrane-associated stromal c-*kit* ligand, hence interfering with subsequent hemopoietic proliferation and differentiation signals that may be stromal mediated. However, since down-modulation of hemopoiesis by MGF was only observed when MGF was coadministered with the otherwise stimulatory GM-CSF or GM-CSF plus IL–3 treatments, it is perhaps more plausible that MGF may down-modulate GM-CSF receptor expression. IL–3 receptor expression, on the other hand, does not appear to be affected since control mice administered MGF plus IL–3 actually exhibited better hemopoietic recovery than the recovery induced by either of these cytokines administered alone.

Little information has been published on *in vivo* effects of c-*kit* ligand in combination with other cytokines. However, Ulich et al. did report the ability of coadministered c-*kit* ligand (SCF) and GM-CSF to synergistically increase bone marrow GM-CFC and neutrophil numbers in normal rats [48]. There are several major differences between Ulich's study and ours which may explain the contrasting effects observed in the two studies. First, Ulich utilized a polyethyleneglycol (PEG) modified c-*kit* ligand (PEGalated recombinant rat SCF). The MGF used in our studies was not PEGalated. PEG modification can increase the *in vivo* bioavailability of proteins by altering pharmacological properties such as extending plasma half-life and increasing resistance to proteolysis [49]. Whether PEGalation alone may account for some of the hematological differences observed between our study and that of Ulich is not certain. Second, *c-kit* ligand:GM-CSF dose ratios and cytokine administration protocols differed significantly between the two studies. The MGF:GM-CSF dose ratio administered in our study was 1:1, while a 5:1 SCF:GM-CSF dose ratio was administered in Ulich's study. Furthermore, in our study cytokines were administered subcutaneously for 17 days, while in Ulich's study cytokines were administered intravenously for only 7 days. Both of these differences may have altered the effects of the injected cytokines. The length of the treatment protocol, in particular, may have had a significant impact. With respect to c-*kit* ligand administration, in normal mice receiving s.c. injections of PEG-SCF (100 μg/kg/d) over a 21-day period, it has been noted that although leukocytosis initially occurs, by day 18 cell counts drop to subnormal levels despite continued SCF treatment [24]. Ulich's study evaluated responses only through 7 days of treatment; had treatment continued, suppressive effects may have also been observed in his study.

Another possible explanation for the differences observed in our two studies could relate to the fact that normal animals were used in Ulich's study, while irradiated animals were used in ours. Previous studies performed in our laboratory with IL–3, GM-CSF, and the combination of these cytokines have revealed conflicting responses elicited in normal versus irradiated primates, despite identical cytokine administration

protocols [28; MacVittie, unpublished]. In fact, Schuening et al. very recently have reported on the effects of coadministered PEG-SCF (recombinant canine SCF; 200 ug/kg/d × 21 days, s.c.) and G-CSF (recombinant canine; 10 ug/kg/d × 21 days, s.c.) in canines exposed to an otherwise lethal 5 Gy irradiation [26]; the effects were different from the synergistic effects observed by others when these two cytokines were coadministered to normal animals [24, 48]. Although in combination-treated irradiated canines Schuening et al. did not report a down modulaton of G-CSF-induced responses as we have observed in irradiated mice coadministered MGF and GM-CSF (or GM-CSF + IL–3), the granulocyte, platelet, and survival responses they observed were not better than those induced by the individual cytokines. Thus, Schuening's results further stress the variation in responses elicited following cytokine administration in compromised animals. Since we have recently demonstrated that endogenous production of several cytokines increases dramatically following radiation exposure such as that used in our studies presented in this paper [47, 50], it seems plausible that cytokine-cytokine interactions could be very different in radiation-induced aplastic animals than in normal animals.

In conclusion, our studies demonstrate that MGF administered *in vivo* either does not affect or in some cases even down-regulates regenerative responses induced by GM-CSF or GM-CSF plus IL–3 in sublethally irradiated mice, and that these responses sharply contrast the *in vitro* effects of these cytokines. Furthermore, these studies emphasize that caution must be taken in attempting to predict cytokine interactions *in vivo* in hemopoietically injured animals based on *in vitro* cytokine effects or cytokine effects in normal animals.

Acknowledgements

We are grateful to Ruth Seemann and Joe Parker for excellent technical assistance, to William Jackson for statistical analysis, and to Modeste Greenville for editorial assistance. This work was supported by the Armed Forces Radiobiology Research Institute, Defense Nuclear Agency, under research work unit 00132. Research was conducted according to the principles enunciated in the Guide for the Care and Use of Laboratory Animals prepared by the Institute of Laboratory Animal Resources, National Research Council.

References

1. Witte ON. *Steel* locus defines new multipotent growth factor. Cell 1990; 63: 5–6.
2. Williams DE, Eisenman J, Baird A, Rauch C, Van Ness K, March CJ, Park LS, Martin U, Mochizuki DY, Boswell HS, Burgess GS, Cosman D., Lyman SD. Identification of a ligand for the c-*kit* proto-oncogene. Cell 1990; 63: 167–74.
3. Zsebo KM, Wypych J, McNeice IK, Lu HS, Smith KA, Karkare SB, Sachdev RK, Yuschenkoff VN, Brikett NC, Williams LR, Satyagal VN, Tung W, Bosselman RA, Mendiaz EA, Langley KE. Identification, purification, and biological characterization of hematopoietic stem cell factor from buffalo rat liver-conditioned medium. Cell 1990; 63: 195–201.
4. Nocka K, Buck J, Levi E, Besmer P. Candidate ligand for the c-*kit* transmembrane kinase receptor: KL, a fibroblast derived growth factor stimulates mast cells and erythroid progenitors, EMBO J 1990; 9: 3287–94.
5. Williams DE, DeVries P, Namen AE, Widmer MB, Lyman SD. The *Steel* factor. Develop Biol 1992; 151: 368–76.
6. Martin FH, Suggs SV, Langley KE, Lu HS, Ting J, Okino KH, Morris F, McNeice IK, Jacobsen FW, Mendiaz EA, Birkett NC, Smith KA, Johnson MJ, Parker VP, Flores JC, Patel AC, Fischer EF, Erjavec HO, Herrera CJ, Wypych J, Sachdev RK, Pope JA, Leslie I, Wen D, Lin CH, Cupples RL, Zsebo KM. Primary structure and functional expression of rat and human stem cell factor DNAs. Cell 1990; 63: 203–11.
7. McNeice IK, Langley KE, Zsebo KM. Recombinant human stem cell factor synergizes with GM-CSF, G-CSF, IL–3, and Epo to stimulate human progenitor cells of the mycloid and erythroid lineages. Exp Hematol 1991; 19: 226–31.
8. Broxmeyer HA, Hangoc G, Cooper S, Anderson D, Cosman D, Lyman SD, Williams DE. Influence of murine mast cell growth factor (c-*kit* ligand) on colony formation by mouse marrow hematopoietic progenitor cells. Exp Hematol 1991; 19: 143–6.
9. Williams N, Bertoncello I, Kavnoudias H, Zsebo KM, McNeice I. Recombinant rat stem cell factor stimulates the amplification and differentiation of fractionated mouse stem cell populations. Blood 1992; 79: 58–64.

10. Anderson DM, Lyman SD, Baird A, Wingnall JM, Eisenman J, Rauch C, March CJ, Boswell S, Gimpel SD, Cosman D, Williams DE. Molecular cloning of mast cell growth factor, a hematopoietin that is active in both membrane bound and soluble forms. Cell 1990; 63: 235–43.
11. DeVries P, Brasel KA, Eisenman JR, Alpert AR, Williams DE. The effect of recombinant mast cell growth factor on purified murine hematopoietic stem cells. J Exp Med 1991; 173: 1205–11.
12. Carow CE, Hangoc G, Cooper SH, Williams DE, Broxmeyer HE. Mast cell growth factor (c-*kit* ligand) supports the growth of human multipotential progenitor cells with a high replating potential. Blood 1991; 78: 2216–21.
13. Moore MAS. Clinical implications of positive and negative hematopoietic stem cell regulators. Blood 1991; 78: 1–19.
14. Bernstein ID, Andrews RG, Zsebo KM. Recombinant human stem cell factor enhances the formation of colonies by CD34+ and CD34+Lin- cells, and the generation of colony-forming cell progeny from CD34+Lin- cells cultured with interleukin–3, granulocyte colony-stimulating factor, or granulocyte-macrophage colony-stimulating factor. Blood 1991; 77: 2316–21.
15. Brandt J, Briddell RA, Srour EF, Leemhuis TB, Hoffman R. The role of c-*kit* ligand in the expansion of human hematopoietic progenitor cells. Blood 1992; 79: 634–41.
16. Heyworth CM, Whetton AD, Nicholls S, Zsebo K, Dexter TM. Stem cell factor directly stimulates the development of enriched granulocyte-macrophage colony-forming cells and promotes the effects of other colony-stimulating factors. Blood 1992; 80: 2230–6.
17. Migliaccio G, Migliaccio AR, Valinsky J, Langley K, Zsebo KM, Visser JWM, Adamson JW. Stem cell factor induces proliferation and differentiation of highly enriched murine hematopoietic cells. Proc Natl Acad Sci USA 1991; 88: 7420–4.
18. Bernstein SE, Russell ES, Keigh'ey G. Two hereditary mouse anemias (*Sl/Sl*^{d} and *W/W*^{v}) deficient in response to erythropoietin. Ann NY Acad Sci 1968; 149: 475–85.
19. Kitamura Y, Go S. Decreased production of mast cells in *Sl/Sl*^{d} anemic mice. Blood 1979; 53: 492–7.
20. Ebbe S, Phalen E, Stohlman FJ. Abnormal megakaryocytopoiesis in *Sl/Sl*^{d} mice. Blood 1973; 42: 865–71.
21. Ruscetti FN, Boggs DR, Torok BJ, Boggs SS. Reduced blood and marrow neutrophils and granulocytic colony forming cells in *Sl/Sl*^{d} mice. Proc Soc Exp Biol Med 1976; 152: 398–402.
22. Zsebo KM, Williams DA, Geissler EN, Broudy VC, Martin FH, Atkins HL, Hsu RY, Birkett NC, Okino KH, Murdock DC, Jacobsen FW, Langley KE, Smith KA, Takeishi T, Cattanach BM, Galli SJ, Suggs SV. Stem cell factor is encoded at the *Sl* locus of the mouse and is the ligand for the c-*kit* tyrosine kinase receptor. Cell 1990; 63: 213–24.
23. Ulich TR, Castillo J, Yi ES, Yin S, McNiece I, Yung YP, Zsebo KM. Hematologic effects of stem cell factor *in vivo* and *in vitro* in rodents. Blood 1991; 78: 645–50.
24. Molineux G, Migdalska A, Szmitkowski M, Zsebo KM, Dexter TM. The effects on hematopoiesis of recombinant stem cell factor (ligand for c-*kit*) administered *in vivo* to mice either alone or in combination with granulocyte colony-stimulating factor. Blood 1991; 78: 961–6.
25. Andrews RG, Knitter GH, Bartelmez SH, Langley KE, Farrar D, Hendren W, Appelbaum FR, Bernstein ID, Zsebo KM. Recombinant human stem cell factor, c-*kit* ligand, stimulates hemopoiesis in primates. Blood 1991; 78: 1975–80.
26. Schuening FG, Appelbaum FR, Deeg HJ, Sulivan-Pepe M, Graham R, Hackman R, Zsebo KM, Strob R. Effects of recombinant canine stem cell factor, a *c-kit* ligand, and recombinant granulocyte colony-stimulating factor on hematopoietic recovery after otherwise lethal total-body irradiation. Blood 1993; 81: 20–6.
27. Patchen ML, Fischer R, Williams DE. C-*kit* ligand enhances multilineage hemopoietic recovery *in vivo* following radiation-induced aplasia. Exp Hematol (In press).
28. MacVittie TJ, Monroy RL, Farese AM, Patchen ML, Seiler FR, Williams DE. Cytokine therapy in canine and primate models of radiation-induced marrow aplasia. Behring Inst Mitt 1991; 90: 1–13.
29. Farese AM, Williams DE, Seiler FR, MacVittie TJ. Combination protocols of cytokine therapy with IL–3 and GM-CSF in a primate model of radiation-induced marrow aplasia. Blood, 1993; 82: 3012–3018
30. Hendri PC, Miyazawa K, Yang YC, Langefeld CD, Broxmeyer HE. Mast cell growth factor (c-*kit* ligand) enhances cytokine stimulation of proliferation of the human factor-dependent cell line M07e. Exp Hematol 1991; 19: 1031–7.
31. Xiao M, Leemhuis T, Broxmeyer HE, Lu L. Influence of combinations of cytokines on proliferation of isolated single cell sorted human bone marrow hematopoietic progenitor cells in the absence and presence of serum. Exp Hematol 1992; 20: 276–9.
32. Urdal DL, Mochizuki D, Conlon PJ, March CJ, Remerowski ML, Eisenmann J, Ramthun C, Gillis S. Lymphokine purification by reversed phase high performance liquid chromatography. J Chromatogr 1984; 296: 171–9.
33. Schulz J, Almond PR, Cunningham JR, Holt JG, Loevinger R, Suntharalingam N, Wright KA, Nath R, Lempert D. A protocol for the determination of absorbed dose for high energy photon and electron beams. Med Phys 1983; 10: 741–71.
34. Patchen ML, MacVittie TJ. Hemopoietic effects of intravenous soluble glucan administration. J Immunopharmacol 1986; 8: 407–25.
35. Till JE, McCulloch EA. A direct measurement of the radiation sensitivity of normal mouse bone marrow cells. Radiat Res 1961; 14: 213–22.
36. Robinson BE, Quesenberry P. Review: Hemopoietic growth factors: Overview and clinical applications, part I. Am J Med Sci 1990; 300: 163–70.
37. Patchen ML, MacVittie TJ, Solberg BD, Souza LM.

Therapeutic administration of recombinant human granulocyte colony-stimulating factor accelerated hemopoietic regeneration and enhances survival in a murine model of radiation-induced myelosuppression. Int J Cell Cloning 1990; 8: 107–22.
38. Patchen ML, MacVittie TJ, Williams JL, Schwartz GN, Souza LM. Administration of interleukin–6 stimulates multilineage hematopoiesis and accelerates recovery from radiation-induced hematopoietic depression. Blood 1991; 77: 472–80.
39. Morrissey P, Charrier K, Bressler L, Alpert A. The influence of IL–1 treatment on the reconstitution of the hemopoietic and immune systems after sublethal radiation. J Immunol 1988; 140: 4204–10.
40. Laver J, Abboud M, Gasparetto C, Gillio A, Smith C, O'Reilly RJ, Moore MA. Effects of IL–1 on hematopoietic progenitors after myelosuppressive chemoradiotherapy. Biotherapy 1989; 1: 293–300.
41. Neta R, Oppenheim JJ. Cytokines in therapy of radiation injury. Blood 1988; 72: 1093–5.
42. Patchen ML, Fischer R, MacVittie TJ. Effects of combination interleukin–6 and granulocyte colony-stimulating factor on recovery from radiation-induced hemopoietic aplasia. Exp Hematol 1993; 21: 338–44.
43. Williams DE, Dunn JT, Park LS, Frieden EA, Seiler FR, Farese AM, MacVittie TJ. A GM/IL–3 fusion protein promotes neutrophil and platelet recovery in sublethally irradiated rhesus monkeys. Biotech Ther 1993.
44. Flanagan JG, Leder P. The c-*kit* ligand: A cell surface molecule altered in *Steel* mutant fibroblasts. Cell 1990; 63: 185–94.
45. Aye MT, Hashemi S, Leclair B, Zeibdawi A, Trudel E, Halpenny M, Fuller V, Cheng G. Expression of stem cell factor and c-*kit* mRNA in cultured endothelial cells, monocytes, and cultured human bone marrow stromal cells (CFU-RF). Exp Hematol 1992; 20: 523–7.
46. Brannan CI, Lyman CD, Williams DE, Eisenman J, Anderson DM, Cosman D, Dedell MA, Jenkins NA, Copeland NG. Steel-Dickie mutation encodes c-*kit* ligand lacking transmembrane and cytoplasmic domains. Proc Natl Acad Sci USA 1991; 88: 4671–7.
47. Chang CM, Baker WH, Limanni A, Williams JL, Fragoso L, Patchen ML. *In vivo* gene expression of interleukin–3, granulocyte-macrophage colony-stimulating factor, and c-*kit* ligand in murine bone marrow and spleen after sublethal irradiation. Exp Hematol 1991; 20: 775.
48. Ulich TR, Del Castillo J, McNiece IK, Yi ES, Alzona CP, Yin S, Zsebo KM. Stem cell factor in combination with granulocyte colony-stimulating factor (CSF) and granulocyte-macrophage CSF synergistically increase granulopoiesis. Blood 1991; 78: 1954–62.
49. Ahern TJ, Manning MC. Stability of protein pharmaceuticals: *In vivo* pathways of degradation and strategies for protein stabilization. New York: Plenum, 1991.
50. Baker WH, Limanni A, Chang CM, Williams JL, Patchen ML. Comparison of interleukin–1 mRNA expression in murine spleens after lethal and sublethal cobalt–60 irradiation. Exp Hematol 1992; 20: 771.

Pergamon

Adv. Space Res. Vol. 14, No. 10, pp. (10)181–(10)201, 1994
1994 COSPAR

0273–1177/94 $7.00 + 0.00

ENERGY AND CHARGE LOCALIZATION IN IRRADIATED DNA

C. E. Swenberg,* L. S. Myers, Jr* and J. H. Miller**

** Armed Forces Radiobiology Research Institute, 8901 Wisconsin Avenue, Bethesda, MD 20889-5603, U.S.A.*
*** Pacific Northwest Laboratory, PO Box 999, Richland, WA 99352, U.S.A.*

ABSTRACT

The relation between the site of energy deposition and the site of its biological action is an important question in radiobiology. Even at 77°K, evidence is clear that these two sites must be separated since energy deposition is random but specific products are formed. Several processes that may contribute to this separation are: 1) hole migration and stabilization through deprotonation to give neutral oxidation product radicals; 2) electron trapping and transfer to form specific radical anions, possibly followed by protonation to give neutral reduction product radicals; and 3) recombination of spatially separated charges or radicals. These microscopic processes will be reviewed critically in an analysis using electron paramagnetic resonance spectroscopy (EPR) evidence for and against long-range transfer of energy and/or charge in frozen, hydrated DNA.

INTRODUCTION

A strongly held tenet of radiobiology is that damage of DNA mediates many of the cellular effects of ionizing radiation. Whether the damage results from attack on DNA by ·OH (hydroxyl free radical) or other radicals formed at a distance from a DNA molecule (indirect effect) or from energy deposited directly in a DNA molecule by radiation (direct effect) has been the subject of debate for many years /1/. Growing evidence indicates that the direct effect, defined to include deposition of energy in DNA and water molecules closely associated with DNA (the hydration layer or layers) plays a critically important role in cellular responses to radiation /2,3/. It follows that investigations of the localization of energy and charge in irradiated DNA are urgently needed.

Experimental studies have shown convincingly that the radiation chemistry of DNA is critically dependent on experimental conditions. The type of salt and its concentration /4/, and the state of DNA hydration /5,6,7/ are among the variables that effect

DNA chemistry. EPR spectroscopy has provided a most valuable experimental tool to develop insight into the fundamental processes involved in DNA damage reactions. EPR spectra ranging from a 0.9mT "singlet" spectrum to a 14mT octet spectrum were reported for irradiated DNA as early as 1972 /8/. Sorting out the factors contributing to spectral variation has taken the efforts of many outstanding investigators. A major contribution in elucidating DNA radiation chemistry at low temperature was the preparation by Rupprecht /9/ of oriented DNA fibers by the wet spinning technique. Samples prepared in different ionic environments have made it possible to compare the radiolysis products of DNA obtained with different types of radiation and with different orientations of the DNA fiber axis relative to the radiation beam direction. Results have been surprising. We note here that exposure of such samples to gamma radiation at 77°K and measured at 77°K resulted in EPR spectra interpreted in terms of G radical cations* and T and/or C radical anions /10,11/. Exposure of samples

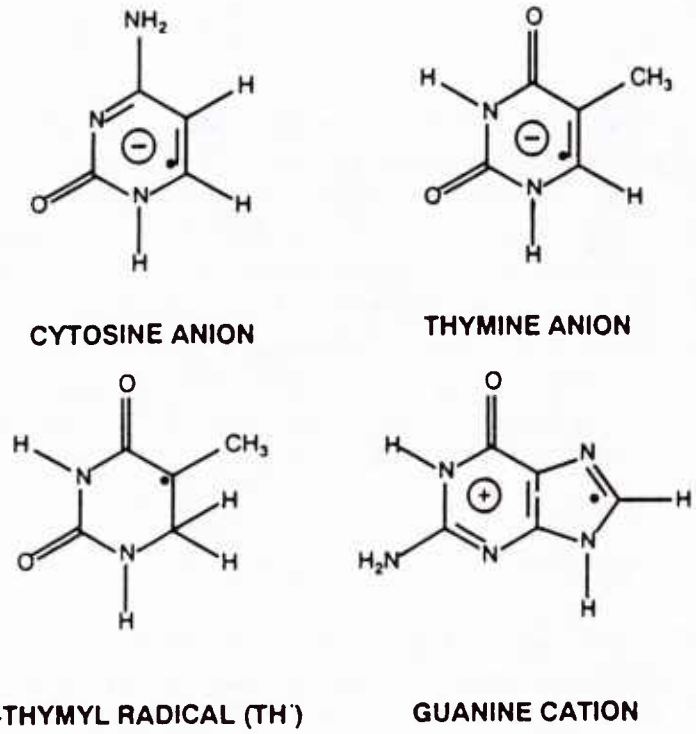

Fig. 1. Free radicals identified by EPR spectroscopy at 77°K in DNA irradiated at 77°K.

under similar conditions to neutrons resulted in similar spectra if the neutron beam was perpendicular to the DNA helix axis; however, if the beam was parallel to this axis, the EPR spectra indicated the presence of the neutral radiation product, the dihydrothymidin-5-yl (TH˙) radical /12/. For proton irradiation, however, the TH˙

---

*The following symbols are used for the DNA bases: G=guanine; A=adenine; C=cytosine; T=thymine

spectrum was observed with both parallel and perpendicular beam orientations /13/. Figure 1 summarizes the free radicals identified in irradiated DNA at low temperatures.

Attempts have been made to explain these results in terms of a variety of microscopic long-range transfer mechanisms, such as triplet exciton migration /12,14/, polaron transport /14/ and solitons /14/. We discuss these mechanisms critically in view of recent research advances. We first consider whether the occurrence of different radicals produced by different kinds of ionizing radiation are artifacts or properties of the systems. We then address whether the microscopic energy deposition pattern is sufficient to explain the results or whether long-range migration of energy and/or charge is required and how this migration might best be described.

Specifically, we question whether neutral triplet or singlet state migration provides an explanation of the neutron results. This is followed by a short discussion as to whether solitons or other DNA collective states or polaron transport are involved in the neutron and proton results. We then address whether other microscopic track phenomena are operative. Charge recombination and charge trapping in dense particle tracks are briefly discussed and their effects on total radical yields are summarized. The paper inconcludes a brief discussion of the reaction(s) that might account for the appearance of $TH^{\cdot}$ at low temperatures and concludes with suggestions for plausible future research.

EXPERIMENTAL BACKGROUND SUMMARY

Samples: All experiments were performed at 77°K with either oriented Na-DNA samples prepared by Rupprecht /9/ using the wet spinning technique or in some of the neutron experiments, by Arroyo et al. /12/ using the procedure of Rupprecht. Samples for the proton irradiations were carefully prepared because of the proton's short-range in the target medium, approximately 0.5 mm for 4 MeV protons. For experiments in which the DNA fibers were oriented perpendicularly to the beam, samples were made by pressing together a sufficient number of sheets of oriented DNA to give a sample thickness greater than the proton range. For the parallel proton irradiation configuration, samples were carefully sliced from a block of oriented DNA so that the ends of samples were not bent over so as to introduce spurious perpendicular components into the EPR data. Although the samples used for the proton experiments were approximately two years old, they were preserved under controlled conditions. X-ray diffraction studies on several specimens (personal communication, A. Rupprecht) demonstrated some distortions due to the pressure required to make the DNA film layers stick together in the original preparation and in the original splicing of the samples, but nothing significant to preclude failure to observed possible orientation effects. The DNA conformation /15/ as determined from independent samples is a mixture of the A-DNA form, where base planes are at 70° angles to the helix axis, and the B-DNA form (57%), where base planes form right angles to the DNA helix axis. All samples were equilibrated with water vapor at 75% relative humidity; this gives a moisture content sufficient to almost fill the primary DNA hydration shell /16/. Figure 2 gives a plot of the number of water

molecules per nucleotide as a function of the relative humidity in the hydration chamber /7/.

Figure 2 emphasizes that even at 0% relative humidity, there are 2.5 H_2O molecules attached to the sodium phosphate groups per nucleotide. These water molecules are not removable via vacuum desiccation of DNA samples /17/. For our purpose we note that the tightly bound H_2O molecules (the first 12-15 water molecules) are impermeable to cations /18/. Another characteristic of this inner hydration shell is that it does not form an ice-like structure. The addition of approximately nine more H_2O molecules per nucleotide completes the filling of DNA primary hydration layer. It is in this latter layer of water molecules where charge transfer could possibly occur. Thus for a relative humidity of 75% the outer hydration layer is nearly filled, and furthermore contains sufficient water molecules to support charge transport along the DNA backbone.

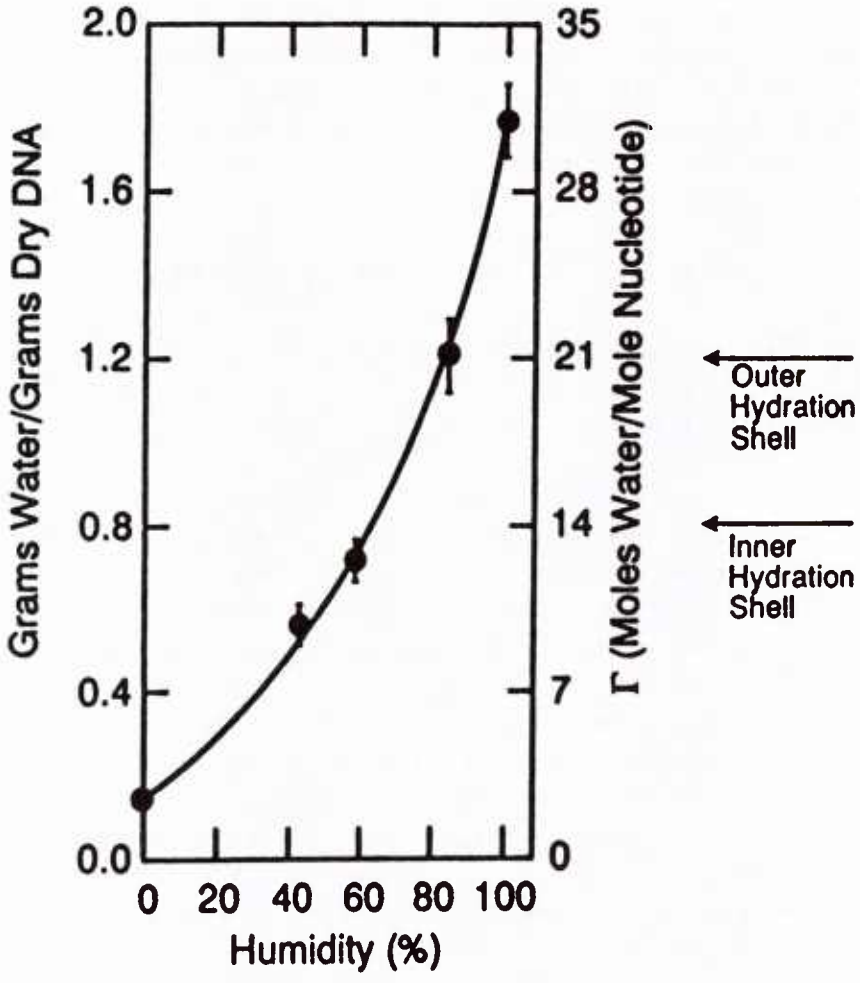

Fig. 2. Hydration of double stranded salmon sperm DNA as a function of relative humidity /7/.

Radiation Sources: The gamma radiation /10,11/ was from a ^{60}Co source. The neutron source was a small TRIGA research reactor. Bismuth shielding was utilized to reduce the gamma component to less than 3% of the total dose. This procedure (unfortunately) introduces a broad neutron spectrum (neutron with energies of 10^4eV to more than 10^7eV) with a broad peak near 1 MeV. Doses were measured by an indium foil technique. The principle neutron reaction for this energy range in tissue-like (water-like) media is elastic scattering of protons. The divergence of the neutron beam induces a diverging recoil proton beam suggesting that any orientation effects observed with neutrons might well be enhanced if a well collimated proton beam were employed. Such beams were obtained from a 2 MV tandem accelerator that provided monoenergetic protons with energy up to 4 MeV. As protons have short track ranges at these energies, only the front surfaces of the DNA samples were irradiated. Table 1 summarizes the parameters for the three experiments.

Table 1 Irradiation Parameters

Investigator	Radiation	Dose (kGy)	Dose-Rate (kGy/hr)
Graslund et al. /4,5/	Gamma	5	9
Arroyo et al. /7/	Neutron	15	25
Miller et al. /8/	Proton	50	150

EPR Analysis: X-band EPR spectra at 100 kHz and 1 to 2 gauss modulation amplitude were obtained with microwave powers of < 3μW (gamma experiments), 20 μW for spectra perpendicular to the incident neutron beam, 200 μW for the parallel radiation configuration and 12.5 mW for the proton experiments. Lower power was used in the gamma experiments to avoid saturation of the ion radical signals.

RESULTS

Irradiation with gamma rays resulted in the spectra shown in Figure 3 /10/. These spectra were interpreted as indicating the presence of the guanine radical cation and the thymine or cytosine radical anion. Recent studies of Bernhard /19,20,21/ indicate that the anion probably is a cytosine and that it may well be protonated /21/. Steenken /22/ has stressed the importance of protonation in influencing electron

attachment. For example, within a base pair, proton transfer will stabilize one electron reduction of cytosine. Bernhard /19/ has shown that the probability of electron attachment follows the relation T > C >> A > G, which is in agreement with calculated electron affinities of the bases /23,24/. The stacking in duplex DNA in aqueous media, however, permits electron transfer between the bases, and proton transfer from a hydrogen bonded partner may occur. Thus the tendency of the hydrogen bonded partner to deprotonate becomes an important factor. The observation that A is a poorer proton donor than G means that $C^{\cdot}$ is stablized by base pairing more than $T^{\cdot}$. Bernhard /19/ has shown that the following relative concentration relationships are expected in double stranded DNA: $[C^{\cdot} H^{+}] >> [A^{\cdot} H^{+}] \approx [T^{\cdot}] >> [G^{\cdot}]$. Note that thymine is the only base that should strongly form an electron adduct but is unlikely to protonate reversibly in this environment. On heating the sample and then recooling to 77°K the EPR spectrum shows the formation of neutral $TH^{\cdot}$ radicals /10,11/, and the disappearance of the ionic radicals and a reduction in the number of total spins. This is critically important in the explanation for the appearance of $TH^{\cdot}$ radicals.

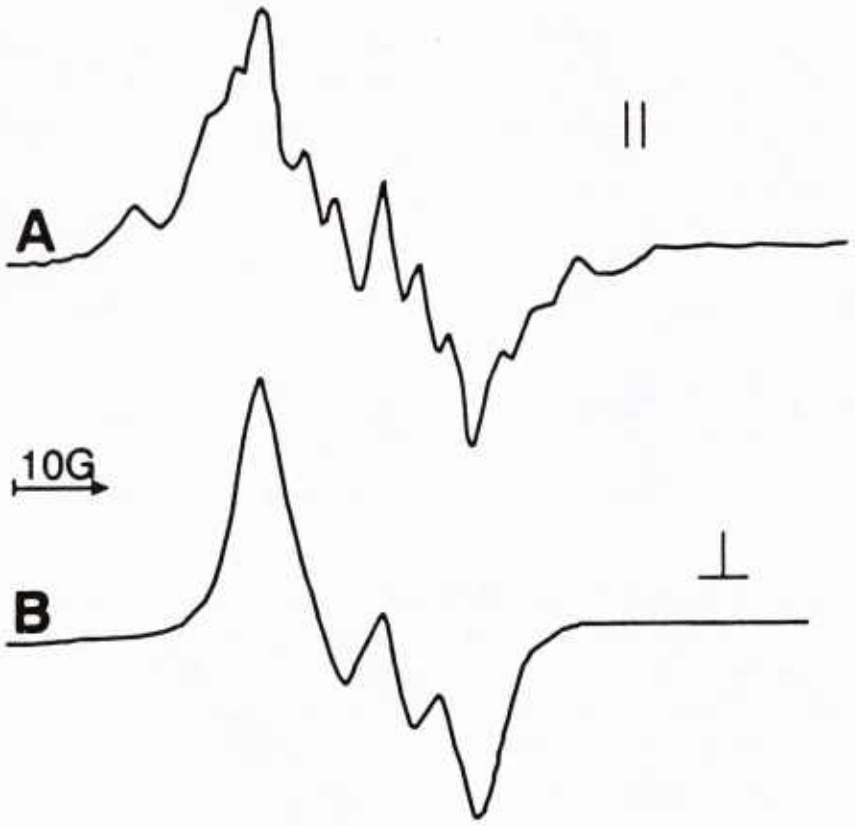

Fig. 3. EPR spectra of calf-thymus Na DNA irradiated with gamma rays /10/.

In contrast to the gamma-induced spectra, proton irradiation gave the spectra shown in Figure 4 /13/, indicative of the presence of neutral $TH^{\cdot}$ radicals.Spectra are similar both for parallel and perpendicular irradiation configuration. For neutron irradiation the EPR spectra obtained at 77°K are shown on Figure 5.

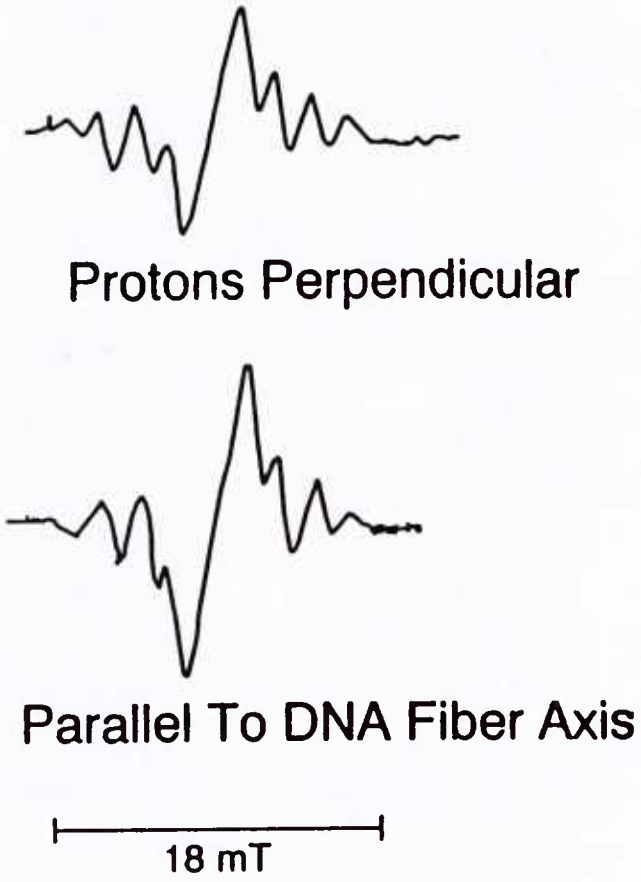

Fig. 4. EPR spectra at 77°K with 4 MeV protons /13/.

When the neutron beam was directed parallel to the DNA fiber axis, the neutral radical $TH^{\bullet}$ was formed; however, when the incident neutron flux was perpendicular to the fiber axis, the spectra showed the presence of radical anions. The EPR data raise the following questions: (1) by what mechanism(s) does proton radiation give the neutral protonated reduction product ($TH^{\bullet}$) whereas gamma radiation at 77°K gives only ionic products? and (2) by what mechanism(s) does neutron irradiation give spin products dependent on the direction of the neutron beam?

Are the results with protons and neutrons due to some problem with the experimental procedures? We have conducted an extensive review of the procedures used for the neutron and proton experiments. In the neutron experiments, two samples were mounted side by side within a liquid nitrogen cooled irradiation chamber so that the fiber orientation of one sample was perpendicular to the neutron beam and the orientation of the second sample was parallel to the incident beam. The samples, irradiated simultaneously, were treated identically so far as is known. Furthermore the experimenters successfully observed the ion radical signals after gamma irradiations, and samples prepared by Rupprecht and by Arroyo /12/ gave the same results. While, of course we can not completely eliminate the possibility that errors were made, we have considerable confidence in the results.

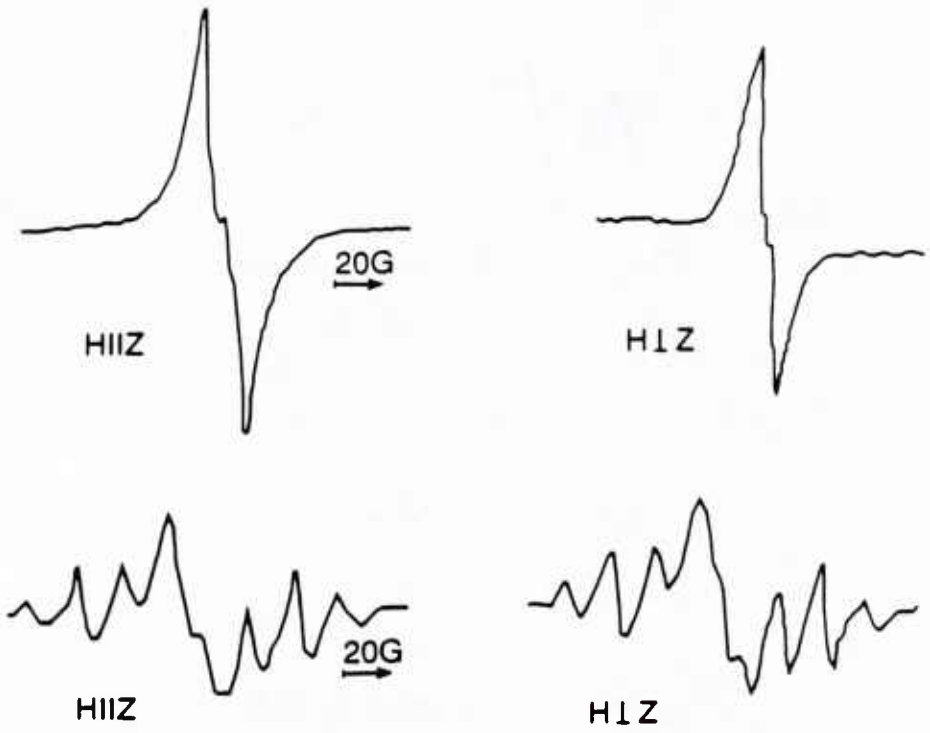

Fig. 5. EPR spectra from calf-thymus Na DNA irradiated with TRIGA-reactor neutrons /12/.

For the proton study, individual samples were irradiated in a liquid nitrogen cooled chamber and transferred to the EPR cavity. During the transfer the samples were exposed to a temperature > 77°K for less than one second. Comparing this time with the times at various temperatures required for the appearance of $TH^{\cdot}$ /11/, we feel confident that this step does not account for the results. Furthermore, the samples were examined by Rupprecht, and by his criteria, which included determination of X-ray diffraction patterns, they were satisfactory for the experiment. Thus we conclude that the results are not a consequence of any obvious or apparent experimental problem.

In the proton experiments, are the results due to macroscopic heat build-up during the irradiation accompanied by inefficient heat transfer from sample to coolant? Elementary calculations show that if all the energy deposited in the sample were retained and converted to heat, the temperature increase would be of the order of 10°K. Using reasonable estimates of the cooling, and considering the dose rate, etc., we estimate a temperature difference of about .002°K between the thermal reservoir at 77° and the irradiated part of the sample. Such a small temperature difference, even if underestimated by a factor of 10^3 would not be nearly enough to cause the formation of $TH^{\cdot}$ by the reaction path observed by Gräslund and coworkers /10,11/.

Does heat generated within the proton tracks in both the proton and neutron experiments explain the appearance of the protonated thymine? Several investigators /25,26,27/ have suggested that fast heavy ions with large stopping power result in

transient localized heated regions around the ion tracks. To estimate this effect we follow the treatment given by Mozumder /28/ who adopted a Gaussian statistical approximation. Solving the standard macroscopic heat equation for low LET radiation one finds the distribution of the excess temperature, where the spur is approximated by a sphere with size parameter r_o, to be:

$$\Delta T^{(1)}(r,t) = T_o\,(1 + 4\,\delta t/r_o^2)^{-3/2}\,\exp\{-r^2/(r_o^2 + 4\delta t)\}$$

Here T_o is the maximum excess temperature at the spur's center, r is the distance from the spur center, and δ is the thermal diffusivity and equals $X/\rho C_v$, the heat conductivity (X) divided by the product of the medium density (ρ) and specific heat (C_v) at constant volume. T_o is determined by the relationship:

$$E = \int_0^\infty \rho C_v\, T_o\, 4\pi\, r^2\, \exp(-r^2/r_o^2)dr$$

where E denotes the average energy deposited per charge pair in the spur, ≈30eV. For high LET ionizing particles traversing a medium a large number of phonons are created resulting in a high density of transient temperature pulses. These heated regions overlap and thereby form a cylindrical excess thermal distribution with initial radius r_o that can be approximated as:

$$\Delta T^{(3)}(r,t) = T_o(1 + 4\delta t/r_o^2)^{-1}\,\exp\{-r^2/(r_o^2 + 4\delta t)\}$$

where r is the transverse distance from the track axis. If S denotes the energy loss per unit distance, then

$$S = \frac{dE}{dx} = \int_0^\infty \rho C_v\, T_o 2\pi r\, \exp\{-r^2/r_o^2\}dr$$

determines the initial temperature T_o at the center of the cylindrical track. Figures 6A and 6B illustrate the time dependence of local heating for several r values assuming $\delta = 10^{-3}cm^2/sec$, $r_o = 20Å$, E = 30eV and S = 5eV/Å.

Variations for ΔT are quite similar and in both cases decay to the ambient temperature in approximately 10^{-10} to 10^{-9} seconds. Although these calculated temperature transients are similar, the effect of the heat spike on reaction rates is strongly dependent on dimensionality. Assuming an activation energy of 8 Kcal/mole, a substrate concentration of 10^{22} molecules/cm^3 and a collision frequency of 10^{11} s^{-1}

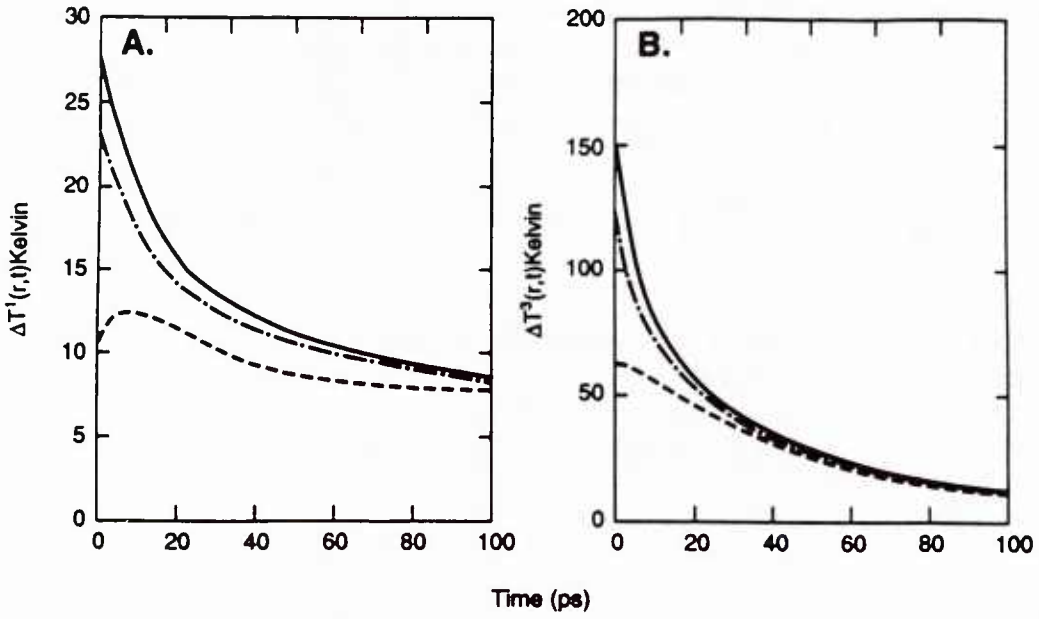

Fig. 6. Excess temperature transients (A) $\Delta T^{(1)}(r,t)$ in a spur (low-LET radiation) and (B) $\Delta T^{(3)}(r,t)$ in a cylindrical track (high-LET radiation) at several distances (——— , r = 10Å,—·—· , r = 15 Å, and - - - - -, r = 20 Å) from the center of the spur or the cylindrical track axis.

$$K = 10^{11}\exp\{-8000/RT\}\ cm^3s^{-1}/molecule$$

gives a low LET reaction time of ≈ 0.5μsec (assuming T_o = 400°K). For high LET irradiation with S = 500eV/Å corresponding to a T_o of 10^4 °K (RT≈ 0.83eV) the reaction time is estimated to be 1.5 x 10^{-11}sec, a time comparable to the duration of the thermal pulse. This simple calculation demonstrates that, at least for low LET radiation, the induced transient increase in the local temperature does not effect chemical processes. This, however, need not be valid for very high LET radiation since the temperature pulse duration can be comparable to chemical reaction times.

Similar calculations for 4 MeV proton tracks yields an initial temperature of about 100°K, which is probably not sufficient to stimulate the formation of TH•. However, errors in the estimates could well bring the temperature into the necessary range of about 200°K. Thus intra-track heating by proton radiation during and shortly thereafter can not be excluded as a possible mechanism involved in the formation of TH•.

Several microscopic processes have been suggested to explain the observed anisotropy in the neutron experiments. We discuss briefly whether any of the quasi-particles, excitons, solitons or polarons or other track phenomenon can account for the anisotropic neutron EPR spectra.

Does the migration of triplet and/or singlet excitons provide an explanation of the neutron EPR spectra? In the original paper by Arroyo et al /12/ it was suggested that the migration of triplet states might provide an explanation of the neutron EPR data. We now believe this transport mode cannot provide the large asymmetry in the transport of energy in DNA (see the discussion on microscopic intra-track spike model) needed to account for the neutron data. Both singlet and triplet exciton migration (within oriented DNA) is probably limited to at most 10 base pairs due to their short life time and extensive trapping expected to exist in highly disordered systems. Although excess hole and electron band widths along the DNA sugar-phosphate backbone are estimated to $\approx$400 cm^{-1} and 1200 cm^{-1}, respectively /29/, the neutral excited state is considerably narrower, about 10 to 70 cm^{-1} /30/. These theoretical values, although admittedly crude, support the contention that mobile neutral excited states have very short transfer distances. Numerous experiments support this viewpoint. As an example we note that exciplex formation in DNA is a rapid process /31/ estimated to be the order of $10^{12}sec^{-1}$; thus excited singlet transfer needs to occur in less than 10^{-12}sec. Denoting the mean transfer distance by d_s we have

$$d_s^2 = 2Fa^2t_T$$

if only nearest neighbor transfers are considered with a Förster rate $F \approx 10^{13}$ sec^{-1}. Here a is the neighboring base pair stacking distance (0.34nm in B-DNA) and t_T is the trapping time. Assuming an exciplex formation time of 10^{-12} sec gives a transfer distance d_s of 1.5 nm or approximately 4 to 5 base pairs. Triplet state transfer has been investigated by Eisinger and Lamola(32) and by Gueron and Shulman (33) to note but a few. Probably the most definitive experimental evidence for triplet migration in DNA has been provided by measuring the quenching of DNA phosphorescence by metal ions. Analysis of the data by Isenberg and coworkers (34) on Ni^{2+}, Co^{2+} and Mn^{2+} quenching gives triplet transfer distances comparable to that of the singlet state, (0.8 to 1.5 nm). We therefore can safely conclude that neutral state migration range is short in DNA and does not constitute an effective mechanism.

Does a microscopic temperature spike model using theoretical track codes account for the anisotropy in neutron EPR data? The most obvious difference in the pattern of energy absorption in the two irradiation geometries is that charged particles traversing the sample nearly parallel to the helical DNA axis have a greater probabliltiy for multiple energy transfers to the same DNA molecule than do particles incident on the sample perpendicular to the fiber orientation. This difference in the spatial pattern of energy absorption should have no effect on the production of free radicals if energy and/or charge move between different DNA fibers as freely as they

are transported along a single DNA chain. The macroscopic model developed by Miller et al. /35/ (the quasi particle being transported is not identified) assumes that an orientation dependence of radical yields is indicative of intramolecular energy and/or charge transfer in DNA. The asymmetric 3-dimensional heat equation is solved in the limit where only the shortest transverse relaxation time ($\tau_t = b^2/5.8D_t$, where b is the DNA radius and D_t is the transverse diffusion coefficient) is included. Miller et al. showed that in this approximation the local termperature at energy deposition site x_k (determined by Monte Carlo track simulation) and at time t is given by

$$T(x,t) = T_s + \exp(-t/\tau_t) \sum_k T_k(x,t/\tau_l)$$

and

$$T_k(x,t) = T_{ko} (1 + t/\tau_l)^{-1/2} \exp\{\frac{-(x-x_k)^2}{2\Delta^2(1 + t/\tau_l)}\}$$

where T_s is the ambient sample temperature, $\tau_l = \Delta/2D_l$ is the longitudinal thermal relaxation time, D_l is the longitudinal diffusion coefficient, Δ is the half-width of the superexcited state (taken to be 3.4Å, the nearest neighbor base-pair distance) and

$$T_{ko} = \epsilon_k/b^2\Delta\rho C(2\pi^3)^{1/2}$$

where C and ρ are the specific heat and sample density and ϵ_k is the absorbed energy at site x_k.

An essential difference between the Henriksen et al /26,27/ application of "heat waves" to calculate conversion of the primary radicals in proteins and the thermal spike model of Miller and coworkers /35/ is that of reformulating the thermal spike model in terms of track structure rather than simply stopping power. In view of recent findings by Bernhard /19,20,21/, electrons liberated in the decay of superexcited states by autoionization (see Figure 7) eventually form C^-.

Energy from other deposition events in the same DNA chain are treated as temperature spikes that spread throughout the sample asymmetrically. Thermal diffusion along DNA chains is assumed to be 1000 fold higher than the transverse thermal diffusion. Although at present we are unware of any experimental evidence to support this large value, it should be noted that anisotropy in electrical conductivity greater than 100 has been reported for organic systems such as polydiacetylene /36/. The longitudinal diffusion coefficient was taken to be comparable to H_2O (10^{-3}

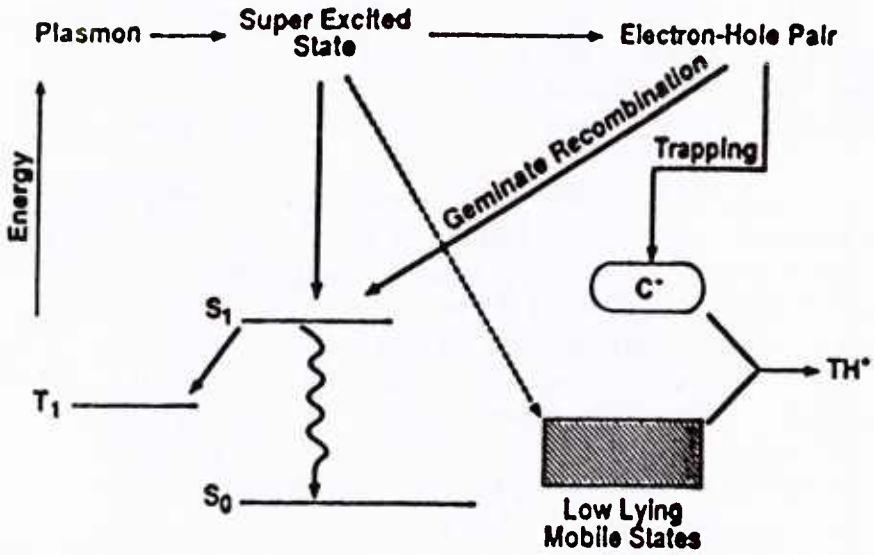

Fig. 7. Possible decay modes of energy absorbed from ionizing radiation in hydrated DNA samples.

cm^2 sec^{-1}) and protonation of the thymine radical was approximated by quasi first-order kinetics with an activation energy between 0.2 and 0.6 eV. The mechanism for conversion of primary radical anions to TH·, which probably involves electron transfer from C to T followed by irreversible protonation at C6, is assumed to be the same as that which operates in thermal annealing experiments /11/. Although the model does predict greater conversion of primary radical anions to TH· for a proton flux oriented parallel to the DNA fibers, it cannot account for the 3 fold greater total radical yields observed in the parallel neutron irradiation configuration without additional considerations of electron trapping and ion recombination. Furthermore, the model predicts that both primary radical anions and TH· should be seen in the parallel case, which does not agree with the observations reported by Arroyo et al. /12/ where radical anion species were detected in the only in the perpendicular case.

Are solitons involved in energy transfer in DNA? Solitons have been proposed as a mechanims of long-range energy transfer in DNA /14,37,38/. These collective states have been invoked to explain the hydrogen-deuterium exchange reaction observed in double-stranded polynucleotides /39,40/; however, problems with this explanation have been noted by Benight et al. /41/. There is currently no generally accepted theory of solitary waves in DNA. As a first approximation, one might visualize a DNA solitary wave as a configuration formed by partial underwinding of the helix over several base pairs with some disruption of interstrand hydrogen bonds. Yomosa /42/ developed a simple DNA soliton model that allows one to estimate their lowest energy E_0, size L_0, and velocity v_0 by fitting model Hamiltonian calculations to the temperature dependence of the equilibrium constant for hydrogen-deuterium exchange /40/. Although details of the Yomosa model of open states are likely to be incorrect (e.g. the assumption of complete base-pair rotation about the phosphate-sugar backbone and the neglect of DNA backbone bending energy), it does provide reasonable estimates of the above parameters. Under the assumption that base stacking is preserved in soliton excitation and with a Hamiltonian which includes interstrand hydrogen bonding, intrastrand stacking, and torsional energy, Yosoma /42/

calculated E_0 = 0.35 eV, which is sufficient to overcome the activation barrier to irreversible protonation of pyrimidine radical anions at C6, L_0 = 10 base pairs, which demonstrates the non-local character of this excitation mode, and v_0 = 8.3 x 10^3 cm/sec, which is less than the velocity of sound in DNA as it should be.

The soliton migration distance d can be estimated by noting that in the radiation-induced thermal spike model of Miller et al. /35/, the heat wave has a lifetime of approximately 1 ns, a value considerably shorter than the measured open-state lifetime of 10^{-7} s /43/; thus d = 83 nm. Hence, intramolecular energy transfer by solitons is a credible mechanism for the necessary long-range energy transfer inferred from Monte Carlo calculations /35/ to explain the neutron data. Unfortunately, a soliton model without charge recombination and trapping cannot account for the observed neutron-induced radical yields. This limitation might be removed by inclusion of the effects of soliton pinning; however, a theory of this process in DNA is not currently available.

Is polaron transport involved in the neutron or proton results? It is possible that long-range migration (LRM), either by electrons or protons could account for the neutron data. Charge transfer in organic systems is well documented /30/. Transport through stacked DNA bases has been shown by van Lith and coworkers /44/ to be the order of 9 nm, which is not long enough to explain the presence of TH· radicals at 77°K. Futhermore, these investigations demonstrated that transport through the phosphate-sugar backbone is also not sufficient. Experimental data do, however, support the possibility of LRM within the structured water layers of DNA hydration. Using transient microwave techniques, van Lith et al. /44/ observed a mobility μ of 2.5×10^{-3} m^2 V^{-1} sec^{-1}, which they associate with transfer of "dry" electrons in the water layer, provided the water concentration was above the critical weight fraction F_0 = 0.44. For comparison, mobilities of 2×10^{-6} m^2 V^{-1} sec^{-1} and 1×10^{-4} m^2 V^{-1} sec^{-1} have been reported for horizonally stacked phthalocyanine columns /45/ and polyethylene /46/, repectively. Above the critical water content, the conductivity is linear in F. If the carrier lifetime (determined primarily by trapping at defects) is an order of magnitude longer than the unsolvated electron in pure ice, then the mean transfer distance at -78° C is about 100 nm. More recent estimates by Warman et al. /45/ give a maximum transfer distance of only 115 base pairs or about 40 nm.

Although electron transfer is sufficient to explain LRM in DNA, proton transport is another posibility. Kunst and Warman /47/ attributed the longer-lived conductivity transient for ice (after electrons are trapped) to mobile protons. If this is the case, then narrow-band polaron transport /48/ is the appropriate theoretical formalism to describe the dependence of mobility on temperature. In this theory

$$\mu = (ea^2/kT)\, \pi^{1/2} \nu_o\, F(T)^{1/2} \exp(-F(T))$$

with

$$F(T) = 2w_p/h\nu_o \, csch(h\nu_o/2kT)$$

where w_p is the polaron binding energy, a is the interatomic distance, and ν_o is the vibrational frequency of the phonon that interacts most strongly with the carrier. Using these equations, we estimate that the proton mobility in hydration layers of DNA is between 0.1 and 1 $cm^2\ V^{-1}\ sec^{-1}$ at 77°K. To achieve a migration distance of 100nm, protons with mobilities in this range would require lifetimes of 4 to 40 ns, which are consistent with existing results on the trapping of electrons and protons in ice /47/. Hence, mechanisms of charge transport exist with sufficient range to account for the orientation effect on radical types reported for neutron irradiation but, as was the case for the thermal spike model, trapping and recombination must be included in any model of radical yields.

What is the role of carrier trapping and recombination in explaining existing EPR data? As noted above, considerations of trapping and recombination in addition to LRM of any quasi-particle are needed to explain the factor of 3 difference between total radical yields observed in parallel and perpendicular neutron irradiation /12/. Miller and Swenberg /38/ have suggested ways to model this effect as well as the absence of TH· radicals in the perpendicular configuration. The observations of van Lith et al. /44/ of electron LRM in hydrated DNA following nanosecond pulses of 3 MeV electrons suggest that autoionization of superexcited states (as illustrated in Fig. 7) produces quasi-free electrons in the hydration layers of DNA where they undergo LRM before relaxation into another trap. Films of oriented DNA may be similar in some repects to the quasi-one-dimensional semiconductors illustrated schematically in Figure 8, below. In the perpendicular irradiation configuration, yields of primary radical anions and cations are mainly determined by the competition between geminate recombination and electron trapping at preexisting defects (denoted by squares in Fig. 8). In the parallel case, the high mobility path of electrons (for polydiacetylene mobility parallel to the fiber direction can be 100 times greater than mobility perpendicular to the fibers /36/) contains trapped positive ions that will reduce the radical yield by nongeminate recombination of the ionic precursors. Solution of the coupled differential equations that describe radical production and decay in this model will be given in a future publication. Here we note only that, in contrast to the soliton model depicted in Figure 7 where collective vibrational excitations are the mobile low-lying states, ejected electrons are the quasi-particle with asymmetic mobility in the model depicted in Figure 8. Vibrational excitations that accompany both the production and decay of ion pairs are assumed to be localized.

Our analysis indicates that no energy or charge transport model can fully account for anisotropy (in the neutron experiments) observed in the EPR data if the effects of carrier trapping and recombination are neglected. Geminate recombination, applicable in the low density limit where an isolated pair of oppositely charged geminate particles can be considered as an isolated system, was developed in the late 1930's by Onsager /49,50/ and was designed as the steady state solution of the

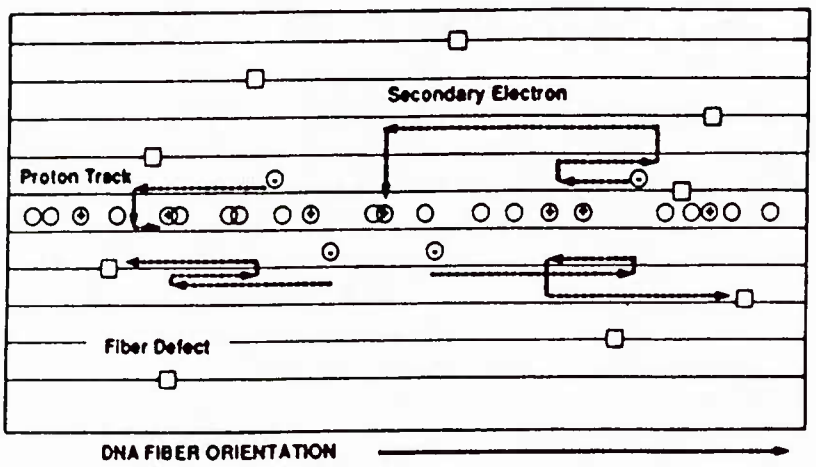

Fig. 8. Schematic diagram of electron trapping and recombination in a quasi one dimensional semiconductor. Squares and circles denote preexisting and radiation-induced traps, respectively. Broken lines represent electron trajectories. (Redrawn from /36/).

charge pair moving in a condensed phase continuum in the presence of an external electric field. This theory has been widely and successfully applied to photogeneration of carriers in organic materials (see Pope and Swenberg /30,51/ for a review). Within the past decade the theory has been extended by Hong and Noolandi /51/ to include transient effects with the refinement of replacing the original Onsager assumption of a point sink at the origin by a recombination sphere of finite radius and recombination velocity. In addition, the seminal theory of Scher and Rackovsky /52/ in which the effects of the lattice and the microscopic molecular process are considered has demonstrated the important role of competing processes, such as the decay rate of the electronically excited precursors to the ion-pair state that dissociates. This improved theory shows how the two parameters of Onsager's theory, the electron thermalization distance and the initial quantum yield of geminate pair generation can be evaluated if an assumption is made regarding the initial distribution of geminate pair distances. Recently, within the context of Onsager's continuum theory, Mozumder /54/ has illustrated by extensive numerical calculations how the fractal geometry of the lattice can influence the geminate escape probability, mean recombination time, and the reaction rate. All these theoretical treatments are applicable only in the low ionization density limit; in the cases where high LET particles are involved the free electrons, ions, and radicals in the track are so high in density that non-geminate processes are dominant (see Schott /55/). When ionization is dense, no similar results as found for geminate processes are known. This is due to two complicating factors; the repulsion between electrons and the inherent problem of tracking the amount of cation charge remaining as electron and cation are neutralized. Both of the effects have been treated in a mean field approximation although one can easily convince oneself that neither a mean field approximation nor

a perturbation approach can be successfully employed. Sano and Baird /56/ have considered the model system of two electrons in the field of a divalent cation (a model analog of the helium atom in atomic theory). Even here the results are mathematically formidable and require numerous numerical calculations. It seems that the only viable approach is to employ a variational approach, and this obviously requires good theoretical insight on the form for the multidimensional distribution functions.

CONCLUSIONS

Several mechanism of energy or charge transport in hydrated DNA have been proposed that have sufficient range to couple energy deposition events in DNA chains in ways that may account for the orientation dependence of radical yields in oriented DNA exposed to neutrons /12/. The details of these mechanisms will be dependent on the identity of the primary radiation-induced species; however, the concepts of relating orientation effects to energy or charge transport is independent of whether thymine or cytosine is the predominant type of electron gain center. The pattern of energy deposition events in an oriented DNA chain interacting with protons depends upon the velocity of the proton (magnitude and direction) relative to the helical axis but should be the same for a primary or secondary flux. Hence, the inconsistancy between experiments with neutrons /12/ and direct proton-beam irradiation /13/ is currently the main impediment to understanding the unusual results observed with neutrons. Determining the reproducibility of these experiments is clearly the most important next step; however, a detailed analysis of the spatial distribution of energy deposited in DNA chains exposed to neutrons from the TRIGA reactor would also be helpful. If the dispersion of secondary protons makes the patterns of energy deposition in DNA chains essentially independent of their orientation relative to the neutron flux, then models for the orientation effects reported by Arroyo et al. /12/ that are based on an assumed difference in this pattern are obviously inappropriate.

REFERENCES

1. P. Alexander and J.T. Lett, Effects of ionizing radiations on biological macromolecules, *Comprehensive Biochem.* **27**, 267 (1967).

2. J.T. Lett, Cellular radiation biology in consolidation and transition, *Brit. J. Cancer (Supplement VIII)*, **55**, 145 (1987).

3. J.T. Lett, Damage to DNA and chromatin structure from ionizing radiations, and the radiation sensitivities of mammalian cells, *Prog. Nucleic Acid Tes, and Mol. Biol.* **39**, 305 (1990).

4. A. Rupprecht and B. Forslind, Variation of electrolyte content in wet-spun lithium and sodium DNA, *Biochim. Biophys. Acta* **204**, 304 (1970).

5 . J.T. Lett and P. Alexander, Crosslinking and degradation of deoxyribonucleic acid gels with varying water contents when irradiated with electrons, *Radiation Res.* **15**, 159 (1961).

6. J. Hütterman, M. Röhreg and W. Köhnlein, Free radicals from iradiation of lypohized DNA: influence of water of hydration, *Int. J. Radiat. Biol.* **61**, 299 (1992).

7. S.G. Swarts, M.D. Sevilla, D. Becker, C.J. Tokar and K.T. Wheeler, Radiation-induced DNA damage as a function of hydration I, Release of unaltered bases, *Radiat. Res.* **129**, 333 (1992).

8. L.S. Myers, Jr. Free Radical damage of nucleic acids and their components by ionizing radiation, *Federation Proc.* **32**, 1882 (1973).

9. A. Rupprecht, Preparation of oriented DNA by wet spinning, *Acta Chem Scand.* **20**, 494 (1966).

10. A. Gräslund, A. Ehrenberg, A. Rupprecht and G. Ström, Ionic base radicals in γ-irradiated DNA, *Biochim. Biophys. Acta* **254**, 172 (1971).

11. A Gräslund, A Ehrenberg, A Rupprecht, B. Tjälldin and G. Ström, ESR kinetics of a free radical conversion in γ-irradiated oriented DNA, *Radiat. Res.* **61**, 488 (1975).

12. C.M. Arroyo, A.J. Carmichael, C.E. Swenberg and L.S. Myers, Jr., Neutron-induced free radicals in oriented DNA, *Int. J. Radiat. Biol.* **50**, 789 (1986).

13. J.H. Miller, D.L. Frasco, C.E. Swenberg and A. Rupprecht, Energy transfer mechanisms in DNA: Relationship to energy deposition in submicroscopic volumes, *Radiation Research: A Twentieth-Century Perspective*, edited by W.C. Dewey, M. Edington, R.J.M. Fry, E.J. Hall, and G.F. Whitmore, (San Diego: Academic Press Inc., vol.II, p.433, 1992).

14. C.E. Swenberg and J.H. Miller, Response to "Are solitons responsible for energy transfer in DNA?", *Int. J. Radiat. Biol.* **56**, 383 (1989).

15. R. Brandes, R.R. Vold, D.R. Kearns and A Rupprecht, A ^{2}H-NMR study of the A-DNA conformation in films of oriented Na-DNA: Evidence of a disordered B-DNA contribution, *Biopolymers* **27**, 1159 (1988).

16. S.A. Lee, S.M. Lindsay, J.W. Powell, T. Weidlich, N.J. Tao and G.D. Lewen, A Brillouin scattering study of the hydration of Li and Na-DNA films, *Biopolymers* **26** 1637 (1987).

17. N.J. Tao, S.M. Lindsay and A. Rupprecht, Structure of DNA hydration shells studied by Raman spectroscopy, *Biopolymers* **28**, 1019 (1989).

18. M.B. Tan and J.E. Heard, On the hydration of DNA II: Base composition dependence of the net hydration of DNA, *Biopolymers* **6**, 1345 (1968).

19. W.A. Bernhard, Initial sites of one electron attachment in DNA, NATO ASI Series, Series H: Cell Biology, Vol 54, *The Early Effects of Radiation on DNA*, E.M. Fielden and P. O'Neill, eds., Springer-Verlag, Berlin, p. 141, 1991.

20. W.A. Bernhard, Free radicals formed by electron gain in oligomers of DNA, *Free Rad. Res. Comm.* **6**, 93 (1989).

21. W.A. Bernhard, Sites of electron trapping in DNA as determined by ESR of one-electron-reduced oligonucleotides, *J. Phys. Chem.* **93**, 2187 (1989).

22. S. Steenken, Purine bases, nucleosides, and nucleotides: Aqueous solution redox chemistry and transformation reactions of their radical cations, e^- and OH adducts, *Chem. Rev.* **89**, 503 (1989).

23. N. Border, M.J.S. Dewar and A.J. Harget, Ground states of congugated molecules XIX, Tautomerism of heteroaromatic hydroxy and amino derivatives and nucleotide bases, *J. Am. Chem. Soc.* **92**, 2929 (1970).

24. N. Berthard, C. Gresssner-Prettre and A. Pullman, Theoretical study of the electronic properties of the purine and pyrimidine components of nucleic acids, I. A semiempirical self-consistent field calculation, *Theor. Chim. Acta* **5**, 53 (1966).

25. A. Norman, Thermal spike effects in heavy-ion tracks, *Radiat. Res.* **7**, 33 (1967).

26. T. Henriksen, Production of free radicals in solid biological substances by heavy ions, *Radiat. Res.* **27**, 676 (1966).

27. T. Henriksen, P.K. Horan and W. Snipes, Free-radical production by heavy ions at 77K and its relation to the thermal spike theory, *Radiat. Res.* **43**, 1 (1970).

28. A. Mozumder, Charge particle tracks and their structure, *Advances in Radiation Chemistry*, edited by M. Burton and J. Magee, (New York: Wiley-Interscience, vol.1, p.1 1969).

29. S. Suhai, Energy bands and electronic delocalization in the sugar-phosphate backbone of DNA, *Biopolymers* **13**, 1739 (1974).

30. M. Pope and C.E. Swenberg, *Electronic Processes in Organic Crystals*, (New York: Oxford University Press, 1982).

31. J.B. Birks, *Photophysics of Aromatic Molecules*, (New York: Wiley-Interscience, 1970).

32. J. Eisinger and A.A. Lamola, The excited states of nucleic acids, In: *Excited States of Proteins and Nucleic Acids*, edited by R.F. Steiner and I. Weinryb, (New York: Plenum Press, p. 107, 1971).

33. M. Guéron and R.G. Shulman, Energy transfer in polynucleotides, *Ann. Rev. Biochem.* **37**, 571 (1968).

34. I. Isenberg, R. Rosenbluth and S.L. Baird, Comparative phosphorescence quenching of DNA's of different composition, *Biophy. J.* **7**, 365 (1967).

35. J.H. Miller, W.E. Wilson, C.E. Swenberg, L.S. Myers, Jr. and D.E. Charlton, Stochastic model of free radical yields in oriented DNA at 77 K, *Int. J. Radiat. Biol.* **53**, 901 (1988).

36. E.L. Frankovich, I.A. Sokolik and A.A. Lymarev, On the photogeneration of charge carriers in quasi-one-dimensional semiconductors: polydiacetylene. *Mol. Cryst. Liqu. Cryst.* **175**, 41 (1989).

37. K.F. Baverstock and R.D. Cundall, Are solitons responsible for energy transfer in oriented DNA?, *Int. J. Radiat. Biol.* **55**, 151 (1989).

38. J.H. Miller and C.E. Swenberg, Radical yields in DNA exposed to ionizing radiation: Role of energy and charge transfer, *Can. J. Phys.* **68**, 962 (1990).

39. M. Nakamshi and M. Tsuboi, Two channels of hydrogen exchange in a double-helical nuclei acid, *J. Mol. Biol.* **124**, 61 (1978).

40. H. Teitelkaum and S.W. Englander, Open states in native polynucleotides I. Hydrogen-exchange study of adenine-containing double helices. Open States in native polynucleotides II. Hydrogen-exchange study of cytosine-containing double helices, *J. Mol. Biol.* **92**, 55 (1975).

41. A.S. Benight, J.M. Schurr, P.F. Flynn, B.R. Reid and D.E. Wemmer, Melting of a self-complementary DNA minicircle: Comparison of optical melting theory with exchange broading of the nuclear magnetic resonance spectrum, *J. Mol. Biol.* **200**, 377 (1988).

42. S. Yomosa, Soliary excitations in deoxyribonucleic acid (DNA) double helices, *Phys. Rev. A* **32**, 474 (1989).

43. M. Guéron, M. Kochovan and J.L. Leory, A single mode of base-pair opening drives imino proton exchange, *Nature* **328**, 89 (1987).

44. D. van Lith, J.W. Warman, M.P. de Hass and A. Hummel, Electron migration in hydrated DNA and collagen at low temperatures, Part 1. Effect of water concentration, Part 2. Effects of additives, *J. Chem. Soc. Faraday Trans. 1* **82**, 2933 (1986).

45. J.M. Warman, M.P. de Haas and P.G. Schouten, Charge migration in hydrated DNA, *Radiation Research: A Twentieth-Century Perspective*, edited by W.C. Dewey, M. Edington, R.J.M. Fry, E.J. Hall, and G.F. Whitmore, (San Diego: Academic Press Inc., vol.II, p.93, 1992).

46. M.P. de Haas and A. Hummel, Charge migration in irradiated polyethelene, *IEEE Transactions in Electrical Insulation* **24**, 349 (1989).

47. W. Kunst and J.M. Warman, Nanosecond time-resolved conductivity studies of pulse-ionized ice, 2. Mobility and trapping of protons, *J. Phys. Chem.* **87**, 4093 (1983).

48. G.G. Roberts, N. Appleby and R.W. Mann, Temperature dependent electronic conductivity in semiconductors, *Physics Reports* **60**, 59 (1980).

49. L. Onsager, Derivation from Ohm's Law in weak electrolytes, *J. Chem. Phys,* **2,** 599 (1934).

50. L. Onsager, Initial recombination of ions, *Phys. Rev.* **54**, 554 (1938).

51. M. Pope and C.E. Swenberg, Electronic processes in organic solids, *Ann. Review Phys. Chem.* **35**, 613 (1984).

52. K.M. Hong and J. Noolandi, Solution of the time dependent Onsager problem, *J. Chem. Phys.* **69**, 5026 (1978).

53. H. Scher and S. Rackovsky, Theory of geminate recombination on a lattice, *J. Chem Phys.* **81,** 1994 (1984).

54. A. Mozumder, Influence of fractal geometry on geminate escape probability, mean recombination time, and homogenous reaction rates, *J. Chem Phys.* **92**, 1015 (1990).

55. M. Schott, Remarks on the process of carrier generation in electron-bombarded crystalline anthracene, *Mol. Cryst.* **5**, 229 (1969).

56. H. Sano and J.K. Baird, Brownian motion of reacting charged particles in ionizing tracks, *J. Chem. Phys.* **77**, 6236 (1982).

Experimental Hematology 22:510–516 (1994)

Experimental Hematology

Effects of radiation on survival and recovery of T lymphocyte subsets in C3H/HeN mice

J.L. Williams,[1] M.L. Patchen,[1] J.H. Darden,[1] W.E. Jackson[2]

[1]Experimental Hematology Department and [2]Computer and Electronics Department, Armed Forces Radiobiology Research Institute, Bethesda, MD

Offprint requests to: Myra L. Patchen, PhD, Experimental Hematology Department, Armed Forces Radiobiology Research Institute, 8901 Wisconsin Avenue, Bethesda, MD 20889-5603

(Received 29 June 1993; revised 19 November 1993; accepted 6 February 1994)

Abstract

The aims of this study were to determine the radiosensitivities of murine thymic and splenic $CD4^+$ and $CD8^+$ lymphocytes and to evaluate the regeneration of these cells in a model of radiation-induced hematopoietic and immune suppression. $CD4^+$ and $CD8^+$ cells were quantitated using two-color flow-cytometric analysis. Cells obtained from C3H/HeN mice 24 hours after exposure to 0.25–8.0 Gy (0.4 Gy/min) ^{60}Co were used to determine D_0 values. Thymic $CD4^+$ cells contained a radiosensitive subpopulation with a D_0 of 0.97 ± 0.05 Gy and a radioresistant subpopulation that survived exposures up to 8.0 Gy. $CD8^+$ cells also contained a radiosensitive subpopulation with a D_0 of 1.24 ± 0.05 Gy and a radioresistant subpopulation with a D_0 of 3.93 ± 2.01 Gy. Double-positive thymic $CD4^+/CD8^+$ cells were uniformly radiosensitive, with a D_0 of 1.03 ± 0.28 Gy. Multiple T lymphocyte subpopulations based on radiosensitivity and CD4/CD8 antigen expression were also observed in the spleen. When mice were exposed to a sublethal 6.5-Gy radiation dose and recovery of T lymphocyte subsets was monitored, the relative radioresistance of $CD4^+$ cells resulted in a selective enrichment of these cells among the surviving thymocytes and splenic lymphocytes. This relative enrichment of $CD4^+$ cells became even more prominent 7 days after irradiation, when atrophy of the organs was greatest. Similar, although less dramatic, effects were observed for $CD8^+$ cells. These studies demonstrate that (1) multiple T lymphocyte subpopulations can be identified based on radiosensitivity and CD4/CD8 antigen expression; (2) both $CD4^+$ and $CD8^+$ cells contain radioresistant subpopulations, with the $CD4^+$ subpopulation being more resistant than the $CD8^+$ subpopulation; and (3) although the number of radioresistant $CD4^+$ cells is quite small, they persist in increased proportions during the periods preceding and corresponding to postirradiation hematopoietic recovery.

Key words: T lymphocytes—Radioresistance—Hematopoiesis

Introduction

Substantial hematopoietic recovery following chemotherapy or radiotherapy requires stem cells to proliferate and differentiate into specific progenitor cells capable of giving rise to functional mature cells. Following sublethal chemotherapy or radiotherapy regimens, hematopoietic recovery will ultimately ensue from surviving endogenous hematopoietic stem and progenitor cells. Following more intense suppressive regimens, however, recovery can be facilitated only by transplanting bone marrow cells from a suitable donor [1].

Hematopoietic recovery in mice given bone marrow transplants has been demonstrated to be enhanced by supplementing donor bone marrow cells with normal syngeneic thymic lymphocytes [2]. Since the cells responsible for this improvement were eliminated by in vitro treatment with an anti-Thy-1 serum and complement, they were subsequently named "anti-theta-sensitive regulatory cells" (TSRC) [3]. These cells were also found in the spleen and bone marrow. Later, in vitro studies of erythropoiesis revealed that TSRC actually consisted of two distinct $Thy\text{-}1^+$ subpopulations; one that enhanced hematopoietic recovery and another that suppressed it [4]. The two TSRC subpopulations differed in a number of criteria [4–8]. For example, TSRC that enhanced hematopoietic recovery were resistant to cyclophosphamide and radiation, while TSRC that suppressed recovery were sensitive to these agents [6]. The fact that helper TSRC appeared to be relatively radioresistant suggested that a portion of these cells may persist in irradiated animals and play a role in facilitating hematopoietic recovery, even following radiation exposures such as those used in bone marrow transplant preparation regimens [2].

Although murine lymphocytes have generally been reported to have a D_0 of less than 2 Gy [1], it has been known for years that a small population of radioresistant $Thy\text{-}1^+$ lymphocytes survive in vivo in heavily irradiated animals (for a review see Anderson and Warner [9]). Cell transfer studies indicate that these radioresistant T lymphocytes function as helper cells in reconstituting immune responses. Suppressor function, on the other hand, is abrogated by exposure to radiation. This differential sensitivity to irradiation between helper and suppressor lymphocytes, as well as similar differences in sensitivity to cyclophosphamide [6], seems to mirror the differential sensitivity patterns to these agents found in helper and suppressor TSRC. Thus, it is tempting to hypothesize that the helper and suppressor cells of the TSRC system may be identical to helper and suppressor T lymphocytes of the immunoregulatory system.

It is now known that helper T lymphocyte function is associated primarily with cells that express the CD4 antigen [10], while suppressor T lymphocytes express the CD8 antigen [11]. However, $CD4^+$ and $CD8^+$ T lymphocytes have not been well characterized with regard to their radiosensitivities and persistence in vivo after irradiation. To better understand the relationship between TSRC and immunoregulatory T lymphocytes, we examined the radiosensitivity of thymic and splenic lymphocyte subsets defined by CD4 and CD8

antigens. Furthermore, we followed changes in these cell populations concomitant with hematopoietic regeneration in sublethally irradiated mice. Our results show that both the thymus and the spleen contain a subpopulation of extremely radioresistant $CD4^+$ cells. As a result of the radioresistance of these cells vis-à-vis the radiosensitivity of other lymphoid cells, irradiated animals become proportionately enriched with $CD4^+$ cells. Although the number of $CD4^+$ cells is quite small, the enrichment persists during the early critical phases of postirradiation hematopoietic regeneration.

Materials and methods

Mice

C3H/HeN female mice (~20 g) were purchased from Charles River Laboratories (Wilmington, MA). Mice were maintained in a facility accredited by the American Association for Accreditation of Laboratory Animal Care (AAALAC) in Micro-Isolator cages on hardwood-chip contact bedding and were provided commercial rodent chow and acidified water (pH 2.5) ad libitum. Animal rooms were equipped with full spectrum light from 6 a.m. to 6 p.m. and were maintained at 21°C ± 1°C with 50 ± 10% relative humidity using at least 10 air changes/h of 100% conditioned fresh air. On arrival, all mice were tested for *Pseudomonas* and quarantined until test results were obtained. Only healthy mice were released for experimentation. All animal experiments were approved by the Institute Animal Care and Use Committee before performance.

Irradiation

Mice were placed in ventilated Plexiglas boxes and exposed bilaterally to gamma radiation from the AFRRI ^{60}Co source. Prior to animal irradiations, the midline tissue (MLT) dose rate was measured by placing a 0.5-cc tissue equivalent ionization chamber (calibration factor traceable to the National Institute of Standards and Technology) at the center of a cylindrical acrylic mouse phantom (2.5-cm diameter). The tissue-to-air ratio (TAR) for this array, defined as the ratio of the dose rate in free air to the dose rate measured in the phantom, was 0.96. Exposure time was adjusted so that each animal received from 0.25 to 8.0 Gy MLT at a dose rate of 0.4 Gy/min. Variation within the exposure field was less than 3%. The techniques used for these measurements were in accordance with the American Association of Physicists in Medicine protocol for the determination of absorbed dose from high-energy photon and electron beams [12].

Cell suspensions

The cell suspensions for each assay represented tissues from three animals. Animals were killed by cervical dislocation, and the thymuses and spleens were aseptically excised. Cells from the organs were pressed through stainless steel mesh screens and collected in McCoy's 5A medium containing 10% heat-inactivated fetal bovine serum. Single-cell suspensions were prepared by repeatedly passing the cells through a 20-gauge needle. Erythrocytes were removed by lysis with hypotonic ammonium chloride, and nucleated cells were resuspended in Hanks' balanced salt solution, without calcium and magnesium, containing 1% fetal bovine serum (HBSS + 1% FBS). The number of nucleated cells in the suspension was determined by a Coulter counter. Cytocentrifuge preparations of the cell suspensions were prepared, stained with Diff-Quick, and used for differential cell counts.

Lymphocyte subset analysis

Cells were diluted to 1×10^7 cells/mL in HBSS + 1% FBS, and 100-µL portions were labeled by concurrent incubation with 5 µL each of phycoerythrin-conjugated anti-CD4 and fluorescein-isothiocyanate (FITC)-conjugated anti-CD8 monoclonal antibodies (Becton Dickinson, Mountain View, CA). The cells were incubated on ice for 30 minutes and washed once with HBSS + 1% FBS. Flow-cytometric analysis was performed using a Coulter EPICS V flow cytometer and the MDADS computer system. Gates were set on the forward-angle light scatter vs. 90-degree light scatter histograms to eliminate dead cells and debris. Two-color analysis was performed with the Quad-Stat program of the MDADS system. The number of cells of a particular subset in an organ was determined by multiplying the number of cells per organ, as determined by Coulter counts, by the proportion of cells with the given phenotype.

D_0 determinations

Mice were exposed to graded doses of radiation from 0.25 to 8.0 Gy, and tissues were collected 24 hours later. Cell suspensions were prepared and subpopulations analyzed by flow-cytometric analysis. The D_0 values were determined by plotting the surviving fraction (where surviving fraction = number of cells surviving after a given radiation dose/number of cells in nonirradiated controls) against the radiation dose. The best fit for linear portions of the curves and the Y-intercepts were calculated by nonlinear least-squares fit and the D_0, the radiation dose where the surviving fraction is equal to 0.37, was extrapolated from the exponential portion of the curves.

Spleen colony-forming unit (CFU-S) assay

CFU-S were evaluated by the method of Till and McCulloch [13]. Each colony has been shown to arise from the clonal proliferation of multipotent hematopoietic stem cells. Recipient mice were exposed to 9 Gy of total body irradiation to eradicate endogenous hematopoietic stem cells. After 3 to 5 hours, 5×10^4 bone marrow or 5×10^5 spleen cells were intravenously injected into the irradiated recipients. Twelve days after transplantation, the recipients were killed by cervical dislocation, and their spleens were removed. The spleens were fixed in Bouin's solution, and the grossly visible colonies were counted. For each experiment, groups of five mice were used, and the experiments were repeated twice.

Granulocyte-macrophage colony-forming cell (GM-CFC) assay

Hematopoietic progenitor cells committed to granulocyte and/or macrophage development were assayed using a double-layer agar GM-CFC assay [14]. Mouse endotoxin serum (5% vol/vol) was added to feeder layers as a source of colony stimulating factor. Colonies (>50 cells) were counted after 10 days of incubation in a 37°C humidified environment containing 5% CO_2. Triplicate plates were cultured for each cell suspension and experiments were repeated twice.

Results

Radiosensitivity of thymic and splenic T lymphocyte populations

$CD4^+$ thymocytes consisted of two subpopulations relative to radiosensitivity (Fig. 1A): a sensitive subpopulation with a D_0 of 0.97 ± 0.05 Gy and a resistant subpopulation that survived radiation exposures up to 8.0 Gy (the highest radiation dose evaluated), making it impossible to calculate the D_0 for this subpopulation. The radiosensitive thymic subpopulation contained approximately 82% of the $CD4^+$ cells, while the remaining 18% were in the radioresistant subpopulation. Thymic $CD8^+$ cells also consisted of two subpopulations, the first with a D_0 of 1.24 ± 0.05 Gy and the second with a D_0 of 3.93 ± 2.01 Gy (Fig. 1B). Thymic $CD4^+/CD8^+$ cells, the predominant thymocyte subset in normal animals, were uniformly radiosensitive, with a D_0 of 1.03 ± 0.28 Gy (Fig. 1C). Figure 1D shows

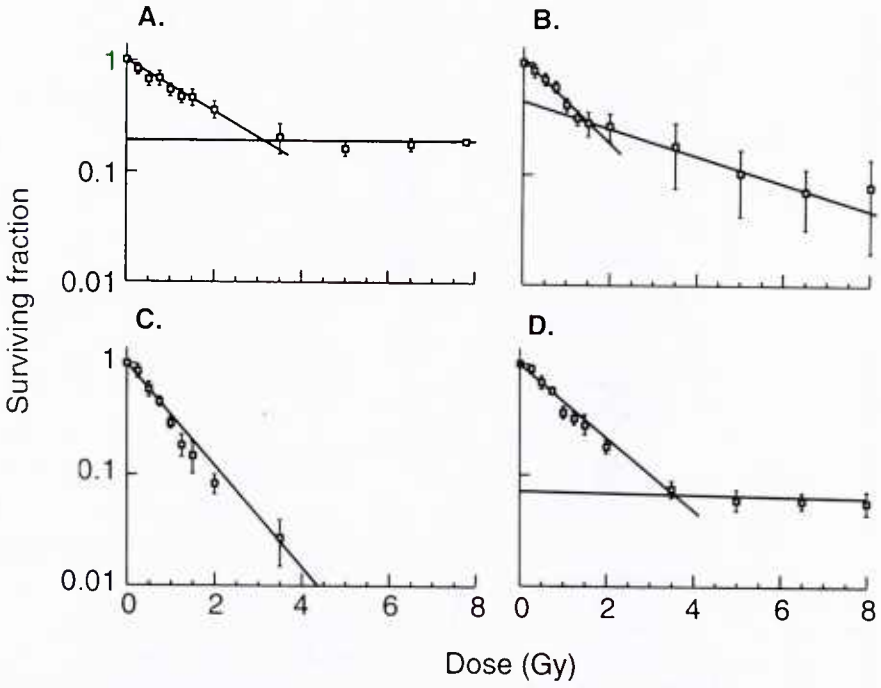

Fig. 1. Radiosensitivity of thymocyte subsets in C3H/HeN mice. Mice were exposed to graded doses of ^{60}Co radiation and thymocyte subset analysis was performed 24 hours later. **A.** $CD4^+$ cells. **B.** $CD8^+$ cells. **C.** $CD4^+/CD8^+$ cells. **D.** Total thymic cellularity. Data represent the mean ± 1 standard error of the mean (SEM) for two or more experiments with thymocytes pooled from three mice for each experiment. The surviving fraction is the ratio of the number of cells positive for the indicated antigens in irradiated animals to the number of cells positive for the indicated antigen in unirradiated controls.

that approximately 93% of the total thymocyte population was radiosensitive, with a D_0 of 1.14 ± 0.08 Gy.

Similar results were seen in the spleen, but precise D_0 values could not be determined because of high levels of autofluorescence in the spleen cells obtained from mice exposed to the higher doses of radiation.

Repopulation of thymic and splenic T lymphocyte populations in mice recovering from myeloablative radiation exposure

Total thymic cellularity at 24 hours after exposure decreased more than 15-fold, from 102.72×10^6 to 6.48×10^6 cells. Concomitant reductions in cell numbers occurred in each of the thymocyte subsets defined by the CD4 and CD8 antigens; however, the degree of cytoreduction varied among the different cell types based on their radiosensitivities (Table 1). $CD4^+/CD8^+$ cells, the predominant thymic cell type, decreased the most of any subset from 73.16×10^6 to 0.45×10^6 cells per thymus (0.6% survival). Single-positive cells were affected to a lesser degree. The number of $CD4^+$ thymocytes fell from 14.68×10^6 to 1.96×10^6 cells per thymus (13.4% survival) while the $CD8^+$ thymocytes decreased from 3.98×10^6 to 0.24×10^6 cells per thymus (6.0% survival). These values compared well with values calculated from the data in the D_0 experiments, which indicated that only 0.7% of the $CD4^+/CD8^+$, 18.5% of the $CD4^+$, and 8.4% of the $CD8^+$ thymocytes should remain 24 hours after a 6.5-Gy radiation exposure.

Large reductions both in total cellularity and in the number of cells in each specific subset also occurred in the spleen. In this organ, the $CD4^+$ cells declined from 14.94×10^6 to 5.92×10^6 cells per spleen (39.6% survival), while $CD8^+$ decreased from 5.41×10^6 to 0.31×10^6 cells per organ (5.7% survival). Double-positive T lymphocytes were not seen in the spleen.

Table 1. Residual T lymphocyte subsets in C3H/HeN thymus and spleen 24 hours after exposure to 6.5 Gy ^{60}Co radiation

Cell type	Control	6.5 Gy
	Thymic cellularity ($\times10^6$)	
Total	102.72±3.13	6.48±0.90
$CD4^+/CD8^+$	73.16±5.85	0.45±0.06
$CD4^+$	14.68±1.70	1.96±0.40
$CD8^+$	3.98±0.43	0.24±0.06
$CD4^-/CD8^-$	10.55±1.52	3.74±0.83
	Splenic cellularity ($\times10^6$)	
Total	97.86±10.80	16.29±6.56
$CD4^+$	14.94±2.63	5.92±4.54
$CD8^+$	5.41±1.09	0.31±0.22
$CD4^-/CD8^-$	74.41±7.91	9.95±1.73

The differences in cytoreduction postirradiation among the various subsets resulted in selective enrichment of $CD4^+$ cells. Specifically, the relative proportion of $CD4^+$ cells in the thymus increased from 15.3 to 30.0% of the total remaining cells, and in the spleen they increased from 14.3 to 33.4%. On the other hand, the percentage of $CD8^+$ cells remained constant at about 3.8% in the thymus and decreased from 5.5 to 1.9% in the spleen. The proportion of double-positive cells in the thymus also decreased dramatically from 71.2 to 0.5%.

The radiation-induced atrophy of the thymus was still evident 7 days after irradiation, and the number of cells in each of the thymocyte subsets remained lower than in controls. At that time, there were $0.76 \pm 0.29\times10^6$ $CD4^+$ cells, 0.29 ±

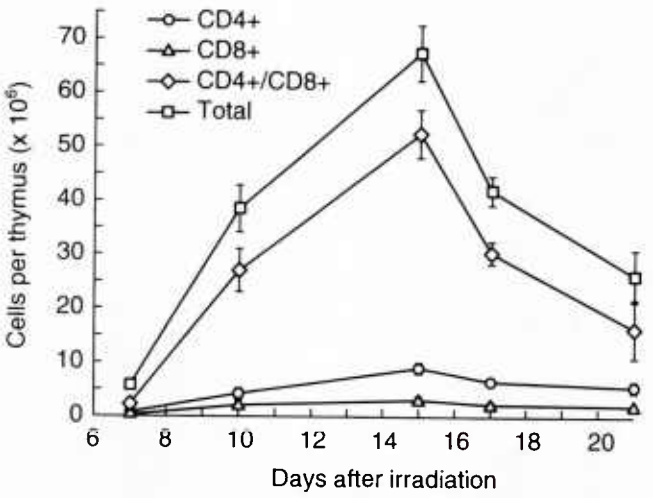

Fig. 2. Recovery of thymocyte subsets after sublethal irradiation. Mice were exposed to 6.5 Gy of ^{60}Co radiation, and the thymuses were harvested at the time points indicated. Thymocyte subset analysis was performed as in Figure 1. Data represent the mean ± 1 SEM for three or more experiments with thymocytes pooled from three mice for each experiment. $CD4^+$ cellularity in nonirradiated control mice was $14.68 \pm 1.70 \times 10^6$ cells per thymus; $CD8^+$ cellularity was $3.98 \pm 0.43 \times 10^5$ cells per thymus; and $CD4^+/CD8^+$ cellularity was $73.16 \pm 5.85 \times 10^6$ cells per thymus.

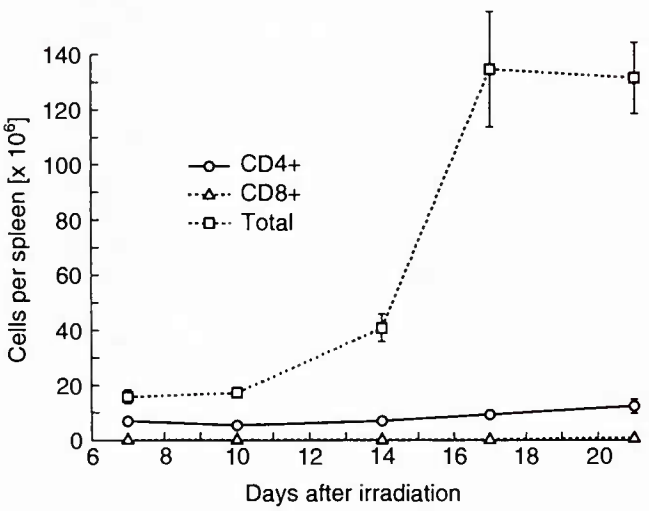

Fig. 3. Recovery of T lymphocyte subsets in the spleen after sublethal irradiation. Mice were exposed to 6.5 Gy of ^{60}Co radiation and the spleens were harvested at the time points indicated. Spleen subset analysis was performed as in Fig. 1. Data represent the mean ± 1 SEM for three or more experiments with cells pooled from three mice for each experiment. $CD4^+$ cellularity in nonirradiated control mice was $14.94 \pm 2.63 \times 10^6$ cells per spleen, and $CD8^+$ cellularity was $5.41 \pm 1.09 \times 10^6$ cells per spleen.

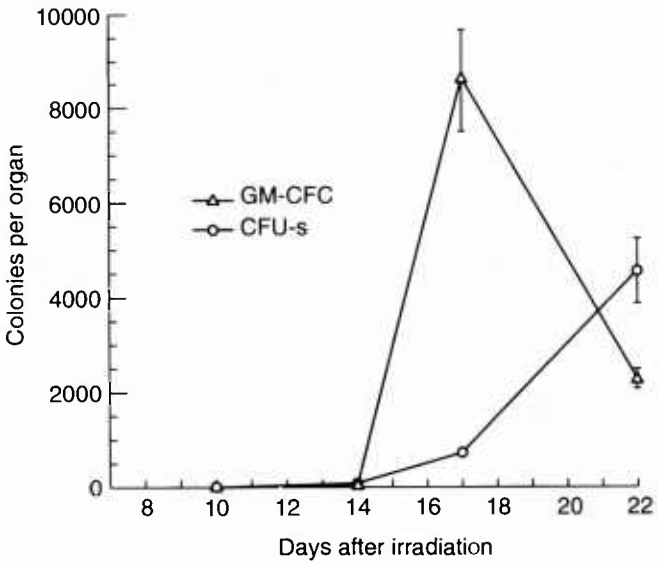

Fig. 4. Recovery of CFU-S and GM-CFC in irradiated C3H/HeN mice. Mice were exposed to 6.5 Gy of ^{60}Co radiation and splenic CFU-S and GM-CFC contents were determined at the time points indicated. Data represent the mean ± 1 SEM of pooled values obtained from two separate experiments. In normal nonirradiated controls, CFU-S content was $7.3 \pm 0.7 \times 10^3$ and GM-CFC content was $4.4 \pm 0.5 \times 10^3$.

0.09×10^6 $CD8^+$ cells, and $2.30 \pm 0.82 \times 10^6$ $CD4^+/CD8^+$ cells per thymus. Cellular regeneration was evident at 10 days, peaked at 14 days, and returned toward normal thereafter (Fig. 2). Double-positive $CD4^+/CD8^+$ cells made up the bulk of the regenerating thymocytes. $CD4^+$ cells and $CD8^+$ cells followed a similar cycle of regrowth but with slower kinetics.

In the spleen, total cellularity remained low for 10 days and then began to increase between 10 and 14 days after irradiation (Fig. 3). The number of spleen cells increased rapidly to a peak value at day 17 postirradiation and remained elevated through the end of the experimental observation period. Splenic $CD4^+$ cells remained low through the first 10 days and then began to slowly increase until the end of the experiment. The $CD8^+$ cells, which were reduced 3.5-fold by irradiation, remained at very low levels throughout the observation period. Concomitant with these studies evaluating T lymphocyte subset recovery, splenic CFU-S and GM-CFC recovery were also monitored in mice exposed to 6.5 Gy ^{60}Co radiation (Fig. 4). CFU-S and GM-CFC numbers decreased to undetectable levels for at least 7 days and then recovered rapidly. By day 22 postirradiation, splenic CFU-S recovery was approximately 65% of normal controls, and GM-CFC recovery was actually 180% of normal controls as early as 17 days postirradiation.

Effect of radiation on survival and repopulation of non–T lymphocytes in the thymus and spleen

Inherent in these studies was also the opportunity to observe the radiation-induced changes in non–T lymphocytes in the thymus and spleen, that is, the cells staining negative for CD4 and CD8. These cells consisted of a mixture of macrophages, natural killer cells, progenitor cells, and, in the spleen, B lymphocytes. The radiosensitivity of the $CD4^-/CD8^-$ cell popula-

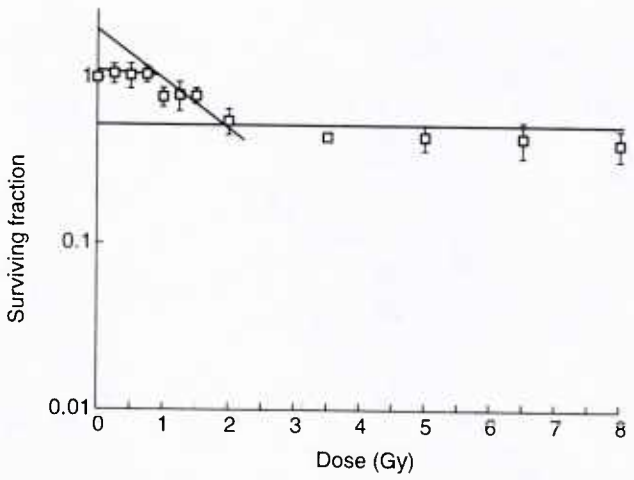

Fig. 5. Radiosensitivity of $CD4^-/CD8^-$ thymocytes in C3H/HeN mice. Mice were exposed to graded doses of ^{60}Co radiation, and thymocyte subset analysis was performed 24 hours later. Data represent the mean ± 1 SEM for two or more experiments with thymocytes pooled from three mice for each experiment. The surviving fraction is the ratio of the number of cells positive for the indicated antigens in irradiated animals to the number of cells positive for the indicated antigens in unirradiated controls.

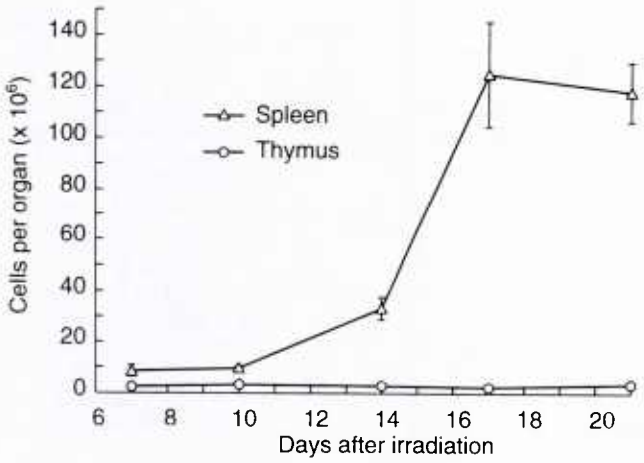

Fig. 6. Recovery of thymic and splenic $CD4^-/CD8^-$ cells after sublethal irradiation. Recovery of the $CD4^-/CD8^-$ thymocytes and splenic lymphocytes was determined from the experiments described in Figures 2 and 3, respectively. $CD4^-/CD8^-$ cellularity in nonirradiated control mice was $10.55 \pm 1.52 \times 10^6$ cells per thymus and $74.41 \pm 7.91 \times 10^6$ cells per spleen.

tion in the thymus is illustrated in Figure 5. These cells contained a radiosensitive subpopulation with a D_0 of 2.28 ± 0.74 Gy and an n of 1.37 ± 0.26. In addition, these cells contained a radioresistant subpopulation with a D_0 greater than 8 Gy. Recovery of the $CD4^-/CD8^-$ cells following a sublethal 6.5-Gy irradiation is illustrated in Figure 6. In the thymus, the number of $CD4^-/CD8^-$ cells remained relatively constant throughout the 21-day postirradiation period, while in the spleen, the observed changes in cellularity during recovery were primarily driven by changes in the number of double-negative cells.

Discussion

Our results indicate that the radiosensitivities of the $CD4^+$ and $CD8^+$ T lymphocytes are comparable, respectively, to the radiosensitivities of helper and suppressor TSRC reported by Sharkis et al. [6]. The $CD4^+$ cells that we observed in the thymuses of irradiated animals exhibited properties characteristic of the TSRC that stimulate hematopoietic recovery. Helper TSRC, which make up less than 10% of the cells in normal thymuses, are reported to be radioresistant [5]. Although, in our studies, the total number of thymus cells was drastically reduced 24 hours after irradiation, radioresistant $CD4^+$ cells were easily found in the thymuses of irradiated animals (Table 1). These results support Huiskamp and van Ewijk's immunocytochemistry studies [15], in which they too observed radioresistant $CD4^+$ cells in the thymuses of mice 24 hours after irradiation. Our use of two-color analysis to simultaneously test for CD4 and CD8 antigen expression confirmed the single-positive phenotype of the radioresistant $CD4^+$ cells, a characteristic typical of mature T lymphocytes in the thymic medulla and the peripheral organs [16]. Exposure of mice to 6.5 Gy radiation left an average of 1.96×10^6 radioresistant $CD4^+$ cells in the thymuses 24 hours after irradiation (Table 1). This corresponds to approximately 2% of the thymocyte population in unirradiated animals and compares well with the estimate of Sharkis et al. [5] for the size of the stimulatory TSRC population.

The D_0 determinations (Fig. 1) show that the surviving fraction of $CD4^+$ cells at radiation doses of 4 to 8 Gy is approximately 0.18. However, the remainder of the $CD4^+$ cells has a D_0 of 0.97 Gy, which is comparable to the D_0 of lymphocytes in general [1]. Radiation-induced apoptosis is the most likely cause of death of the radiosensitive cells, since resting lymphocytes are known to be extremely sensitive to this process while mitogen-activated lymphocytes are known to be resistant to this form of cell death [17]. The mechanisms responsible for this are unknown but may be related, in part, to the cell cycle. It is well known that cells in late S-phase of DNA synthesis are more radioresistant than cells in other phases of the cell cycle [18]. This increase in radioresistance is mediated by DNA repair and results in an increase in the n value and a decrease in the slope of the survival curves in the D_0 studies [19]. However, the percent of $CD4^+$ cells in S-phase is only 5 to 7% [20], which does not account for the 18% survival of $CD4^+$ cells reported here.

Sharkis et al. [5] have shown that helper TSRC that survive an initial radiation exposure appear to persist in irradiated animals. Likewise, radioresistant $CD4^+$ cells detected in our studies appear to persist in irradiated animals, since these cells were still present on each day tested between 7 and 21 days postirradiation (Fig. 2). Huiskamp and van Ewijk [15] reported that radioresistant $CD4^+$ thymocytes could be seen as late as 10 days after irradiation. However, due to the qualitative nature of their immunocytochemistry techniques, they were unable to provide a quantitative estimate of the size of this population. Using quantitative techniques based on flow cytometry, our data shows that the number of $CD4^+$ cells decreased between days 1 and 7 after irradiation, but even at the nadir of thymic cellularity (5.8×10^6 cells per thymus) approximately 7.6×10^5 $CD4^+$ cells could be detected.

Tomooka et al. [21] have also examined the changes in thymocyte subsets after irradiation using techniques very similar to those we used in this report. Their results are comparable to ours, but their interpretation differs significantly with respect to the persistence of the $CD4^+$ cells in the thymus. They report an absence of mature thymocytes at day 7 postirradiation; however, even after exposure to 8 Gy ^{60}Co radiation, a population of phenotypically mature $CD4^+$ cells is evident at each time point depicted in their flow-cytometric data. Taken together, the data presented in our studies and the data from the reports cited above support the postulate that a small population of $CD4^+$ cells persists in the thymuses of irradiated mice and may contribute to thymic as well as hematopoietic regeneration.

In the thymus, most $CD8^+$ cells were sensitive to the doses of radiation previously reported to eliminate the inhibitory TSRC [6]. However, D_0 studies (Fig. 1B) revealed a radioresistant population of these cells also. In contrast to the $CD4^+$ cells, where the D_0 curve flattens out at 4 to 8 Gy, the D_0 curve of the radioresistant $CD8^+$ cells is sloped, indicating a continued degree of radiosensitivity in this resistant fraction. Hence, the populations of residual regulatory cells potentially affecting the hematopoietic system of an irradiated animal vary significantly depending on the radiation dose given. At doses below 4 Gy, the proportion of each of the regulatory cell types examined in this study decreased as the dose changed. Above 4 Gy, the residual $CD4^+$ cell population remained constant while the $CD8^+$ cell content continued to decrease as the radiation dose increased. However, the importance of the changes in the numbers of $CD8^+$ cells at high doses may be ameliorated somewhat by the fact that the overall number of these cells was extremely small after irradiation (Figs. 2 and 3).

Huiskamp et al. [22] previously determined the radiosensitivity of thymocyte subsets using a panel of antibodies that included the CD8 cell marker. The D_0 curve for $CD8^+$ cells, as well as those for each of the other subsets, was biphasic and hence apparently comparable to the results reported in this paper. Although both studies report differences in radiosensitivities based on phenotype, direct comparison of the two sets of data is difficult. This difficulty arises primarily from Huiskamp et al.'s use of cytofluorometry with only one fluorochrome, which cannot distinguish between single-positive $CD8^+$ cells and double-positive $CD4^+/CD8^+$ cells. Consequently, their D_0 curve for the $CD8^+$ cells represents a composite of the radiosensitivity of these two types of cells. Our Figure 1 shows that the D_0 curves for these two populations are markedly different. Resolution of $CD8^+$ and $CD4^+/CD8^+$ as well as identification of $CD4^+$ cells requires the use of two-color analysis with CD8 and CD4 antibodies labeled with different fluorochromes. Comparison of the results between Huiskamp's studies and ours is further impeded not only by their use of fission neutron and X-ray irradiation as opposed to our use of ^{60}Co irradiation, but also by their determination of postirradiation cell survival on days 2 and 5 vs. the 24-hour evaluation time used in our studies. However, both series of studies illustrate a selective survival of phenotypically mature thymocytes following radiation exposure.

We also evaluated the radiosensitivities of splenic lymphocytes and found effects similar to those found in the thymus (Table 1). The effect of radiation on splenic $CD4^+$ cells was similar to that found in the thymus (Table 1). Most of the $CD4^+$ cells were eliminated, but a radioresistant population was readily apparent. Approximately 40% of the splenic $CD4^+$ cells remained after irradiation, as opposed to 13% in the thymus. This may reflect differences in the sensitivity noted between newly formed virgin T cells from the thymus and antigen-experienced T cells found in the peripheral lymphoid organs [9]. The extensive splenic necrosis seen after irradiation, along with the greater heterogeneity of cell types in the spleen as compared to the thymus, may have contributed to the variability seen in the splenic $CD4^+$ cell counts. This variability prevented precise D_0 determinations for the $CD4^+$ spleen cells, but both sensitive and resistant populations were evident (data not shown). Seven days after irradiation, when the variability was greatly reduced, the increased proportion of $CD4^+$ cells in the residual spleen cell population was readily detectable (Fig. 3).

Neither the $CD4^+/CD8^+$ cells nor the $CD4^-/CD8^-$ cells appear to be viable candidates for either the helper or suppressor TSRC. Although $CD4^+/CD8^+$ cells are radiosensitive like the suppressor TSRC, they are restricted to the thymus, while both types of TSRC are found in the bone marrow, spleen, and peripheral blood [3]. $CD4^-/CD8^-$ cells are radioresistant like the helper TSRC but they lack the characteristic peripheral T cell markers.

In the radiation recovery studies presented here, we employed a high sublethal dose of ^{60}Co radiation to induce hematopoietic depletion, which, however, is followed by vigorous recovery initiated from endogenous stem and progenitor cells that survive the irradiation (Fig. 4). The proliferation and differentiation of such stem and progenitor cells are known to be regulated by a variety of cytokines produced by the cells that constitute the hematopoietic environment. These cells include both the stromal elements that make up the framework of the hematopoietic organs and the monocytoid accessory cells from peripheral blood, such as T lymphocytes and macrophages [23]. Our results show that when CFU-S and GM-CFC become detectable in the spleen around day 14, they reside in an environment enriched with $CD4^+$ cells. The finding that in vivo antibody-mediated ablation of $CD4^+$ cells prior to irradiation reduces bone marrow CFU-S and GM-CFC suggests a role for $CD4^+$ cells in hematopoietic recovery [24]. Immunological studies have shown that $CD4^+$ cells produce extensive quantities of a wide range of cytokines [25] such as granulocyte, granulocyte-macrophage, and macrophage colony-stimulating factors (G-CSF, GM-CSF, and M-CSF), interleukin-3 (IL-3), and IL-6, all of which are known to be stimulators of hematopoiesis [26]. Recently many of these cytokines have been used to stimulate hematopoietic recovery in irradiated animals [27–32]. If the residual radioresistant $CD4^+$ cells reported in these experiments produce cytokines, either as a direct result of radiation injury or because of subsequent antigenic stimulation, they may contribute to hematopoietic recovery as proposed by Pantel and Nakeff [33]. Whether these cells are identical to the helper TSRC reported by Sharkis et al. [2] is not definite, but certainly they exhibit similar characteristics based on radiosensitivity. Since these cells are readily identifiable after exposure to radiation, they should be easy to isolate and evaluate for their ability to produce cytokines relevant to hematopoiesis. Studies designed to resolve this issue are currently under way.

Acknowledgments

This work was supported by the Armed Forces Radiobiology Research Institute, Defense Nuclear Agency, under work unit 00132. Research was conducted according to the principles enunciated in the Guide for the Care and Use of Laboratory Animals prepared by the Institute of Laboratory Animal Resources, National Research Council. The authors are grateful to Brian Solberg and Barbara Calabro for expert technical assistance.

References

1. Bond VP, Fliedner TM, Archambeau JO (196S) Mammalian radiation lethality. New York: Academic Press
2. Sharkis SJ, Wiktor-Jedrzejczak W, Ahmed A, Santos GW, McKee A, Sell KW (1978) Antitheta-sensitive regulatory cell (TSRC) and hematopoiesis: regulation of differentiation of transplanted stem cells in W/W^v anemic and normal mice. Blood S2:802
3. Wiktor-Jedrzejczak W, Sharkis S, Ahmed A, Sell KW, Santos GW (1977) Theta-sensitive cell and erythropoiesis: identification of a defect in W/W^v anemic mice. Science 196:313
4. Sharkis SJ, Spivak JL, Ahmed A, Misiti J, Stuart RK, Wiktor-Jedrzejczak W, Sell KW, Sensenbrenner LL (1980) Regulation of hematopoiesis: helper and suppressor influences of the thymus. Blood SS:S24
5. Sharkis SJ, Cremo C, Collector MI, Noga SJ, Donnenberg AD (1986) Thymic regulation of hematopoiesis. III. Isolation of helper and suppressor populations using counterflow centrifugal elutriation. Blood 68:787
6. Sharkis SJ, Colvin MO, Sensenbrenner LL (1981) Effect of radiation and 4-hydroperoxycyclophosphamide on thymic regulators of erythropoietic growth. Stem Cells 1:269
7. Sieber F, Sharkis SJ (1982) Modulation of murine erythropoiesis in vitro by syngeneic thymocytes: interactions of enhancing and suppressing subpopulations with fluorescent antitheta antibody and polyamino acids. Blood 60:84S
8. Sharkis SJ, Luk GD, Collector MI, McCann PP, Baylin BB, Sensenbrenner LL (1983) Regulation of hematopoiesis. II. The role of polyamine inhibition on helper and suppressor influences of the thymus. Blood 61:604
9. Anderson RE, Warner NL (1976) Ionizing radiation and the immune response. Adv Immunol 24:215
10. Dialynas DP, Quan ZS, Wall KA, Pierres A, Quintans J, Loken MR, Pierres M, Fitch FW (1983) Characterization of the murine T cell surface molecule, designated L3T4, identified by monoclonal antibody GK1.S: similarity of L3T4 to the human Leu3/T4 molecule. J Immunol 131:244S
11. Ledbetter JA, Herzenberg LA (1979) Xenogeneic monoclonal antibodies to mouse lymphoid differentiation antigens. Immunol Rev 47:63
12. Schultz J, Almond PR, Holt JG, Loevinger R, Suntharalingam N, Wright KA, Nath R, Lempert D (1983) A protocol for the determination of absorbed dose from high energy photon and electron beams. Med Phys 10:741
13. Till JE, McCulloch EA (1961) A direct measurement of the radiation sensitivity of normal mouse cells irradiated and proliferating in vivo. Radiat Res 14:213
14. Patchen ML, MacVittie TJ (1986) Hemopoietic effects of soluble glucan administration. J Immunopharmacol 8:407
15. Huiskamp R, van Ewijk W (198S) Repopulation of the mouse thymus after sublethal fission neutron irradiation. I. Sequential appearance of thymocyte subpopulations. J Immunol 134:2161
16. Dialynas DP, Wilde DB, Marrack P, Pierres A, Wall KA, Havran W, Otten G, Loken MR, Pierres M, Kapler J, Fitch FW (1983) Characterization of the antigenic determinant, designated L3T4a, recognized by monoclonal antibody GK1.S: expression of L3T4a by functional T cell clones appears to correlate primarily with class II MHC antigen-reactivity. Immunol Rev 74:29
17. Sellins KS, Cohen JJ (1987) Gene induction by gamma irradiation leads to DNA fragmentation in lymphocytes. J Immunol 139:3199
18. Sinclair WK, Morton RA (1966) X-ray sensitivity during the cell generation cycle of cultured Chinese hamster cells. Radiat Res 29:4S0
19. Hall EJ (1988) Radiobiology for the radiologist. 3rd ed. Philadelphia: Lippincott
20. Egerton M, Scollay R, Shortman K (1990) Kinetics of mature T cell development in the thymus. Proc Nat Acad Sci 87:2579
21. Tomooka S, Matsuzaki G, Kishihara K, Tanaka K, Yoshika Y, Taniguchi K, Himeno K, Nomoto K (1987) Sequential appearance of thymocyte subpopulations and T cell antigen receptor gene messages in the mouse thymus after sublethal irradiation. J Immunol 139:3986
22. Huiskamp R, Davids JAG, van Ewijk W (1986) The effect of graded doses of fission neutrons or X rays on the lymphoid compartment of the thymus in mice. Radiat Res 10S:247
23. Torok-Storb B (1988) Cellular interactions. Blood 72:373
24. Pantel K, Nakeff A (1990) Differential effect of L3T4$^+$ cells on recovery from total-body irradiation. Exp Hematol 18:863
25. Kelso A, Gough MN, Metcalf D (1991) Production of hemopoietic colony stimulating factors by murine T lymphocytes. In: S Cohen (ed) Lymphokines and the Immune Response. Boca Raton, FL: CRC Press, 213
26. Metcalf D (1989) Haemopoietic growth factors. I. Lancet 1S April 82S
27. Kobayashi Y, Okabe T, Urabe A, Suzuki N, Takaku F (1987) Human granulocyte colony-stimulating factor produced by *Escherichia coli* shortens the period of granulocytopenia induced by irradiation in mice. Jpn J Cancer Res 78:763
28. Tanikawa S, Nakao I, Tsuneoka K, Mara N (1989) Effects of recombinant granulocyte colony-stimulating factor (rG-CSF) and recombinant granulocyte-macrophage colony-stimulating factor (rGM-CSF) on acute radiation hematopoietic injury in mice. Exp Hematol 17:883
29. Patchen ML, MacVittie TJ, Solberg BD, Souza LM (1990) Therapeutic administration of recombinant human granulocyte colony-stimulating factor accelerates hemopoietic regeneration and enhances survival in a murine model of radiation-induced myelosuppression. Int J Cell Cloning 8:107
30. Talmadge JE, Tribble H, Pennington R (1989) Protective, restorative, and therapeutic properties of recombinant colony-stimulating factors. Blood 73:2093
31. Okano A, Suzuki C, Takatsuki F, Akiyama Y, Koike K, Ozawa K, Hirano T, Kishimoto T, Nakahata T, Asano S (1989) In vitro expansion of the murine pluripotent hemopoietic stem cell population in response to interleukin 3 and interleukin 6. Application to bone marrow transplantation. Transplantation 48:495
32. Patchen ML, MacVittie TJ, Williams JL, Schwartz GN, Souza LM (1991) Administration of interleukin-6 stimulates multilineage hematopoiesis and accelerates recovery from radiation-induced hematopoietic depression. Blood 77:472
33. Pantel K, Nakeff A (1989) Lymphoid regulation of hematopoiesis. Int J Cell Cloning 7:2

DISTRIBUTION LIST

DEPARTMENT OF DEFENSE

ARMED FORCES INSTITUTE OF PATHOLOGY
ATTN: RADIOLOGIC PATHOLOGY DEPARTMENT

ARMED FORCES RADIOBIOLOGY RESEARCH INSTITUTE
ATTN: PUBLICATIONS DIVISION
ATTN: LIBRARY

ARMY/AIR FORCE JOINT MEDICAL LIBRARY
ATTN: DASG-AAFJML

ASSISTANT TO SECRETARY OF DEFENSE
ATTN: AE
ATTN: HA(IA)

DEFENSE NUCLEAR AGENCY
ATTN: TITL
ATTN: DDIR
ATTN: RARP
ATTN: MID

DEFENSE TECHNICAL INFORMATION CENTER
ATTN: DTIC-DDAC
ATTN: DTIC-FDAC

FIELD COMMAND DEFENSE NUCLEAR AGENCY
ATTN: FCFS

INTERSERVICE NUCLEAR WEAPONS SCHOOL
ATTN: TCHTS/RH

LAWRENCE LIVERMORE NATIONAL LABORATORY
ATTN: LIBRARY

UNDER SECRETARY OF DEFENSE (ACQUISITION)
ATTN: OUSD(A)/R&AT

UNIFORMED SERVICES UNIVERSITY OF THE HEALTH SCIENCES
ATTN: LIBRARY

DEPARTMENT OF THE ARMY

AMEDD CENTER AND SCHOOL
ATTN: HSMC-FCM

HARRY DIAMOND LABORATORIES
ATTN: SLCHD-NW
ATTN: SLCSM-SE

SURGEON GENERAL OF THE ARMY
ATTN: MEDDH-N

U.S. ARMY AEROMEDICAL RESEARCH LABORATORY
ATTN: SCIENTIFIC INFORMATION CENTER

U.S. ARMY CHEMICAL RESEARCH, DEVELOPMENT, AND ENGINEERING CENTER
ATTN: SMCCR-RST

U.S. ARMY INSTITUTE OF SURGICAL RESEARCH
ATTN: DIRECTOR OF RESEARCH

U.S. ARMY MEDICAL RESEARCH INSTITUTE OF CHEMICAL DEFENSE
ATTN: SGRD-UV-R

U.S. ARMY NUCLEAR AND CHEMICAL AGENCY
ATTN: MONA-NU

U.S. ARMY RESEARCH INSTITUTE OF ENVIRONMENTAL MEDICINE
ATTN: SGRD-UE-RPP

U.S. ARMY RESEARCH OFFICE
ATTN: BIOLOGICAL SCIENCES PROGRAM

WALTER REED ARMY INSTITUTE OF RESEARCH
ATTN: DIVISION OF EXPERIMENTAL THERAPEUTICS

DEPARTMENT OF THE NAVY

NAVAL AEROSPACE MEDICAL RESEARCH LABORATORY
ATTN: COMMANDING OFFICER

NAVAL MEDICAL COMMAND
ATTN: MEDCOM-21

NAVAL MEDICAL RESEARCH AND DEVELOPMENT COMMAND
ATTN: CODE 40C

NAVAL MEDICAL RESEARCH INSTITUTE
ATTN: LIBRARY

NAVAL RESEARCH LABORATORY
ATTN: LIBRARY

OFFICE OF NAVAL RESEARCH
ATTN: BIOLOGICAL SCIENCES DIVISION

DEPARTMENT OF THE AIR FORCE

BOLLING AIR FORCE BASE
ATTN: AFOSR

BROOKS AIR FORCE BASE
ATTN: AL/OEBSC
ATTN: USAFSAM/RZ
ATTN: OEHL/RZ

OFFICE OF AEROSPACE STUDIES
ATTN: OAS/XRS

SURGEON GENERAL OF THE AIR FORCE
ATTN: HO USAF/SGPT
ATTN: HO USAF/SGES

U.S. AIR FORCE ACADEMY
ATTN: HO USAFA/DFBL

OTHER FEDERAL GOVERNMENT

ARGONNE NATIONAL LABORATORY
ATTN: ACQUISITIONS

BROOKHAVEN NATIONAL LABORATORY
ATTN: RESEARCH LIBRARY, REPORTS SECTION

CENTER FOR DEVICES AND RADIOLOGICAL HEALTH
ATTN: HFZ-110

GOVERNMENT PRINTING OFFICE
ATTN: DEPOSITORY RECEIVING SECTION
ATTN: CONSIGNED BRANCH

LIBRARY OF CONGRESS
ATTN: UNIT X

LOS ALAMOS NATIONAL LABORATORY
ATTN: REPORT LIBRARY/P364

NATIONAL AERONAUTICS AND SPACE ADMINISTRATION
ATTN: RADLAB

NATIONAL AERONAUTICS AND SPACE ADMINISTRATION
GODDARD SPACE FLIGHT CENTER
ATTN: LIBRARY

NATIONAL CANCER INSTITUTE
ATTN: RADIATION RESEARCH PROGRAM

NATIONAL DEFENSE UNIVERSITY
ATTN: LIBRARY

U.S. DEPARTMENT OF ENERGY
ATTN: LIBRARY

U.S. FOOD AND DRUG ADMINISTRATION
ATTN: WINCHESTER ENGINEERING AND ANALYTICAL CENTER

U.S. NUCLEAR REGULATORY COMMISSION
ATTN: LIBRARY

RESEARCH AND OTHER ORGANIZATIONS

AUSTRALIAN DEFENCE FORCE
ATTN: SURGEON GENERAL

BRITISH LIBRARY (SERIAL ACQUISITIONS)
ATTN: DOCUMENT SUPPLY CENTRE

CENTRE DE RECHERCHES DU SERVICE DE SANTE DES ARMEES
ATTN: DIRECTOR

INHALATION TOXICOLOGY RESEARCH INSTITUTE
ATTN: LIBRARY

INSTITUTE OF RADIOBIOLOGY
ARMED FORCES MEDICAL ACADEMY
ATTN: DIRECTOR

KAMAN SCIENCES CORPORATION
ATTN: DASIAC

NBC DEFENSE RESEARCH AND DEVELOPMENT CENTER OF THE FEDERAL ARMED FORCES
ATTN: WWDBW ABC-SCHUTZ

NCTR-ASSOCIATED UNIVERSITIES
ATTN: EXECUTIVE DIRECTOR

RUTGERS UNIVERSITY
ATTN: LIBRARY OF SCIENCE AND MEDICINE

UNIVERSITY OF CALIFORNIA
ATTN: LABORATORY FOR ENERGY-RELATED HEALTH RESEARCH
ATTN: LAWRENCE BERKELEY LABORATORY

UNIVERSITY OF CINCINNATI
ATTN: UNIVERSITY HOSPITAL, RADIOISOTOPE LABORATORY

XAVIER UNIVERSITY OF LOUISIANA
ATTN: COLLEGE OF PHARMACY